Enhancing the Efficiency of RF Sources for Future Colliders

Victoria (Catherine Rubina) Hill, BEng (Hons)

Engineering Department

Lancaster University

A thesis submitted for the degree of

Master of Philosophy

September, 2024

Declaration

I declare that the work presented in this thesis is, to the best of my knowledge and belief, original and my own work. The material has not been submitted, either in whole or in part, for a degree at this, or any other university. This thesis does not exceed the maximum permitted word length of 80,000 words including appendices and footnotes, but excluding the bibliography.

Victoria (Catherine Rubina) Hill

Dedication

For my beloved fiancé, this work is dedicated to you. You have been my unwavering source of support and love throughout this journey. Your steadfast presence, throughout the highs and the lows (and God knows there were so many lows), has been my guiding light. In the midst of my numerous setbacks and the moments of sheer panic, you remained by my side always offering me comfort and reassurance with every step.

Your selflessness knows no bounds as you willingly sacrificed your own comfort to be there for me during those late nights. Even choosing to sleep in the living room with the lights on and Guinness snuggled uncomfortably beside you, just to keep me company. During those times your presence was more than just physical, it was a constant reminder that I was not alone.

Your patience knows no bounds as you stood by me through my moments of frustration, panic, and exhaustion. Your calming presence and unwavering belief in me helped me navigate through even the most sleepless of nights.

For all the times you held me up when I felt like I was disintegrating bag of potatoes, for every encouraging word that kept me going, and for your boundless love that sustained me through it all.

I would also love to say a few words about my Mum. Throughout my university journey, you were not just Mum but also my best friend. You allowed me to move into your new home during my education and constantly loved and encouraged me throughout the challenges. Even when my rowdy and noisy friends stormed through your home after long days at university, you welcomed them with open arms, embracing them as if they were your own (and on a good few occasions even joined in). Your kindness and generosity knew no bounds.

And lastly, to my cherished friends Sarah, Storm, James, Leah, and Luke who all brought me immense joy and laughter into my mums home. I owe you all a debt of gratitude for always being there for me too.

Enhancing the Efficiency of RF Sources for Future Colliders

Victoria (Catherine Rubina) Hill, BEng (Hons).
Department of Engineering, Lancaster University

A thesis submitted for the degree of *Master of Philosophy.* September, 2024

Abstract

This study addresses the effectiveness of employing the Core Stabilization Method (CSM) in the pursuit of high-efficiency klystron design. Through simulations and design considerations, the suitability of CSM as a technique for achieving high efficiency is rigorously assessed. Initially, simulations were conducted on a 1 GHz klystron design to evaluate the efficiency of CSM in a 2.5D simulations compared to 1D simulations. Subsequently, AJDisk 1D simulations were employed to investigate the impact of the gap coupling factor (M) on minimizing electron crossovers, observed through Applegate diagrams. Adjustments to the gap coupling factors were made to enhance minimal electron crossovers and, consequently, efficiency. Magic 2D simulations were then performed on 800 MHz CSM 23 klystron preceding the gap coupling optimisation, yielding notable efficiency improvements. Furthermore, a novel fuzzy logic method is introduced, demonstrating its usefulness in expediting klystron optimization for 1/1.5D simulations and markedly reducing the optimisation time compared to conventional methods. The results show the potential of CSM and fuzzy logic optimization in enhancing klystron efficiency, augmented by the time saving gains facilitated by the fuzzy logic optimization approach.

Contents

List of Figures

List of Tables

Chapter 1

Introduction

On July 4th 2012, the ATLAS (A Toroidal LHC Apparatus) and CMS (Compact Muon Solenoid) proton-proton collisions at CERN's LHC (Large Hadron Collider) announced the discovery of a new particle [1]. This particle had a mass of around 126 GeV and was linked to the Brout-Englert-Higgs mechanism that provides elementary particles with mass, thus earning the name "Higgs-like boson". After more investigation the particle observed showed to have properties consistent with the Higgs boson predicted by the Standard model and in March 2013 the particle-physics community had enough evidence to name this new boson "a Higgs boson". This discovery contributed to the understanding of the origin of mass of subatomic particles and is the first-ever fundamental scalar particle observed in nature, however, it remains an open question whether this is thee Higgs boson of the Standard Model or another Higgs-like boson. However, further explanation and understanding of this question is unlikely to be investigated using the LHC. When the LHC is running at full design power the protons are accelerated from 450 GeV to 7 TeV per beam giving a total collision energy of 14 TeV [2]. Hadrons like the proton are not elementary particles and are composed of quarks, gluons and virtual antiquark pairs. Therefore, to obtain a more detailed analysis of a Higgs boson particle, an accelerator that would allow elementary particles to collide directly would be beneficial.

1.1 RF Sources Used In Particle Accelerators

Advancements in modern physics and engineering have propelled the demand for cutting-edge technologies, notably in the realm of high-energy particle accelerators. Particle physics relies on sophisticated tools to explore the fundamental constituents of the universe. Among these tools, radio frequency (RF) sources play a pivotal role in particle accelerators. These sources provide the necessary energy to propel particles to high speeds, allowing researchers to study their behavior at the subatomic level. RF sources' precision and adaptability make them vital components in advancing particle physics. These high-energy particle accelerators require high-power amplifiers capable of providing frequencies between 0.5 Ghz and 30 GHz and output RF powers of up to 2 MW for continuous wave (CW) and 150 MW for pulsed [3]. The two main types of amplifiers used are solid-state devices and vacuum tubes and the choice between these amplifiers often hinges on the specific requirements of the particle accelerator's design, considering factors such as power needs, frequency range, and reliability.

Figure 1.1.1 highlights these historical origins and the emergence of high power microwaves from the 1920s through to the 2010s.

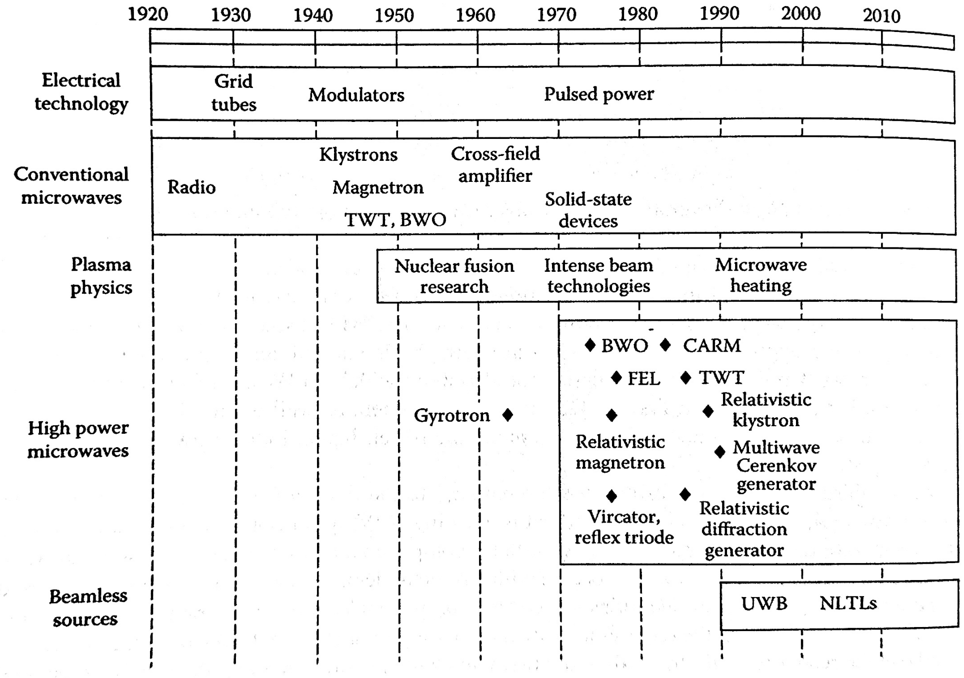

Figure 1.1.1: Origins and emergence of high power microwaves [4].

1.2 Solid State Amplifiers

Solid state amplifiers (SSA), or commonly referred to as solid state tubes, are used to mainly operate in the VHF (very high frequency) and UHF (ultra-high frequency) range. Solid-state amplifiers operate using transistors rather than vacuum electron tubes. Initially, RF silicon devices employed bipolar junction transistors (BJTs); however, these encountered challenges like thermal runaway and secondary breakdown. Consequently, measures such as temperature-compensated bias circuits were introduced to mitigate these issues and reduce the safe operating areas of the BJTs. Vacuum electron tubes became the preferred choice for medium and high-power applications, while solid-state amplifiers primarily served as driver stages, delivering output continuous wave (CW) power up to several hundred watts at frequencies within the range of tens of megahertz. Coming after the BJT, silicon bipolar transistors, silicon MOSFETS (metal-oxide-semiconductor field-effect transistor), or silicon carbide static induction transistors (SIT) were operated in parallel to obtain the high powers necessary for accelerators. Nowadays, higher frequencies employ GaN and GaAs FETs and silicon (Si) lateral diffused metal-oxide-semiconductor (LDMOS) devices for lower frequencies.

The shift from BJTs to more modern transistor types such as MOSFETs and LDMOS helped improve the performance of SSAs by reducing issues related to thermal instability, increasing their safe operating area, and enhancing reliability. Despite these improvements vacuum electron tubes like klystrons continued to dominate in very high-power applications due their ability to handle much higher power levels. However, SSAs have steadily advanced, benefiting from semiconductor innovations that now allow them to operate efficiently at higher frequencies and power levels, making them a competitive alternative in many applications.

The European Synchrotron Radiation Facility (ESRF) upgraded their RF system by replacing a klystron transmitter with 150 kW SSAs operating at 352.2 MHz. Each 150 kW SSA consists of two 75 kW “towers”. Using a coaxial combiner tree with $\lambda/4$ transformers, these towers chain together 128 RF modules, which produce 680 W each [5]. SSA capabilities were documented to reach average powers of hundreds of watts in CW mode and over 1 kW in pulsed mode, supporting a range of frequencies between 110 MHz to over 1 GHz [6]. Other operating advantages include the absence of high biasing voltages, leading to substantial power savings. ESRF quoted that operation of the four SSAs used only a third of the power required to operate the klystron transmitter [7]. Furthermore, the greatest main improvement proposed for using SSAs instead of klystrons is their reliability. This enhanced reliability is achieved by connecting the transistors in parallel as opposed to in series. In a parallel configuration, if one transistor fails, the others can continue to function. This redundancy increases the system's reliability compared to a series connection, where the failure of one transistor can disrupt the entire circuit.

Furthermore, the breakdown of one transistor will have a negligible effect on the overall power drop. Conversely, it has been noted that only a limited number of transistors can fail before major problems arise. ESRF documented that during a site acceptance test (SAT), having six unpowered RF modules (under mismatched conditions) led to arcing in the output circuits of the unpowered modules and the failure of their "protection" circuits, with up to 100% reflection [7]. It is appreciated that SSA transistors are vulnerable to inadvertent overload of power, given that they are driven so close to their design limit [8].

Despite their increasing use and reliability SSAs are not without their challenges when compared to klystrons. One of the key disadvantages of SSAs is their sensitivity to power overloads due to the transistors operating close to their maximum design limits. In contrast, klystrons require higher bias voltages and have a wider margin of safety when it comes to power handling. Furthermore, klystrons generally have a higher power output capacity making them the preferred choice for extremely high-power applications such as large particle accelerators, where SSAs would need to be operated in parallel to achieve comparable output. However, the reduced need for high-voltage power supplies and the inherent reliability of SSAs, due to their parallel transistor design giving them an edge in many medium-power RF applications. This reliability, combined with the lower operational power requirements, makes

SSAs particularly attractive for continuous operation over long periods, such as in synchrotrons and other scientific installations.

In general, the SSA technology efficiencies are typically around 60%. One study at the Thomas Jefferson National Accelerator Facility (TJNAF, JLab) observed operating efficiencies of more than 60% [9], with ESRF quoting efficiencies of 57 to 58% [7] and SOLEIL synchrotron facility observing SSA efficiencies of 60%, after five years of operation [10]. This efficiency level, while lower than the most efficient klystrons remains competitive along with the additional savings from reduced power supply demands. Over time, ongoing advancements in transistor technology, such as the use of wide-bandgap materials like GaN, are expected to further increase the efficiency and operational power of SSAs, making them a more viable alternative to klystrons in a wider range of applications.

1.3 Triodes and Tetrodes

In the triode a process called thermionic emission allows electrons to be released from the metal cathode by heating it with a separate current carrying filament. The electrons emitted are attracted to the positive anode (plate) through a grid. This grid modulates the electron flow between the two plates by changing the voltage between the grid and cathode. The tetrode was an improvement of the triode design by adding another grid to reduce capacitance between the cathode and the anode; the screen grid. However both the tetrode and triode have limited performance at high frequencies due to their transit time: the time required for the electron to travel between two electrodes [8]. The transit time is an important factor because at higher frequencies the time it takes for an electron to travel from the cathode to the anode becomes comparable to the oscillation period of the signal being amplified. When the transit time approaches or exceeds the signal period the device begins to suffer from phase delays and efficiency losses and therefore limits its ability to function effectively. In triodes and tetrodes, the physical distance between the electrodes and the speed of the emitted electrons is determined by this transit time. Although the introduction of the screen grid in the tetrode improved amplification efficiency by reducing capacitance, it did not resolve the underlying issue of electron transit time, particularly at higher frequencies. This limitation is a fundamental challenge for both triodes and tetrodes, as it directly affects their high-frequency performance.

1.4 Inductive Output Tubes

The essential components of an Inductive Output Tube (IOT) include the electron gun, anode, output gap, and collector. The electron gun, typically based on the conventional Pierce gun model, plays a crucial role in modulating the electrons emitted from the cathode. RF input voltage is applied between the cathode and grid, enabling modulation before the electrons traverse the RF output interaction area. Critical parameters such as the grid's characteristics significantly impact tube performance and include factors like gain and linearity. Maintaining precise separation between the cathode and grid throughout the tube's lifespan is required for optimal functionality. The IOT operates in a grounded anode mode and uses coils to create the necessary magnetic field for focusing the electron beam.

The input cavity, designed as a quarter-wave resonator, is positioned atop the electron gun and uses the cathode-grid gap as the interaction space for beam modulation. The input cavity is similar to that of the control grid in the tetrode by which it modulates the electron beam's current. RF input power is applied to the cavity, creating an oscillating electric field between the cathode and the grid. This field controls the flow of electrons from the cathode, modulating their velocity and density as they pass through the grid. The inner wall of the input cavity connects to both the cathode and grid and are at significant negative potentials, whilst the outer wall is grounded.

The IOT differs from the klystron as it lacks intermediate cavities and therefore the output cavity comes immediately after the input. This results in only a moderate gain and bandwidth compared to the klystron. To improve performance, modifications to the output cavity can be made, such as transitioning from conventional pillbox-type resonators to alternative designs like the double-gap or extended interaction structures. To address the risks associated with RF voltages within the output cavity, RF arc detector sensors are installed along with a cooling system to manage heat dissipation.

Similar to a klystron, an IOT uses an electron gun to produce a beam of high-velocity electrons. These electrons pass through a control grid, which modulates the current of the beam in a manner comparable to the tetrode. The electrons are then accelerated towards a high-voltage DC anode and pass into a resonant RF cavity, where they decelerate, allowing RF energy to be extracted and coupled out.

IOTs operate mainly in the frequency range of 100 MHz to 3 GHz and can produce CW RF output powers of up to 1 MW at lower frequencies and above 10 kW at higher frequencies. IOTs offer the advantage of high efficiency, around 70%, and are typically shorter, making them more cost-effective to produce than klystrons. However, their power range is more limited, and they have lower RF gain compared to klystrons [8].

1.5 Klystron

In 1937 Russel and Sigurd Varian produced the first working two-cavity klystron that was able to produce small amounts power at around 2GHz [11]. Originally patent granted in 1941 under the name "Electrical Translating System and Method" and having the US patent number US-2242275-A, this amplifying tube, as shown in Figure 1.5.1 laid the foundation for subsequent developments in microwave technology [12]. Since then klystron technology has continued to advance, and at frequencies of 300MHz and above are the main power amplifiers used in particle accelerators today. It extracts power similar to that as an IOT, however it uses a mechanism of velocity modulation rather than current modulation to bunch the electron beam. This allows for a higher output power but with similar efficiencies to the IOT. Table 1.1 and Table 1.2 show the typical characteristics of many klystron tubes that are being used in accelerators today [8].

Table 1.1: Table showing typical CW parameters of super-power klystrons

Type	**TH 2089B**	**K 351C**	**YK 1303**	**TH 2103**	**Units**
Frequency	352	352	508	3700	MHz
Beam Volatge	100	100	90	60	kV
Beam Current	20	20	18.2	20	A
Power	1300	1300	1	0.5	kW
Efficiency	65	65	61	43	%
Gain	40	40	41	45	dB
Length	4.8	3.8	3.75	2.0	m

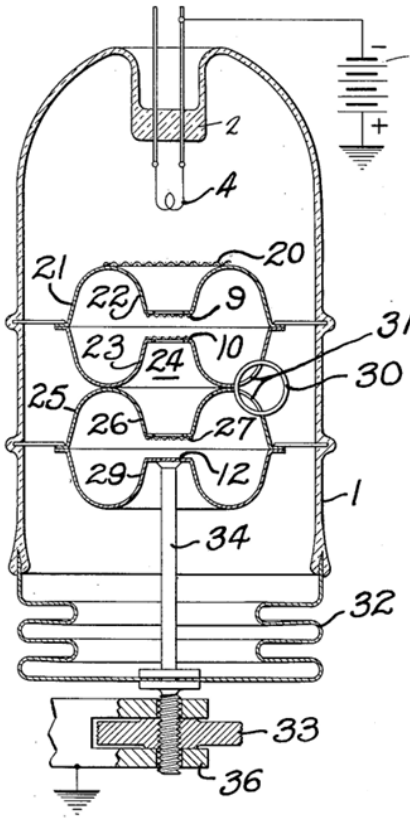

Figure 1.5.1: The first figure of an amplifying tube as filed under the patent number US2242275A by inventor Russel H. Varian. The numbering system used in the above Figure coincides with the features of the invention as described in the patent. [12]

Table 1.2: Table showing typical pulsed parameters of super-power klystrons

Type	**TH 2153**	**SLAC**	**VKS 8333A**	**Units**
Frequency	3.0	2.87	2.998	GHz
Beam Volatge	576	470		kV
Beam Current	600	612		A
Power	150	150	150	MW
Efficiency	43	50		%
Gain	48	52		dB
Pulse Length	1.2	3	3	μs

1.5.1 Basic Klystron Theory and Operation

A klystron is a specialised electron tube used in electronic and microwave applications for the amplification and generation of high-frequency radio waves. Simply put, a klystron functions as a vacuum tube that uses the principles of velocity modulation to amplify and generate electromagnetic waves at microwave frequencies. A klystron typically includes an electron gun, an input cavity for electron velocity modulation, and an output cavity where the amplified signal is extracted. The signal is amplified by modulating the velocity of an electron beam produced by the electron gun. Through the application of a small radio frequency (RF) signal at the input cavity the electrons within the beam experience variations in their velocity. These variations are caused by the sinusoidal behaviour of the RF signal that alternately accelerates and decelerates the electrons resulting in electron bunching. This electron bunch then arrives at the output cavity and further excites an RF field larger than that at the input cavity, therefore providing an amplified signal [8].

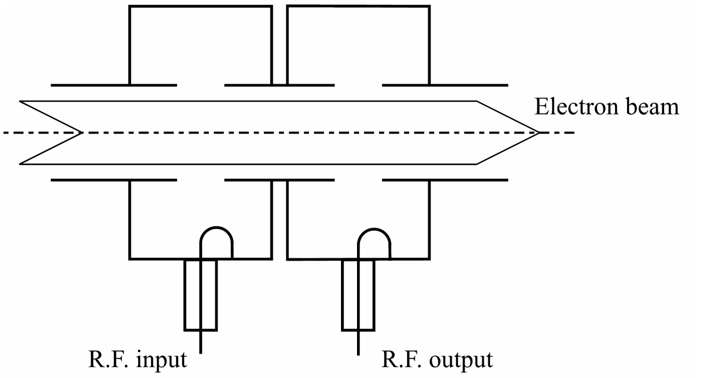

Figure 1.5.2: Schematic of a two-cavity klystron.
[8]

The two-cavity klystron in Figure 1.5.2 shows the principle operation of the klystron amplifier in more detail. By applying a voltage between the two electrodes in the electron gun, electrons emitted by the cathode are accelerated towards the anode and leave with a constant velocity. A small RF signal with a resonant frequency close to that of the transverse magnetic mode TM010 is coupled to the input cavity through a coaxial cable or waveguide. This RF signal excites an RF voltage across the interaction gap of the cavity. As the electron beam transverses through this cavity it is acted upon by the RF voltage which velocity modulates the beam, i.e. the beam is either accelerated or retarded depending on the phase of the electric field. After leaving the cavity the electron beam has experienced no current modulation and travels in a field free space called the drift tube or beam pipe. Along this length of tube faster electrons catch up with slower electrons which causes the beam to form bunches of charge [8]. These bunches can be simply represented graphically by Applegate diagram as shown in Figure 1.5.3.

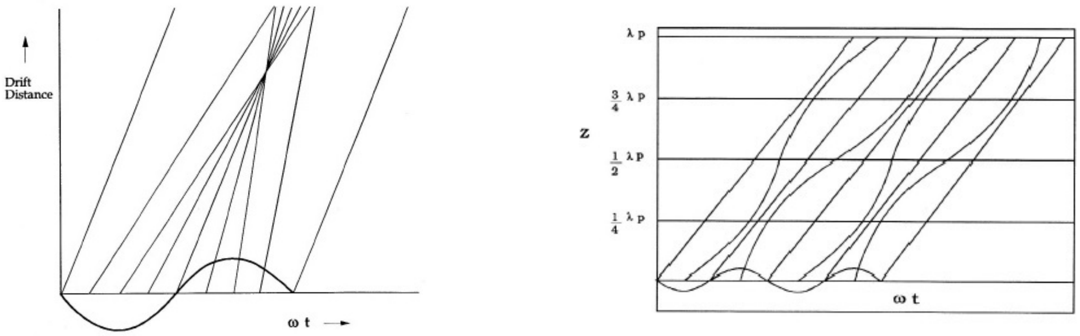

(a) Diagram ignoring space charge

(b) Diagram including space charge

Figure 1.5.3: Applegate diagram showing convergence of electrons in a field free drift region, where each line depicts the trajectory of an electron (9 electron trajectories) with the slope of each trajectory being proportional to its velocity over one RF phase [11].

Both graphically depict the trajectories of the electrons when you ignore or include space charge forces. Omission of space charge allows convergence of tight bunches and for electron overtaking (see Figure 1.5.3a). Whereas inclusion of the space charge forces (see Figure 1.5.3b) shows the electrons taking distorted paths due to the repelling nature of such forces. As the electrons get closer together the space charge force between them increases, limiting the convergence of electrons into tight bunches and vastly decreasing the chance of electron overtaking [11]. The output cavity is tuned to the repetition rate of the bunches, and placed further down the tube in a beam region where bunching of the electrons is greatest. To extract the RF energy from the beam the electric field across the gap of the output cavity is in anti-phase with the beam current. Therefore, any electrons crossing the gap within 90° of the bunch centre are decelerated. This allows them to transfer their kinetic energy to RF energy in the cavity. To get an appropriate amplified signal the convergence and tightness of these bunches is very important. The more electrons that transverse across the output gap during the deceleration phase compared the accelerating phase, the larger the gain in RF energy coupled out [8].

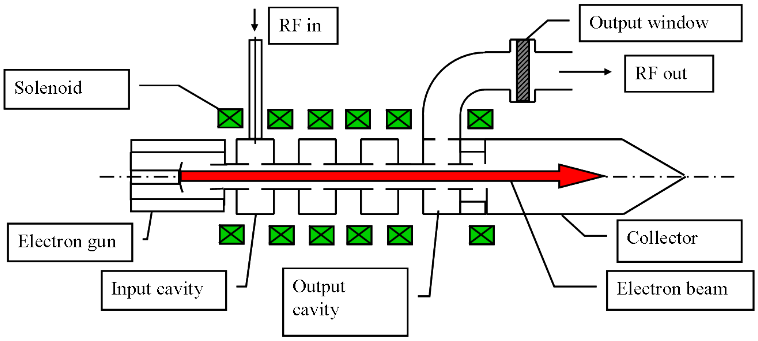

Figure 1.5.4: Schematic of two-cavity klystron [8]

To further enhance the velocity modulation or bunching of electrons, one or more resonant cavities can be inserted between the output and input cavities called “idler” cavities[11]. Unlike the input and output these intermediate idler cavities do not contain any coupler circuits. These additional cavities were added to the two-cavity klystron to create the multi-cavity tube, as shown in Figure 1.5.4. When the cavities are tuned to the correct resonant frequencies and placed along positions of maximum RF current, the multi-cavity klystron showed an increase in the gain, efficiency and bandwidth of the tube compared to the two-cavity klystron[8].

1.5.2 Electron Gun

The electron gun shown in Figure 1.5.5, is used in all klystrons to produce and control a beam of electrons, formed by the cathode, designed to match the beam requirements for that particular tube. The main difficulties that arise with electron gun design are space charge forces, which cause the beam to diverge, the expected current density of the beam and cathode lifetime [13]. The main parameters of the electron beam are the beam radius b, the electron velocity and the beam current I_b. Whilst beam radius is defined by the size of the beam tube, the beam current and electron velocity are determined by the cathode emission and the accelerating voltage between the cathode and anode.

There are several methods of control that can be applied to modulate the beam. Continuous wave operation and pulsed control are two techniques used in different systems. Pulsed RF power is usually required for radar or high power scientific applications, whilst continuous wave is used in communication broadcasting [11]. There are several techniques that can be used for beam current control as seen in Figure 1.5.6). The simplest method of current control is by modulating the voltage between the anode and cathode (Cathode pulsing, shown in Figure 1.5.6a). The anode is kept at ground potential and the cathode is pulsed at negative to turn the beam on. To turn off the beam, the cathode is increased to ground potential. Figure

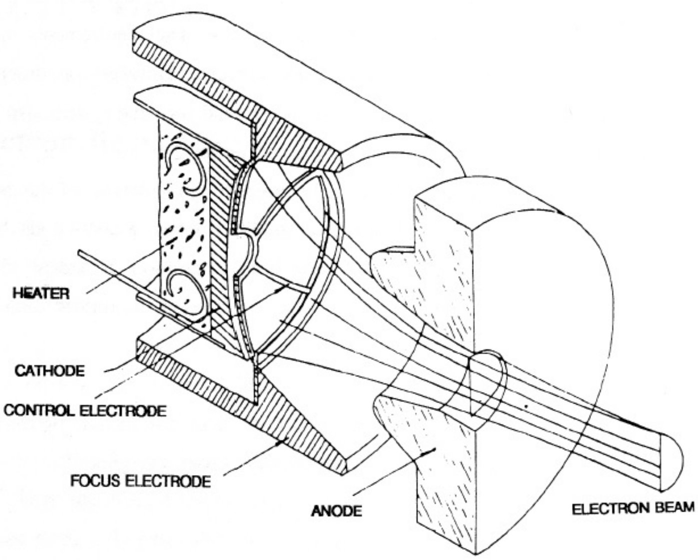

Figure 1.5.5: Schematic diagram of electron gun used in pulsed applications. [11].

1.5.6b utilises an additional modulating anode to control the beam power. The most common technique is to use one or more grids, placed very close to the cathode shown in Figure 1.5.6d. To turn the beam "off" a negative voltage is applied to the grid compared to the cathode, creating an electric field at the cathodes surface. This stops the acceleration of the electrons towards the grid, suppressing electron emission. The beam is turned "on" by switching the grid voltage to positive, with respect to the cathode, allowing the electrons to accelerate through the grid. Finally, Figure 1.5.6c shows the use of a focus electrode, however this technique is not wildly used due to severe defocusing of the beam current [13].

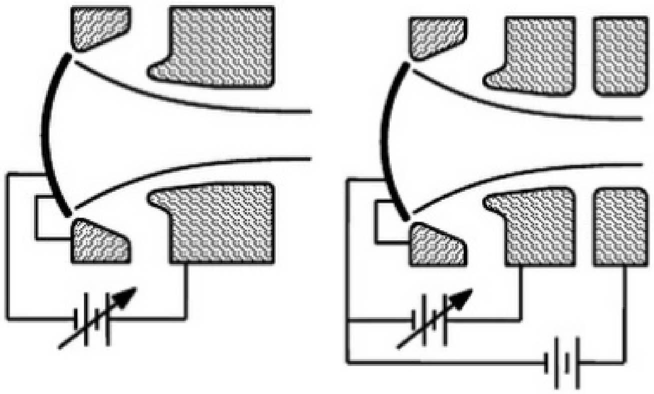

(a) Cathode. (b) Modulating anode.

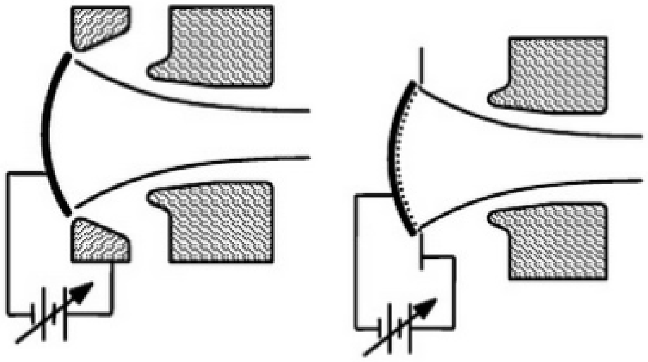

(c) Focus electrode. (d) Grid.

Figure 1.5.6: Methods used for beam control.
[13]

1.5.3 Thermionic Cathodes

Cathodes that use a heat source to expel electrons from their surface, that is through thermionic emission, are referred to as thermionic cathodes. This occurs when electrons that are situated in the upper conduction bands of the cathode material are given enough energy (via heating) to exceed the Fermi level. The minimum thermodynamic energy required to move an electron from the conduction band to a level in the vacuum (immediately outside the cathode material) is called the work function denoted by $e\phi$, where e is the charge on an electron. The Richardson-Dushman equation for thermionic emission shows the current density of the electrons emitted from the surface of the cathode:

$$J = A_0 T^2 e^{\frac{-e\phi}{kT}} \tag{1.5.1}$$

where J is the current density, T is the surface temperature of the cathode in kelvin, k is Boltzmann's Constant and A_0 is a universal constant and has a value of:

$$A_0 = 1.20e6 A/m^2 deg^2 \tag{1.5.2}$$

From the Richard-Dushman equation you can see that to increase the current density from the cathode you need to increase the surface temperature or use a work function value [13].

Barium is the most commonly used material used in cathodes. It has a low work function, 2.7 eV and has a reasonable melting temperature of 725°C. Barium also, when introduced to other elements, (example oxygen or tungsten) can create materials with a lower work function and higher melting point. [13].

Early radio tubes used pure tungsten for their thermionic cathodes. These cathodes had a high work function (4.54 eV) and therefore had an operating temperature of 2200°C to produce an emission rate of 0.3 A/cm^2 [13]. It was discovered that by introducing oxides of alkaline earth metals to the substrate metal, the work function of the material could be decreased dramatically [11]. The oxide is added by applying a carbonate mixture to a metal base (usually nickel) which is then heated in a vacuum reducing the carbonates to oxides. The most common carbonate mixtures to add are barium and strontium (Ba Sr)C0_3. These cathodes were commonly known as oxide cathodes and could operate at 1200K with a current density of 0.3 - 1A/cm^2. However, at a high current density the barium on the surface of the cathode would be evaporated. This reduction in barium (or other alkaline earth metal) decreased the lifetime of the cathodes, as a result of the element not being replenished. These cathodes were widely used through to the 1950s, but due to their low dc emission, short life span and susceptibility to being poisoned the L cathode was developed [13].

This early design of the L cathode, used a technique to store (Ba Sr)C0_3 in a cavity behind a thin porous tungsten plug surrounded by a molybdenum body. Behind the reservoir is a heater potted in an alumina mixture, this heater is to breakdown the carbonates to barium oxide. The tungsten layer reacts with these oxides to form free barium which pass through the porous plug and are released onto the cathode surface producing a thin active layer. These cathodes had a longer lifespan and produced good current densities (around 4 A/cm^2), however it had many fabrication issues with the leak-tight seals and narrow activation temperatures to stop side reactions with the tungsten [11].

The development of the B-Type dispenser cathode followed which impregnated the porous tungsten with Ba0, Ca0 and Al$_2$0$_3$, removing the original reservoir. This provided emission densities of above 4 A/cm^2 at operating temperatures of 1100°C. As a result of the high temperature, the lifetime of the cathode was only a few thousand hours [13]. Significant improvement in the dispenser cathode was found when the emitting surface of the B cathode was covered in a thin layer of osmium, iridium, ruthenium or rhenium. This reduced the work function by around 0.2eV and vastly decreased the cathode operating temperature to around 90°C(depending on the film metal) [13]. This new cathode, called the M-type cathode is now being presently used in high power klystrons. Problems can start to arise with these cathodes when the tungsten heavily diffuses into the metal coating. This causes the cathode to initially increase in current emission then eventually degraded. Further degradation causes the cathode to revert back to its B-type pre-requisite [13].

The current research into cathode chemistry involves the use of scandate oxide. Two proposed models have been devised through theoretical and experimental studies; the Ba-Sc-O monolayer and a semiconductor layer. The work function of these cathodes have been shown to reach 100A/m^2 continuous emission rate and 40A/m^2 pulsed at an operating temperature of 950°C. These cathodes have not been implemented as of yet due to inadequate attachment of the scandate to the surface [14].

1.5.4 Cathode loading and convergence

Other design aspects that need to be considered are cathode loading and gun convergence. Cathode loading is defined as the amount of current produced by the cathode per unit area. It is directly related to the operational life of the cathode, and thus, it is advantageous to keep this value low in order to extend the device's lifespan.

$$J_c = \frac{I_b}{A} \tag{1.5.3}$$

Where J_c is the current density of the cathode, A is the area of the cathode, and I_b is the beam current.

Area convergence in an electron gun is defined as the ratio between the diameter of the cathode surface and the diameter of the beam at its narrowest point (the beam waist). This concept arises because the beam's cross-sectional current density must often exceed the current density that can be generated by the cathode surface alone. To achieve this, the cathode surface is typically curved, as shown in Figure 1.5.5, to increase its effective area and thereby enhance electron emission.

The emitted electrons are then focused and compressed by electrostatic or magnetic fields to achieve the required beam diameter and current density at the beam waist. A high area convergence ratio indicates that the electron beam is being significantly compressed from the cathode to the beam waist, which increases the design complexity of the electron gun. Poor focusing can occur at high convergence values, leading to beam aberrations.

One way to improve focus is by reducing the cathode diameter, but this also increases the cathode loading, which in turn shortens the cathode's lifespan.

1.5.5 Operating Regions of the Cathode

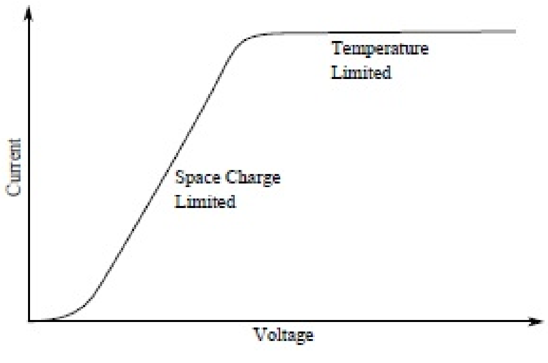

Figure 1.5.7: Graph illustrating the space charge limited and temperature limited operating regions in a cathode.
[15].

Figure 1.5.7 shows that the cathode operates in two separate regions of applied voltage and current. These regions are defined as the space-charge limiting region and the temperature limiting region.

As the electric field at the surface of the cathode increases it emits current (I_b) proportional to the field (V_b) raised to the three halves power. This is called the space-charge operating region. In this region the current drawn only depends on the geometry of the cathode and not the temperature or the work function of the material. Further increases in the electric field beyond this region, the temperature limited section, current is still emitted, it is not however proportional to the three halves power to the electric field. The current drawn from the applied voltage is far less and unpredictable, therefore it is desirable to have the cathode always operating in the space charge limiting region [11] .

1.5.5.1 Perveance

One of the most important characteristics of an electron gun is the perveance, K, usually measured in microns (micro-perveance). The most commonly used definition for measuring the perveance of klystrons is the ratio between the beam current and the beam voltage raised to the three-halves power with respect to the cathode.

$$K = \frac{I_b}{V^{\frac{3}{2}}} \tag{1.5.4}$$

This relationship between the current density (J) and the applied voltage (V) was first described by the Child-Langmuir three-halves power law: [11]

$$J = \frac{4\epsilon_0}{9d^2}\sqrt{\frac{2e}{m}}V^{\frac{3}{2}} \tag{1.5.5}$$

where m is the mass of an electron. This describes the simplest case of an electric field in a planar diode between the cathode and anode of infinite extent, separated by a distance, d [11].

A generalised relativistic measure of perveance which includes space charge is as follows:

$$K_{rel} = \frac{I_0}{([1 + \frac{V_0}{2U_e}]V_0)^{\frac{3}{2}}} \tag{1.5.6}$$

where U_e is the electron speed. Perveance can also be an indication of space charge forces. If the perveance is low then space charge forces between the electrons is weaker and this allows for tighter bunches and less debunching. This consequently leads to a higher efficiency compared to a klystron with high perveance. However, a low perveance means that a higher beam voltage is required. This can lead to problems with voltage breakdown at the gun which can reduce the klystrons reliability.

Most klystrons have a desired micro-perveance between 0.5 and 2.5 but in some cases, such as high power klystrons, a lower perveance is chosen, despite the higher beam voltage [16]. The relationship between the beam perveance and the RF efficiency has been documented as:

$$\eta(\%) = 90 - 20K(\mu perv) \tag{1.5.7}$$

This equation shows that a theoretical limit of 79% efficiency can be obtained with a low perveance [17].

1.6 RF Section

1.6.1 Resonant Cavities

A resonant cavity is described as a structure enclosed by metal walls that can support an oscillating electromagnetic field. RF cavities are used for several different reasons: to either store energy to accelerate a beam; extract beam energy; or to modulate the beams velocity or current. These cavities can easily be represented by a lumped element circuit to show how the electric and magnetic field are stored, by using a capacitor and inductor in parallel as shown in Figure 1.6.1.

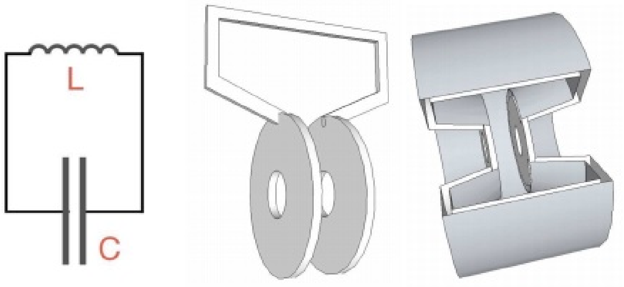

Figure 1.6.1: Diagram showing transition from lumped element circuit to resonant cavity.

[18]

All RF cavities share a set of fundamental characteristics that govern their operation and performance. These include the following:

- **Resonant frequency** (ω_0): This is the natural frequency at which the cavity resonates and is generally predetermined by its physical dimensions and design. The resonant frequency is a key parameter because the cavity must be driven at or near this frequency to achieve efficient energy transfer to the charged particles passing through it. The resonant frequency is calculated as ω_0=$2\pi f_0$, where f_0

is the resonant frequency in Hz.

- **Harmonic number** (h): The harmonic number represents the ratio between the RF frequency (ω_{RF}) and the revolution frequency (ω_0) of the particles in a circular accelerator. Mathematically, this relationship is expressed as $\omega_{\mathrm{RF}}=h\omega_0$. The harmonic number defines how many RF oscillations occur per particle revolution.

- **Shunt impedance** (Z): The shunt impedance is a measure of the efficiency of the cavity in converting RF power into accelerating voltage. It is defined as the ratio of the square of the accelerating voltage (V_{RF}) to the power dissipated in the cavity walls. A higher shunt impedance requires less power to achieve a given accelerating voltage.

- **RF voltage** (V_{RF}): This is the peak voltage generated across the gap of the RF cavity and is responsible for accelerating the charged particles. The RF voltage depends on the input power and the cavity's shunt impedance and helps in determining the energy gain of the particles through the cavity.

- **Quality factor** (Q): The quality factor is a dimensionless parameter that describes how well the cavity stores energy. It is defined as the ratio of the stored energy to the energy lost per RF cycle. A higher Q factor indicates that the cavity has lower energy losses and can sustain oscillations for longer periods with minimal input power and is an important measure of the cavity's efficiency.

- **Transit time factor** (T): The transit time factor accounts for the fact that the particles take a finite amount of time to cross the cavity and experience the accelerating voltage. It is a correction factor that reduces the effective accelerating voltage seen by the particles. The transit time factor depends on the velocity of the particles and the geometry of the cavity.

The simplest form a resonant cavity can take is the pill-box cavity, which is a cylindrical vacuum chamber with a conducting surface. The electromagnetic waves within these cavities can be classified into TM mode cavities (transverse magnetic), TE mode cavities (transverse electric), or TEM mode cavities (transverse electromagnetic). For RF cavities, the TM mode is of particular interest, as it generates a longitudinal electric field that can accelerate or decelerate charged particles, with no longitudinal magnetic field at the center of the cavity. The simplest mode in this configuration is the TM_{010} mode. This mode is characterised by zero full-wave variations in the azimuthal direction, ϕ, one zero-crossing of the longitudinal field in the radial direction, r, and zero half-wave variations of the field components along the length, z [18].

The field equations for this mode, expressed in cylindrical coordinates, are as follows:

$$\begin{aligned} &E_z(r,\phi,z,t) = E_0 J_0(k_r r)\cos(\omega t) && H_z = 0 \\ &E_r = 0 && H_r = 0 \\ &E_\phi = 0 && H_\phi(r,\phi,z,t) = -\frac{E_0}{Z_0} J_1(k_r r)\sin(\omega t) \end{aligned} \tag{1.6.1}$$

Here, each term is defined as follows:

- $E_z(r,\phi,z,t)$: The longitudinal electric field component, which is the primary accelerating field inside the cavity.
- $H_z(r,\phi,z,t)$: The longitudinal magnetic field component, which is zero in the

TM mode.

- E_ϕ, E_r: The azimuthal and radial components of the electric field, respectively, both of which are zero in this mode.
- $H_\phi(r, \phi, z, t)$, H_r: The azimuthal and radial components of the magnetic field, where only the azimuthal magnetic field, H_ϕ, exists in this mode.
- E_0: The amplitude of the longitudinal electric field, representing the maximum field strength.
- $J_0(k_r r)$, $J_1(k_r r)$: The zeroth and first-order Bessel functions of the first kind, which describe the spatial variation of the electric and magnetic fields in the radial direction.
- k_r: The radial wave number, which is related to the cavity's geometry and defines how the fields vary with the radius.
- $\omega = 2\pi f$: The angular frequency, where f is the operating frequency of the cavity.
- Z_0: The wave impedance in free space, defined as $Z_0 = \sqrt{\frac{\mu_0}{\epsilon_0}} = 377\,\Omega$, where μ_0 is the magnetic permeability of free space, and ϵ_0 is the electric permittivity of free space [18].

The angular frequency ω of the pill-box cavity is determined by the geometry of the cavity, particularly the cavity radius, R_{cav}. For a pill-box cavity operating in the TM_{010} mode, the angular frequency can be expressed as:

$$\omega_0 = k_r c = \frac{2.405c}{R_{cav}} \tag{1.6.2}$$

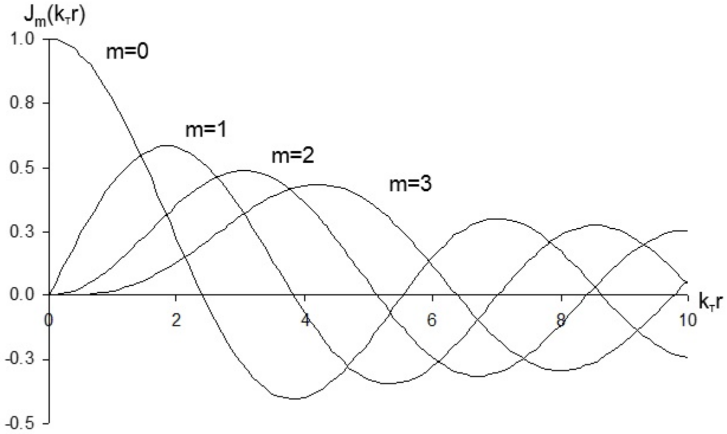

Figure 1.6.2: Graph showing first four Bessel functions.
[19]

Where ω_0 is the angular frequency of the cavity, k_r is the radial wave number, specifically $k_r = \frac{2.405}{R_{cav}}$, where 2.405 is the first root of the zeroth-order Bessel function J_0, which defines the field distribution in the radial direction for the TM_{010} mode, c is the speed of light in vacuum (2.8×10^8 m/s) and R_{cav} is the radius of the cavity.

The field components E_z and H_ϕ, as described above, exhibit a specific spatial variation described by Bessel functions, which are solutions to the wave equation in cylindrical coordinates. The zeroth-order Bessel function $J_0(k_r r)$ defines the electric field distribution along the radial direction, and the first-order Bessel function $J_1(k_r r)$ describes the corresponding magnetic field. These functions are depicted in Figure 1.6.2, illustrating the first few Bessel functions and their oscillatory behavior.

The wave impedance Z_0, which is the ratio of the transverse electric field to the transverse magnetic field in free space, is defined as:

$$Z_0 = \sqrt{\frac{\mu_0}{\epsilon_0}} = 377\,\Omega \tag{1.6.3}$$

This wave impedance applies only in the frequency domain and is a fundamental property of electromagnetic waves in vacuum [18]. It plays an important role in determining the energy transfer efficiency within the cavity and how well the cavity resonates at its designated frequency.

The electric and magnetic field pattern that is generated by the TM_{010} is shown in Figure 1.6.3.

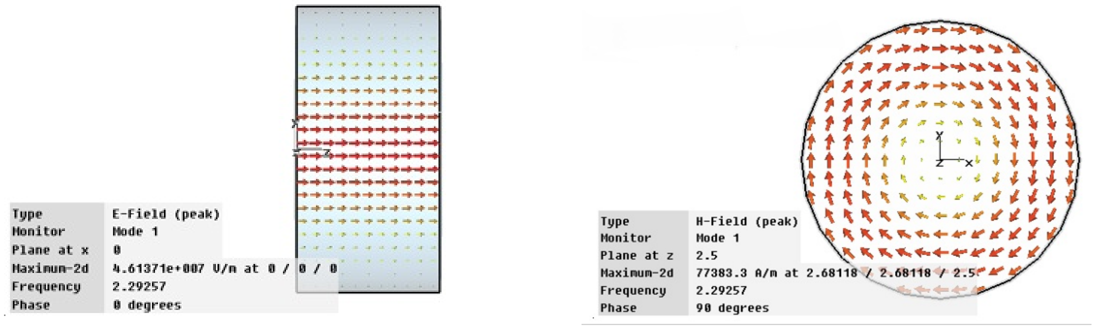

Type	E-Field (peak)
Monitor	Mode 1
Plane at x	0
Maximum-2d	4.61371e+007 V/m at 0 / 0 / 0
Frequency	2.29257
Phase	0 degrees

Type	H-Field (peak)
Monitor	Mode 1
Plane at z	2.5
Maximum-2d	77383.3 A/m at 2.68118 / 2.68118 / 2.5
Frequency	2.29257
Phase	90 degrees

(a) Electric field

(b) Magnetic field

Figure 1.6.3: The electric and magnetic field in a pill box cavity.
[19]

For a practical resonant cavity there needs to be a hole, including nose cones, on either side of the pill box cavity for the drift tube (beam pipe). This allows the electron beam to enter the cavity and cross the acceleration gap. The nose cones concentrate the electric field across this gap by increasing the capacitance, C. In order to maintain the resonant frequency of the cavity the inductance, L must also be lowered.

$$\omega_0 = \frac{1}{\sqrt{LC}} \tag{1.6.4}$$

The basic design of a conventional klystron will have two or more resonant cavities; the input, output and (in most cases) idler cavities. These cavities, generally cylindrical in shape, are usually re-entrant resonant cavities and are used for their ability to create strong electric fields across a short gap and provide enhanced coupling to the beam. The cavity is able to provide an axial field in the direction of the beam by operating in the TM010 mode.

1.6.1.1 Input Cavity

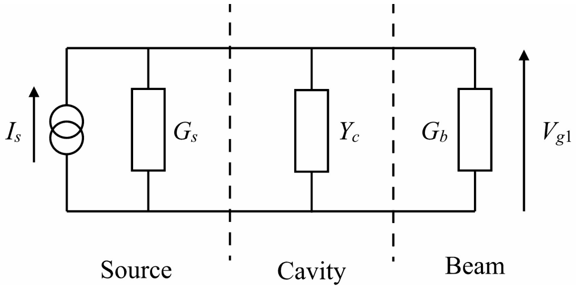

Figure 1.6.4: Equivalent lumped resonating circuit for the input cavity [8]

Figure 1.6.4 shows the equivalent circuit of the input cavity of a conventional klystron. Where V_g is the gap voltage , I_s is the source current, G_s and G_b are the source and beam conductance respectively, whilst Y_c and Y_b denotes the cavity and beam admittance respectively. The input coupler modifies the source current and conductance from those of the external source. Subsequently, the input gap voltage is determined by

$$V_g = \frac{i_g}{G_s + Y_c + Y_b}, \tag{1.6.5}$$

where the cavity admittance is derived as depicted in

$$Y_c = G_c(1 + jQ_u(\frac{\omega}{\omega_0} - \frac{\omega_0}{\omega})), \tag{1.6.6}$$

wherein G_c is the shunt conductance, Q_u is the unloaded quality factor. The input power can further be calculated by

$$P_{in} = \frac{i_s^2}{8G_s}, \tag{1.6.7}$$

giving an input gap voltage of

$$|V_{g1}|^2 = \frac{8G_s}{|G_s + Y_c + Y_b|^2} P_{in}, \tag{1.6.8}$$

1.6.2 Intermediate Cavities

Figure 1.6.5 shows the equivalent circuit for the idler cavities. The beam is modeled as a current source with a magnitude of I_g and an admittance equivalent to the beam admittance (Y_b). In small-signal analysis, it is common practice to utilize the beam loading admittance of an unmodulated beam across all cavities, although this approach is not strictly accurate. When the imaginary part of Yb is significantly smaller than the real part (G_b), Yb may be approximated by G_b without significant error. The cavity operates by extracting power from the modulated beam and utilizing it to introduce fresh modulation to the beam. Due to the high impedance of the cavity, a small induced current results in a substantial gap voltage. Neglecting cavity losses, the kinetic power of the beam exiting the cavity is equivalent to the power entering it.

1.6.3 Output Cavity

The output cavity of a klystron is designed to extract energy from the electron beam and convert it into a high-frequency RF signal. The basic function can be described by the following equations and by the equivalent circuit of the output cavity, shown in Figure 1.6.5.

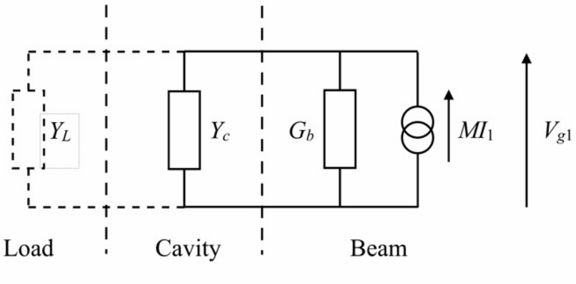

Figure 1.6.5: Equivalent lumped resonating circuit for the output or idler cavity. [8]

$$v = c\sqrt{1 - \frac{1}{\gamma^2}} \tag{1.6.9}$$

The above equation is the relativistic beam velocity where v is the electron beam velocity, c is the speed of light, and γ is the Lorentz factor given by

$$\gamma = \frac{1}{\sqrt{1 - \frac{v^2}{c^2}}} \tag{1.6.10}$$

Next the electron beam current current (I_{beam}) is related to the charge of the electrons (e) and the number of electrons per unit time (N_e given by the following equation

$$I_{beam} = eN_e v \tag{1.6.11}$$

Thirdly, the resonant frequency (f_{res}) of the output cavity is determined by its dimensions and the speed of light:

$$f_{res} = \frac{c}{2L} \tag{1.6.12}$$

Finally the power (P_{out}) in the output cavity is related to the beam current and the quality factor (Q) of the cavity:

$$P_{out} = \frac{1}{2}(I_{beam})^2 \tag{1.6.13}$$

These equations provide a basic description of the function of the output cavity in a klystron. The electron beam, with its associated current, interacts with the resonant structure of the output cavity, leading to the extraction of RF power at the resonant frequency. Whilst the quality factor of the cavity influences the efficiency of power transfer from the electron beam to the RF signal.

1.7 Small Signal Analysis

1.7.1 Space charge wave theory

If space charge forces could be disregarded when dealing with the trajectories of individual electrons, analysis of this motion would be considered uncomplicated. However, as previously explained, this is not the case for klystrons. There are considerable space charge forces acting within the electron beam due to velocity modulation at the input cavity. The basic properties of velocity modulation (or any modulation for that matter) can be defined as space-charge waves propagating down the electron beam. To make these calculations it is best to describe the electron beam as a space-charge continuum or plasma.

1.7.2 Gap coupling factor

Placement of the output cavity is very important to gain the maximum excitation of the RF currents in cavity. Analysis of the fundamental component of the RF beam current (i) will show where the amplitude is at a maximum:

$$i = 2I_0 J_1(X) \tag{1.7.1}$$

Where J_1 is a Bessel function of the first kind of the first order(see section 6.1), I_0 is the DC beam current and X is the bunching parameter:

$$X = \frac{\alpha M_\theta \omega z}{2u_0} \tag{1.7.2}$$

Where ω = angular frequency, u_0 = velocity of electron at beam voltage

V_0, M_θ = gap coupling coefficient and α is the depth modulation which is the ratio between the RF gap voltage, V_g and the DC beam voltage V_b:

$$\alpha = \frac{V_g}{V_b} \tag{1.7.3}$$

1.8 Large Signal Analysis

Large signal analysis, compared to small signal analysis, reverts to a ballistic model. This involves examining the interplay between electrons and the RF electric fields within the resonant cavities. The model becomes more complicated due to the concentration of space charge, leading each electron to repel others at varying degrees. From introducing this higher level of complexity, finding an analytical solution can become challenging. Instead, we can resort to iterative solutions employing steady-state time domain simulations based on a simplified representation. One common simplification involves adopting the disk model, where a sequence of charged disks, each characterized by axial position and velocity, serves as a representation of the beam. Such examples include AJDisk and KlyC. In these models, radial motion is disregarded, and the calculation is divided into two stages: the drift between interaction gaps; and the interaction with cavities.

Nevertheless, there are limitations to this approach. For example, the radial size of the beam is not constant due to bunch expansion caused by space charge. Additionally, the electric field in the gaps is not constant radially, and quantization errors arise from the creation of disks. To address these limitations, enhancements can be made by dividing the disks into rings to account for radial effects.

For a more precise yet computationally intensive large signal simulation, the Particle in Cell (PIC) approach is employed. An example of such a PIC code is Magic 2D. This code organizes numerous electrons into a reduced number of macro particles that serve as approximations for the beam. This approach allows for the consideration of radial movement and mitigates quantization errors associated with disks or rings.

Table 1.3 gives a description of all the main beam parameter measurements and terms commonly used when comparing different types of klystrons along with techniques used for achieving higher efficiency.

Table 1.3: Description of main beam parameters measured

Beam Parameter	**Description of Beam Parameter**
Current (J1) peak	Value at the peak of the first harmonic current curve.
Harmonic Amplitude	Value at the peak of the second and third harmonic currents.
Harmonic Current	Current values measured at each cavity, in the middle gap for the first, second and third harmonics.
Harmonic Spread	The difference (the spread) between the second and the eighth harmonic current values at the output cavity.
Position of Imax(n)	The position in z(mm) where the peaks of the first to the eighth harmonic currents lies, where (n) is the harmonic number.
Sub-Bunches, Beamlets	Area's of high density electron bunching within a single bunch that can be seen on the Applegate Diagram.
Velocity Spread	The difference between the velocities of the electrons during their trajectory through the tube during one RF cycle.
Stratification	Radial bunch stratification is the radial variations of the RF current modulation depth. In a system with axial symmetry ,with respect to the beam centre, such effect is originated by radial variations of the space charge forces and cavities impedance's.
Bunch Length	The length of a single bunch measured just before the gap of the output cavity
Gradient just before the knee.	The knee defined as the largest gradient change along the length of the tube for the first harmonic.
Velocity Spread vs Shape of Bunch, Pz, Before Output	The phase trajectory of a bunch, a qualitative look at the shape of the bunch before it enters the output cavity. A further indication of stratification.
Over Bunching	Over bunching is an overlap of electrons or a large change in velocity near the bunch in an Applegate diagram. This effect is generally caused by the defocusing of intermediate cavities.

Chapter 2

Literature Review

2.1 Current and Developing Technologies

The current requirement under the CLIC specification (CLIC Conceptual design report) for klystron efficiency is 70% [20]. Whilst the specification report for FCC-ee (Future Circular Collider) requires a total RF power of 100 MW CW [21]. For both the CLIC and FCC-ee projects achieving high klystron efficiency is particularly important in order to meet these increasing power requirements.

2.1.1 Perveance and Multi Beam Klystrons

One of the more traditional techniques that has been used to increase efficiency was by measuring the perveance of the electron gun. In general, the lower the measured perveance the higher the efficiency. Perveance is defined as the ratio between the beam current and the beam voltage raised to the three-halves power with respect to the cathode, see Equation 1.5.4. This measurement gives an insight into the magnitude of the longitudinal space charge effects in a beam and is the most commonly used description (non-relativistic). Wherein, Equation 1.5.5 shows the relativistic measure of perveance as being the more generalized perveance equation (a dimensionless measure). As seen from Equation 1.5.4, to lower the perveance either the beam current has to be small for a given voltage or an increase in the beam voltage is required. Ideally a low current and a higher voltage is desirable. This is preferred for the fact that a smaller beam current results in the space charge forces within the beam being reduced. Therefore, enabling better bunching at the core of the electron beam and ultimately a higher induced harmonic current at the output cavity. However, this is limited at higher powers due to the maximum voltage that can be applied to a given cathode. Typically, the upper technical limit to the voltage that can be applied is 300 - 500 kV. SLAC's X-band klystrons having operated at voltages up to 450 kV and some experimental high-power klystrons having reached 500 kV [22]. Due to these technical limitations on the maximum voltage that can be applied, achieving low perveance requires operating at a low current. In single-beam klystrons, this poses a challenge for generating high power. The multibeam klystron (MBK) concept addressed this issue by using multiple individual beams that interact with shared RF circuits. This approach allows the perveance to be managed for each individual beam, while the total power output is the combined result of all beams. By using MBKs it was therefore theoretically possible to achieve these high powers and high efficiencies as required by CLIC and FCC.

An example of an multiple beam klystron (MBK) klystron design that used low perveance to achieve higher efficiencies was the 10MW L-band MBK [23]. The Toshiba MBK measured 2.3 meters in length, operated at a beam voltage of 115 kV, and emitted six beam-lets. These beam-lets were generated by a diode electron gun consisting of six cathodes and a single focusing electrode. With a relatively low perveance of 0.56 per beam-let, the use of multiple low-perveance beams in parallel was designed to enhance the RF efficiency by reducing space charge forces and enable tighter beam bunching. As a result, the MBK klystron achieved an efficiency of 66%. Using the MBK technology and knowledge of low perveance it was therefore shown to be theoretically possible to achieve these high powers and efficiencies as required by CLIC and FCC. With Table 2.1 highlighting the specifications for L-band low perveance and Figure 2.1.1 showing the road map of the developing MBK designs.

Table 2.1: Table showing specifications for L-band low perveance MBKs for CLIC and FCC.

	CLIC	**FCC (ESS)**	Units
Frequency	1	0.8	GHz
Pulse length	150	(CW)	μ secs
Power	20	1.5	MW
No. of beams	40-60	10-16	
Microperveance per beam	0.3-0.2	0.2	
Operating voltage	<60	40 - 50	kV
Expected efficiency	>90	>85	%

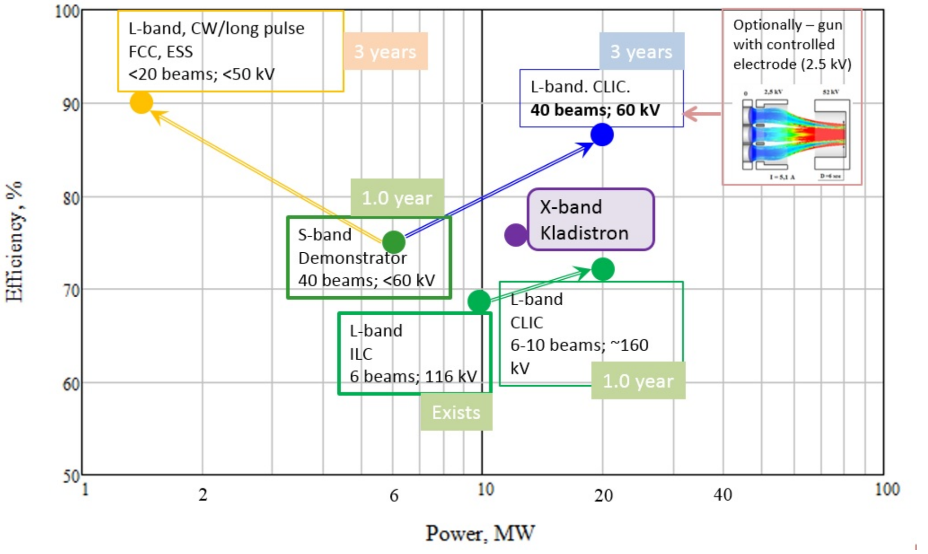

Figure 2.1.1: Graph showing efficiency and power road map of developing MBK designs.

[15]

2.1.2 Congregated Bunch

It has also been previously reported that the ideal structure of a bunch at the input of the penultimate cavity is the “congregated bunch structure”. This method indicates that to further increase efficiency at the output cavity, collecting the electrons at the peripheral of the core is as important as the bunch tightness. The theory suggests that the input velocities must be arranged such that each successive electron has a higher velocity before entering the output cavity. This leads to a progressive bunching effect wherein the electrons converge and rotate before the output cavity leading to a uniform velocity dispersion after deceleration. When the electrons within this bunch have identical velocities after deceleration, the energy transfer to the RF field can be maximised due to minimal kinetic energy losses.

Figure 2.1.2 represents the stages of how this congregated bunch is formed.

Stages one and two shows the electrons of a fully saturated bunch with the same phase velocity being compressed to form a tighter bunch. As this bunch enters the gap of the cavity the electrons experience a different electric field due to the sinusoidal nature of the longitudinal electric field, as shown in stage three. This rotates the bunch in preparation for the bunch entering the output cavity. This rotation ensures that each consequent electron entering the output cavity has higher velocity than preceding one. At stage 4 the electrons are decelerated by the voltage at the output cavity, thus they leave the cavity exit with equal velocities. This technique allows for maximum kinetic energy to be extracted from the electrons into RF power, therefore further improving the efficiency of the overall tube.

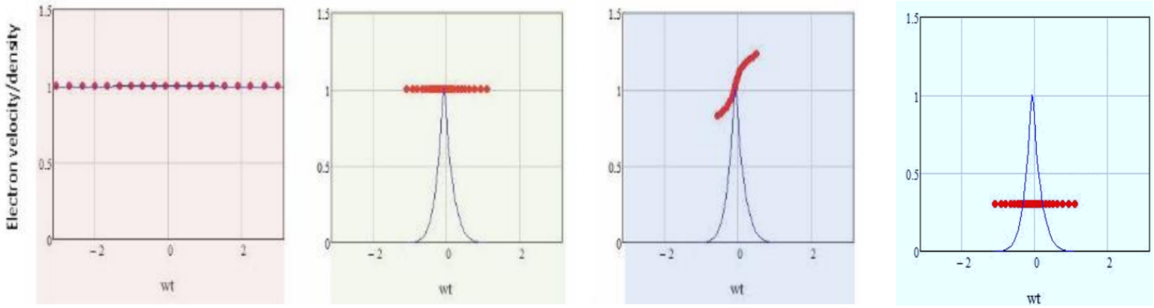

Figure 2.1.2: Four stages showing the formation of the congregated bunch

2.1.3 Core Oscillation Method (COM)

Another technique that has been shown to increase efficiency is the bunch core oscillation method [24]. This method differs from traditional monotonic electron bunching by allowing the core of the electron beam to debunch due to space charge forces. This permits the outside particles (also known as electrons situated in the anti-bunch), subject to weaker space charge forces, to achieve a greater phase shift towards the core. This method has also been shown to predict efficiencies of up to 90% by improving the containment of peripheral electrons with the central core [25]. However, the peripheral electrons require a very long drift space in between the cavities for the desired effect to occur, therefore resulting in a very long tube [25]. The difference between "classical" bunching and new bunching with core oscillations can be seen in Figure 2.1.3. In a specific design, such as the X-band klystrons, the COM approach has shown potential for over 65% efficiency at output power levels of around 50 MW [22].

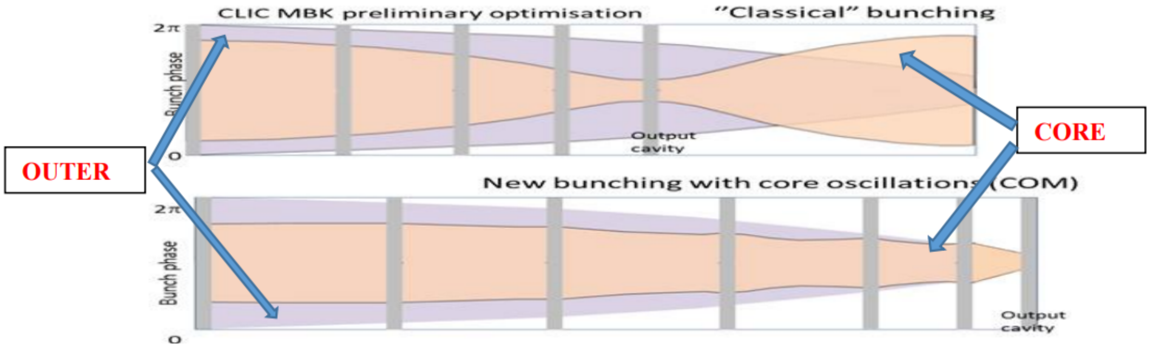

Figure 2.1.3: Representation of the differences between the classical and COM bunching methods. It highlights the two separate bunching regimes. The core (orange), is where the bunch periodically contracts and expands around the centre of the bunch and the outer edges (purple), are were the outsiders monotonically go to the centre of the bunch.

2.1.4 Bunch, Alignment and Collection (BAC) Method

A new method to reduce the length of these tubes was proposed by I.Guzilov [26]. This method was called BAC (Bunching, Alignment and Collection) and it focused on intensifying the process of electron oscillations at the core of the bunch, with Figure 2.1.4 graphically highlighting these three stages on an Applegate diagram. This was achieved by increasing the number of cavities and in the klystron tube and by using strong external forces of specially tuned idler cavities this accelerated the oscillation process and the process of collecting particle 'outsiders'. Each oscillation in the BAC method experiences three stages. The initial, beginning in the first cavity gap, involved the traditional bunching of the core oscillations. The next process occurred in the second cavity gap were the electrons had their velocities spread aligned. Lastly the third cavity gap involved collection of the outsider electrons from the peripherals of the core bunch. As an example, two S-band BAC multiple-beam BT258 klystrons were designed and tested at DBT with support from CERN. These klystrons achieved a peak efficiency of 66% at an output power of 6.6 MW, with potential to increase the output power to between 10 and 20 MW [27].

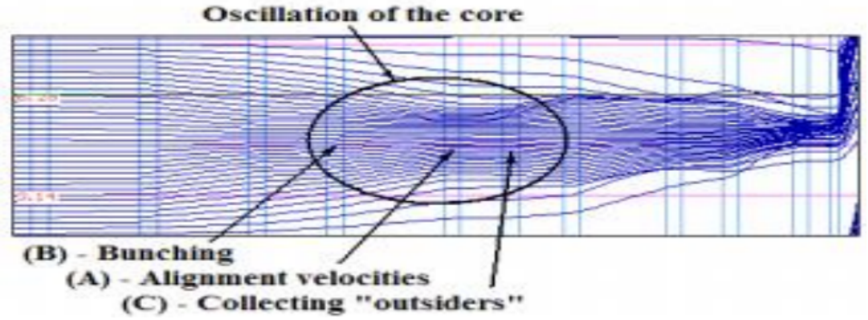

Figure 2.1.4: Graph showing the three stages of electron oscillation at the bunch core in BAC (Bunching, Alignment and Collection) method.

2.1.5 Adiabatic Bunching

Another bunching technique that could further increase efficiency is called Adiabatic bunching. This method was implemented in the Kladistron model and was designed from an existing and well established tube the the 4.9 GHz, 50 kW CW TH2166 klystron developed by Thales and a predicted efficency of 67%. A kladistron (kl-adi(adiabatic)-stron) is a high-efficiency klystron with a large number of cavities, up to three times as many compared to a standard klystron. This method involved continuous bunching at a very low voltage and therefore a large number of cavities were required to bunch the electron beam slowly by keeping the velocity spread small.

2.1.6 Multi Beam Klystrons

Multi beam klystrons (MBK) refer to a configuration where multiple single-beam klystrons operate in parallel. The cavities, excluding the common input and output components, as well as the focusing systems, can either be shared or independent. SLAC developed X-band 75 MW single-beam pulsed klystrons operating at 480 kV voltage (chosen for low perveance) initially intended for JLC and NLC applications. The high voltage, coupled with a high frequency beam, necessitates a strong focusing field and encounters breakdown issues, making it less appealing. The Multiple Beam Klystron configuration addresses these challenges by distributing power across multiple beams, effectively resolving the mentioned issues.

This configuration offers several advantages, particularly in terms of achieving a given output power while reducing the gun voltage. This reduction in gun voltage results in a decrease in the perveance of each beam, enabling higher efficiencies. Additionally, these configurations are relatively compact when compared to similar single-beam klystrons or groups of individual single-beam klystrons, making them easier to cool [28].

The MBK configuration is well-suited for achieving high efficiency in operation. The requirement for low perveance is met by distributing the current over a larger cathode area with multiple cathodes, allowing for a suitable lifetime, albeit with a complex electron gun design. However, beam focusing can pose a challenge due to the off-axis nature of the beams, often necessitating the maintenance of high cathode loading to ensure the beams remain as central as possible [28].

Opting for a single common collector is the likely most cost-effective design. For instance, when CPI designed a 6-beam klystron for TESLA, six isolated collectors were employed, although this was mainly for diagnostic purposes and was not intended for the final models [28].

2.1.7 Sheet Beam Klystrons

The concept of the sheet beam klystron, also known as the “waveguide klystron”, dates back to the 1950s but experienced a resurgence of interest in the 1980s when it was considered as a potential X-band power source for the Next Linear Collider (NLC). However, during that time, it was determined that transporting beams with significant power levels (200 MW) resulted in substantial beam losses, exceeding 50% [29][30], leading to the sheet beam klystron falling out of favor for high frequency applications.

2.1.8 Methodology

There are many codes that can be used for simulating the interaction of the electron beam with the cavity structures in a klystron. What code to choose depends on the specific task or analysis the user requires, for example an initial design or a detailed evaluation. There are two main types of simulation code used for these considerations, 1D disk models and 2D/3D PIC codes. The two main simulation software that was use over the course of this project was AJDISK, KLYC and MAGIC2D. Below is a brief description of all three.

2.1.9 AJDISK

This code adopts the disk model to depict electrons as charged disks confined within a cylindrical drift tube. These disks (see Figure 2.1.5) undergo acceleration propelled by the beam voltage, ensuring their individual charges align with the current in the beam. The resultant electromagnetic field, emanating from these charged disks, is delineated by a "Green's function." This function is intricately linked to several parameters, including the dimensions of the disks (beam) and drift tube, the current, the voltage, and the axial component z. Notably, the disks possess the ability to penetrate and overtake each other within the drift tube.

The characteristics of the klystron cavities are dual-fold. Firstly, they are characterized as lumped circuits, contingent on various parameters such as quality factors (Qs), R/Q ratios, and resonant frequencies. Secondly, the klystron cavities are defined by the electromagnetic field developed across their gridless gaps. This gap field is mathematically expressed as a Gaussian function, incorporating variables such as beam and drift tube diameters along with the gap length. A simplified flow chart of the AJDISK algorithm is shown in Figure 2.1.6.

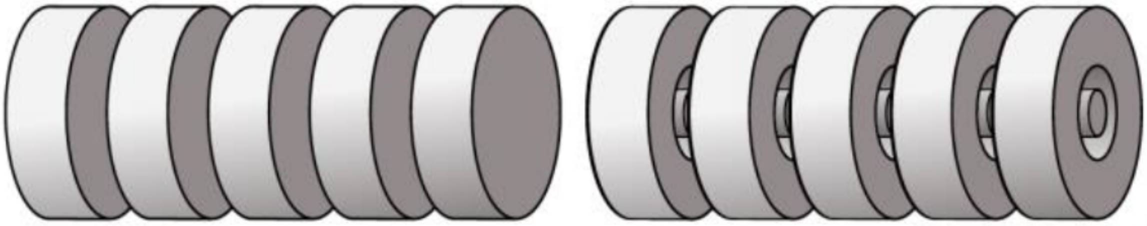

Figure 2.1.5: Representation of disks used to represent electrons in simulation software

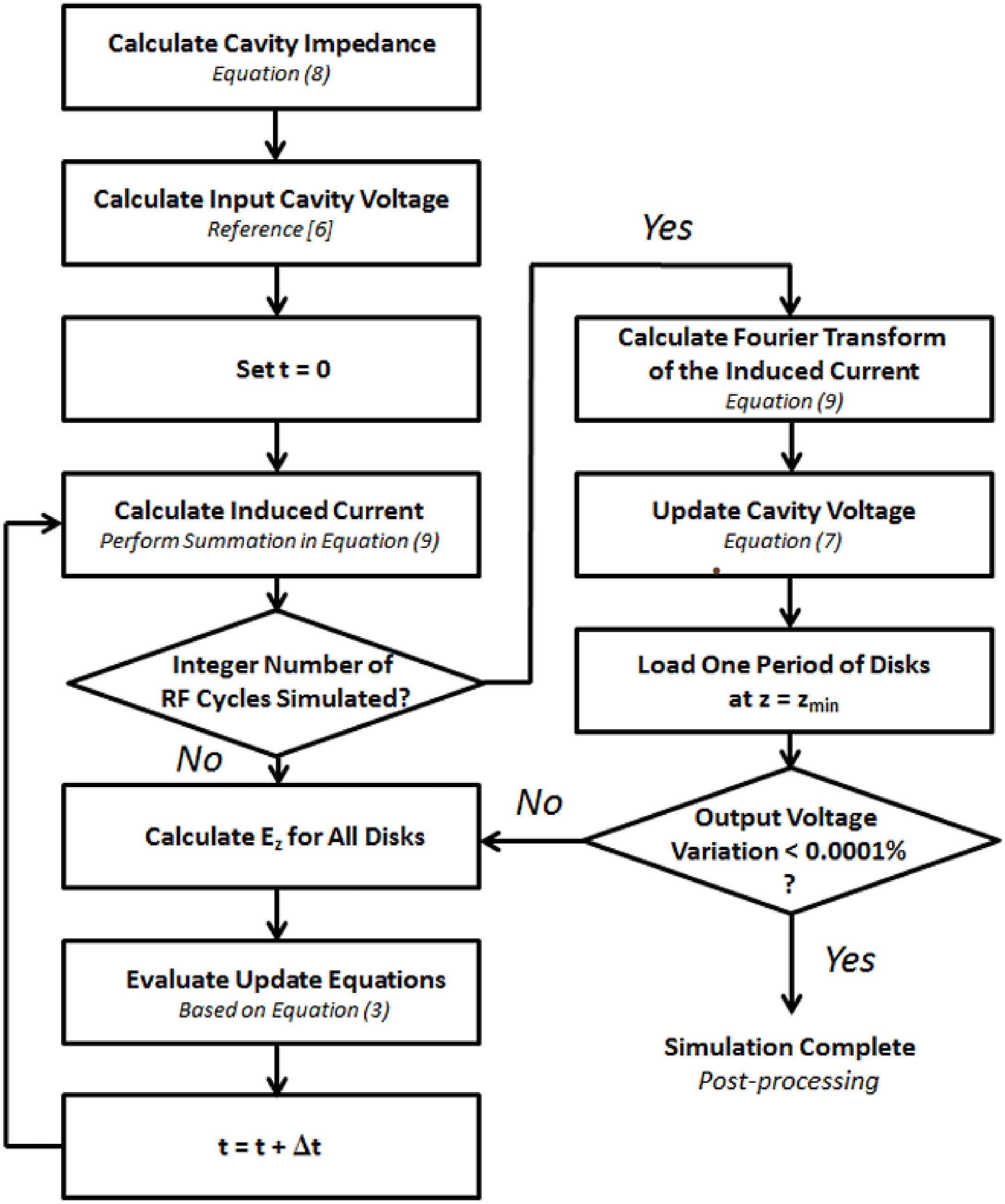

Figure 2.1.6: Simplified AJDisk Algorithm
[31]

2.1.10 KlyC

Recently developed at CERN, the klystron code, denoted as KlyC1D/1.5D, aimed to address a critical need by bridging the gap between fast yet approximate 1D models and the time- and resource-intensive Particle-in-Cell (PIC) codes. The nomenclature "1D/1.5D" is aptly chosen to reflect the code's versatility, allowing it to seamlessly transition between a one-dimensional (1D) and a quasi-two-dimensional (1.5D) representation of the electric field. It's noteworthy that, despite the option for a 2D electric field map, the particle motion within the KlyC code remains confined to one dimension. Just like AJdisk as described above the KlyC/1-D model models charged particles as disks. In the KlyC/1.5-D model, an analogous representation is achieved by utilising a set of rings with varying radii, forming an array of charged particles at the emission plane. These rings are evenly spaced radially with each maintaining an identical charge density. Consequently, for a given beam radius, the current within each ring is contingent upon both the number of rings and their radial positions. As these rings propagate along the tube, they steadfastly retain their radial positions.

2.1.11 Magic 2D

MAGIC is an electromagnetic particle-in-cell code, more commonly referred to as a PIC code, employs a finite-difference, time-domain (FDTD) approach to simulate processes in plasma physics. This encompasses interactions between space charge and electromagnetic fields. Commencing from a predefined initial state, the code dynamically models the evolution of a physical process over time. The comprehensive set of Maxwell's time-dependent equations is diligently solved to derive electromagnetic fields. Simultaneously, the complete Lorentz force equation is tackled to ascertain relativistic particle trajectories, while the continuity equation is addressed to furnish current and charge densities essential for Maxwell's equations.

This methodology, commonly known as electromagnetic particle-in-cell (PIC), ensures self-consistency by intricately capturing the interactions between charged particles and electromagnetic fields. Furthermore, the code incorporates robust algorithms designed to represent complex structures, material properties, incoming and outgoing waves, particle emission processes, and more. Consequently, the versatility of the code extends its applicability to a wide array of challenges within the realm of plasma physics.

Chapter 3

Evolution of the 1GHz F Tube

3.1 Introduction

Originally proposed by E. L. Lien in 1970 [32], it was shown that by using a cavity resonating at the second harmonic in a low microperveance klystron, higher efficiencies could be obtained. Lien was able to demonstrate that with a 5 cavity klystron, replacing the 3rd with a second harmonic cavity that an efficiency of greater than 65% (100kw output power) could be achieved, compared to an efficiency of 54% without the 2nd harmonic cavity. It was discovered that the use of a 2nd harmonic cavity allows for two smaller sub-bunches to form in the electron beam which combine again at the penultimate cavity in the klystron. These sub-bunches lower the space charge forces acting in the core of the bunch and allow for better "collection" of the particles far from the bunch core. Figure 3.1.1 is an Applegate diagram showing the phase evolution of the electrons as they pass through several cavities, with the third cavity being a second harmonic cavity. Initially, the electrons are distributed in phase, with a broad spread of velocities. As the bunches pass through the first and second cavities, they experience velocity modulation due to the RF fields. The electrons are alternately accelerated or decelerated depending on their phase relative to the applied RF field. These alternating phases of acceleration and deceleration are indicated by the red "+" and blue "-" markers, which show where electrons are gaining or losing velocity as they interact with the cavity fields. The third cavity, being a second harmonic cavity operates at twice the frequency of the fundamental mode causing the formation of sub-bunches within the electron beam. This second harmonic interaction is responsible for creating two distinct bunches, shown as the two darker portions in the middle of the diagram. These sub-bunches represent regions where the electron density has increased due to the second harmonic cavity's modulation. After the third cavity and the beam moves toward the fourth cavity, the sub-bunches begin to congregate together and the sub-bunches merge together to form a single bunch. This process continues through to the final cavity, where the phase lines converge even more. By the time the electrons reach the output cavity, they are tightly bunched together, with much less phase spread compared to the earlier stages.

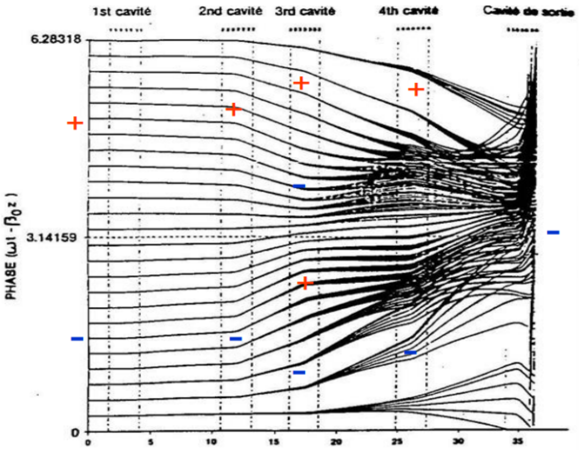

Figure 3.1.1: Phase diagram showing formation of the sub-bunches after 2nd cavity.

These sub-bunches are also highlighted in Figure 3.1.2 which shows a graph of velocity variation (β) of the electron bunch after exiting a second harmonic cavity. The oscillations in β highlight the alternating phases of acceleration and deceleration experienced by the electrons due to the oscillating electric fields in the cavity.

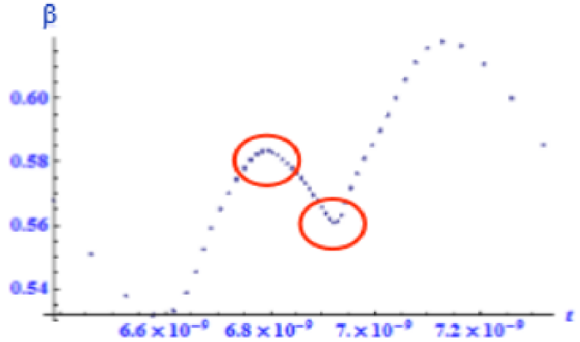

Figure 3.1.2: Graph showing the formation of the sub-bunches with a second harmonic cavity. Normalised velocity vs. time.

To further develop this concept, a third harmonic cavity has been introduced into the model of a six-cavity, 1 GHz klystron (F-Tube), as designed by Chiara Marrelli. The F-Tube incorporates both a second and a third harmonic cavity. With the addition of a second harmonic cavity, the method to increase efficiency became known as the "Core Stabilisation Method." This approach uses the sub-bunching effect created by the harmonic cavities to mitigate space charge forces near the core of the electron beam, while peripheral electrons are collected. Whilst the second harmonic cavity generates two sub-bunches the third harmonic cavity adds a third sub-bunch, further improving the stability of the beam and overall efficiency.

Figure 3.1.3 is a summary of all the main different bunching techniques, and highlights the major visual differences between each. In particular, this figure is a visual representation of the harmonic cavities and the creation of the sub-bunches and the advantage of therein. Whilst the role of the first harmonic fifth cavity is to recombine these sub-bunches along with the peripheral electrons within one RF phase, resulting in a much shorter tube compared to the COM method and much fewer cavities when compared to BAC method. The reduced size and reduced number of cavities of the CSM klystron translates into lower material costs, as fewer resources are required for construction thus providing a financial incentive. Furthermore, smaller klystrons typically consume less power, resulting in reduced operational costs over their lifespan. Lastly, the compact size of the CSM klystron also enables integration into systems where space is limited.

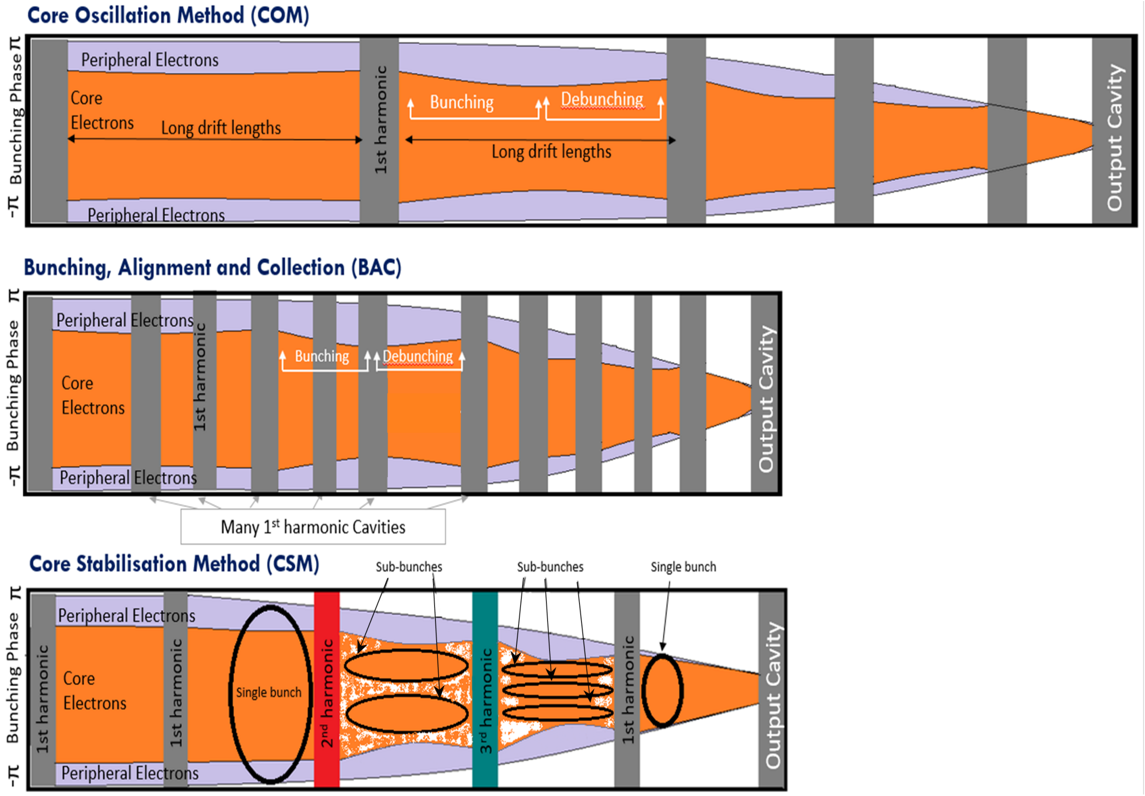

Figure 3.1.3: Diagram showing the differences between the COM, BAC method and CSM method

3.1.1 Initial 1D Simulations

Originally designed and simulated (AJDisk) by C.Marrelli in CERN, Geneva the F-Tube is a third harmonic, 1 GHz, klystron with a beam current of 8.21 A and beam voltage of 115 kV. A low perveance of 0.21 was chosen to ensure an efficiency of greater than 75%, along with a low input power of 97W. The initial optimisation was performed using AJDISK, therefore allowing for a quick investigation on the power or efficiency of a new klystron design. After the initial analysis using AJDISK the tube was further optimised using SUPERFISH and HFSS in order to design real geometric parameters for the cavities which would satisfy the coupling coefficient, R/Q gap length and frequency. These steps were repeated until a final design was reached that satisfied all required parameters. Table 3.1 shows the main final design parameters used in the AJDISK simulation.

Parameter	Value
Operating Frequency	1.0 GHz
Beam Voltage	115 kV
Beam Current	8.21 A
Power In	95 W
Tube Radius	0.009 m
Beam Radius	0.055 m
Total Length of Tube	1.57 m

Table 3.1: Main beam and tube parameters used for the F-Tube.

3.1.4 shows the phase of each disk as a function of its distance in the klystron for the F-Tube. This plot not only showed that the bunching regime for the 2nd and 3rd harmonic cavities, predicted by previous research, was occurring but also that there were signs of bunch core oscillations being formed too.

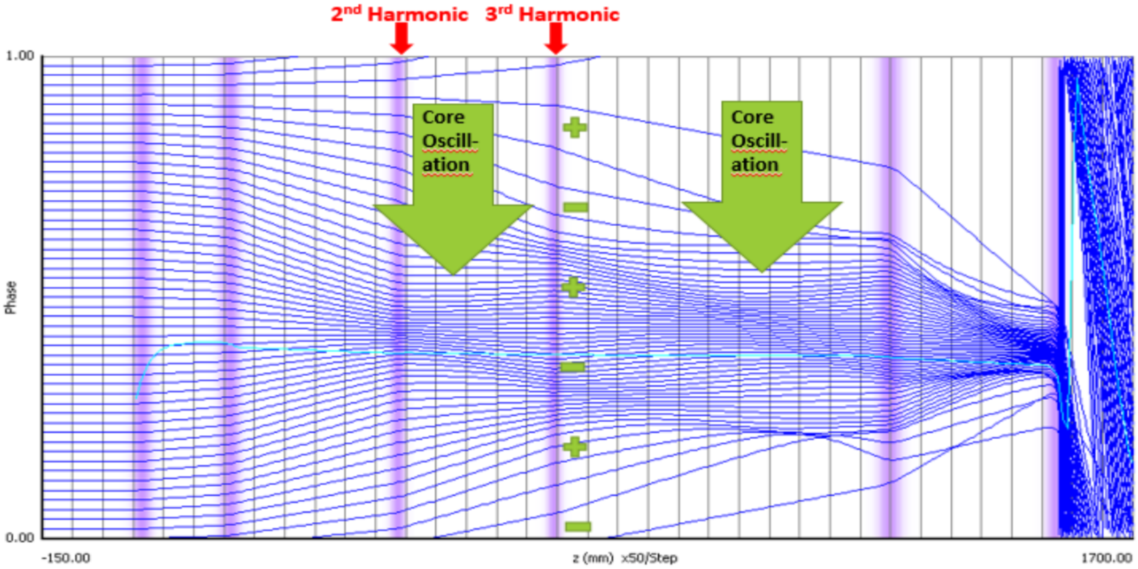

Figure 3.1.4: Normalised phase plot of the F-Tube vs. z (mm). Showing the position of the 2nd and 3rd harmonic cavities and the occurrence of the bunch core oscillation as designed by C. Marrell.

Figure 3.1.5 shows the plot of the harmonic current (I1/I0, blue first harmonic curve and I2/I0, red first harmonic curve) as a function of distance. There was a very high harmonic current recorded at the start of the output cavity, 1.9 A and 1.78 A for the 2 nd induced harmonic current. It can be noted that the 3rd and 4th cavity allowed for a smooth rate of increase in the harmonic current. The predicted efficiency of the F-Tube from AJDISK was 84.11 %, with an output power of 790 kW and a gain of 39 dB. The HFSS cavity design used for the first five cavities of the klystron is shown in Figure 3.1.6.

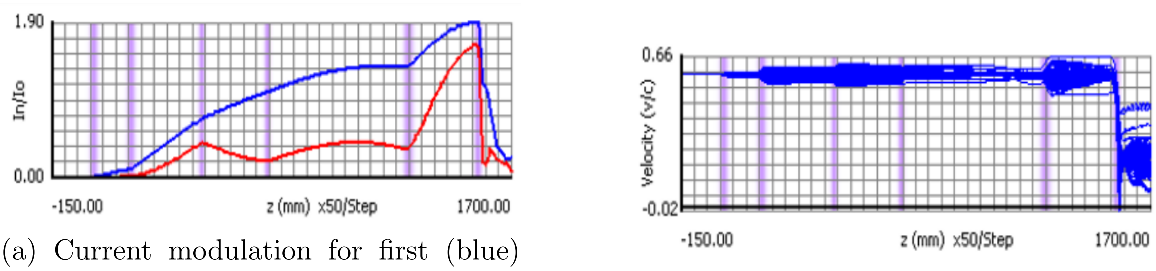

(a) Current modulation for first (blue) and second harmonics (red) as a function of distance.

(b) Velocity distribution plot.

Figure 3.1.5: AJDISK 1D results as designed by C.Marrelli

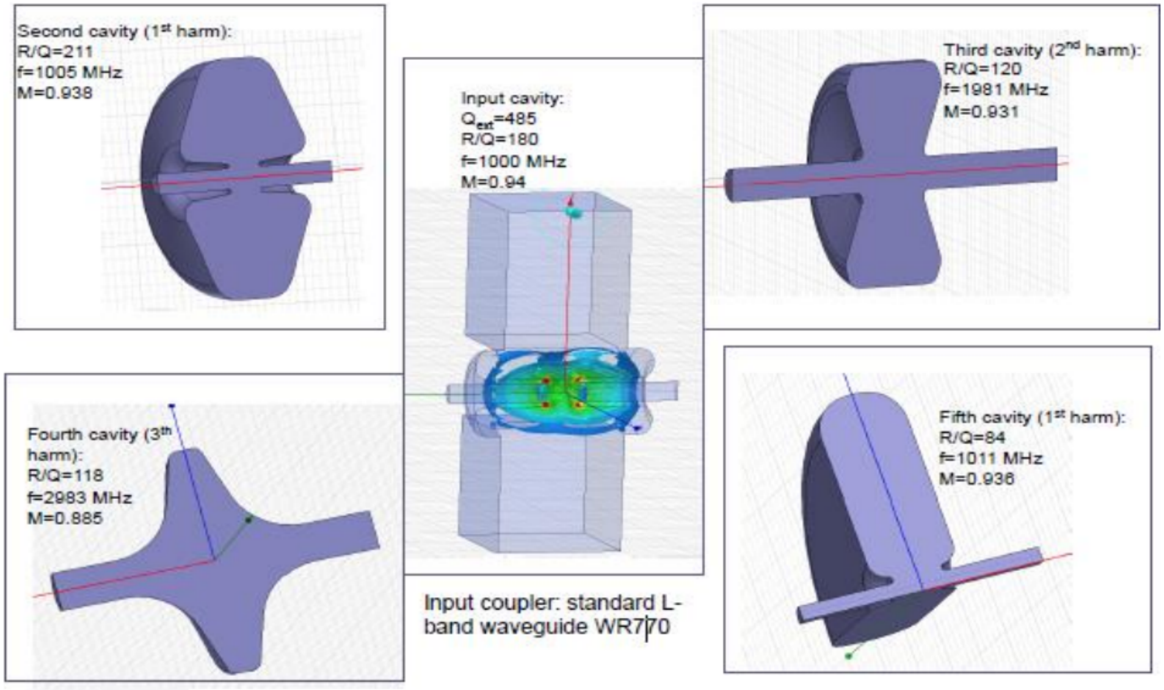

Figure 3.1.6: HFSS cavity design of the first five cavities designed and simulated by C.Marrelli

3.1.2 CST Cavity Simulations

Using a standard re-entrant geometry all cavities were simulated in CST (an electromagnetic simulation software) to measure if the frequencies and R/Qs were similar to the results that were obtained by the given AJDISK simulations. The parameters used from AJDisk are shown in table 2 and SUPERFISH dimensions for each cavity are shown in the appendix.

Table 3.2: AJDisk input parameters

Cavity	R/Q(ohms)	M	Qe	Qo	f(MHz)	z(m)	Harmonic
1	186.181	0.922	618.003	10000	1000.4	0.02	1
2	189.146	0.917	95000	10000	1005	0.17	1
3	67.144	0.816	95000	10000	1990	0.45	2
4	74.666	0.662	95000	10000	2987	0.72	3
5	92.835	0.885	95000	10000	1013	1.29	1
6	202.956	0.93	56.998	10000	1000	1.57	1

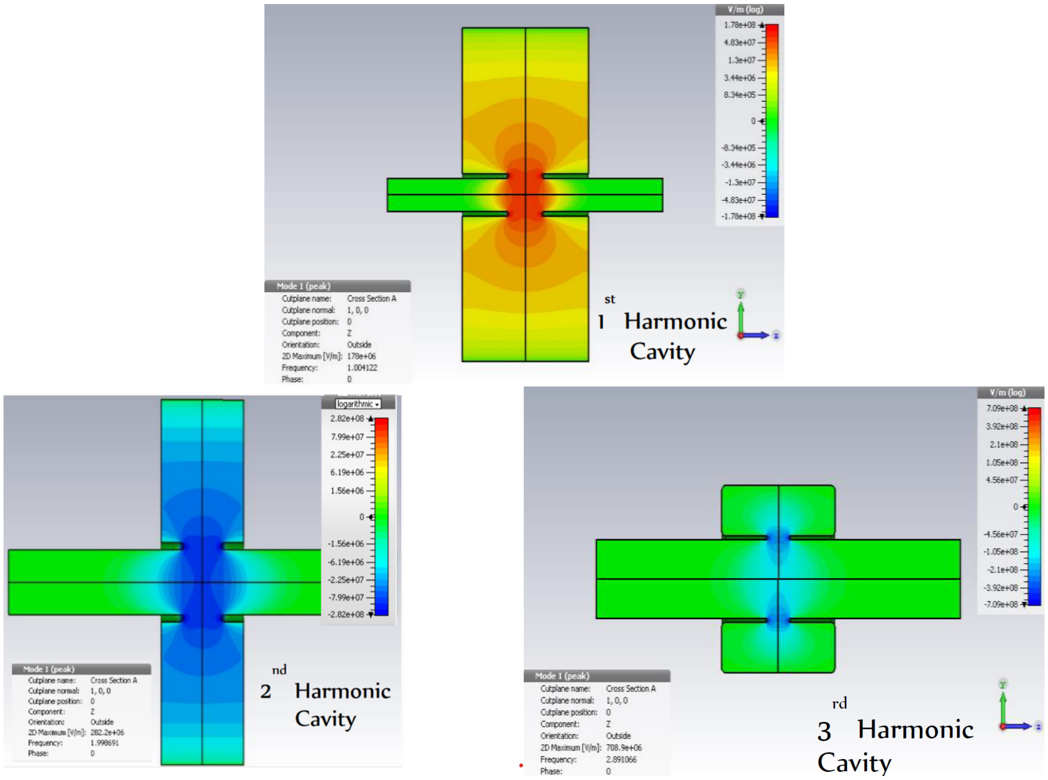

Mode 1 (peak)
Cutplane name: Cross Section A
Cutplane normal: 1, 0, 0
Cutplane position: 0
Component: Z
Orientation: Outside
2D Maximum [V/m]: 178e+06
Frequency: 1.004122
Phase: 0

Mode 1 (peak)
Cutplane name: Cross Section A
Cutplane normal: 1, 0, 0
Cutplane position: 0
Component: Z
Orientation: Outside
2D Maximum [V/m]: 282.2e+06
Frequency: 1.998691
Phase: 0

Mode 1 (peak)
Cutplane name: Cross Section A
Cutplane normal: 1, 0, 0
Cutplane position: 0
Component: Z
Orientation: Outside
2D Maximum [V/m]: 708.9e+06
Frequency: 2.891066
Phase: 0

Figure 3.1.7: CST Geometries

Figure 3.1.7 shows cavities for the 1st, 2nd and 3rd harmonic cavities.

There was good agreement with the CST and AJDisk simulations (frequency and R/Q), confirming that the basic geometries were correct before tuning in Magic.

3.1.3 Magic 2D PIC Simulations

Prior to simulating the F-Tube with all cavities under hot test, several tuning techniques were carried out to ensure correct beam and cavity parameters were used. These included:

1. Initial Tuning (Individual cavity tuning);
2. Fine Tuning (Individual cavity tuning);
3. Frequency Test (Individual cavity tuning); and
4. Hot test (Simulation of all cavities).

3.1.3.1 Initial Tunings

For the initial tuning of the F-Tube klystron two steps were implemented to ensure that the each cavity geometry resonated at the required frequency and R/Q (specified by the AJDISK results). These steps were an eigenmode test and a cold test. The eigenmode simulation was used to compute frequency eigenvalues for each cavity at a given geometry and mesh. Figure 3.1.8 shows the specific geometries that was input for each cavity.

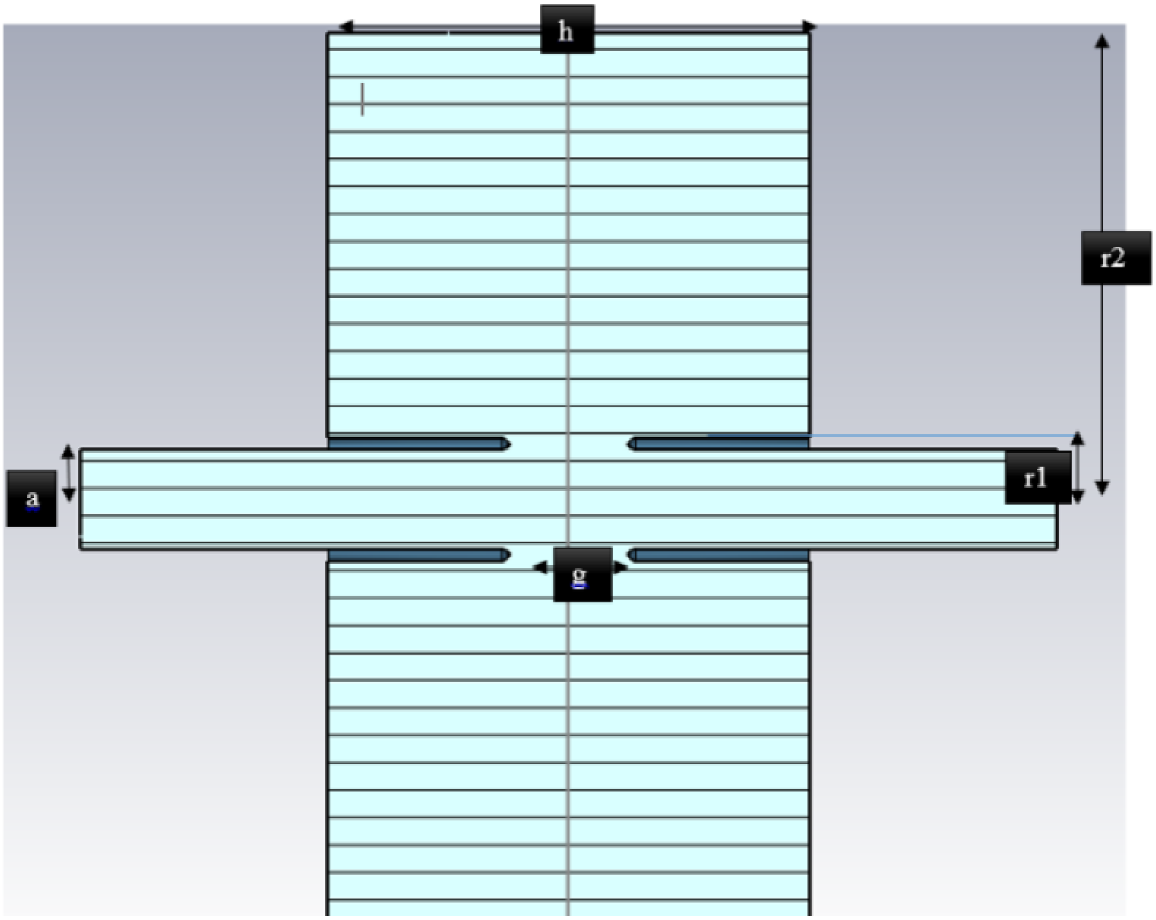

Figure 3.1.8: Input parameters for initial tuning in Magic 2D eigenmode test

Were g = gap length, a = beam tunnel radius, r1 = beam radius plus height of the nose cone, h = cavity radius and r2 = height.

To achieve the correct frequency for each cavity involved an iterative process. The parameters h and r2 were independently changed whilst all other dimensions where kept constant. All frequencies were recorded for a given minimum and maximum and step value (the parameter space) for r2 and h. Once all frequencies are obtained (usually around 225 results per cavity), a cold test was run to get the corresponding R/Qs for each individual cavity. The cold test simulation involved the input of all dimensions (constants and r2 and h) and frequencies from the eigenmode tests. Figure 11. Input parameters for initial tuning in Magic 2D eigenmode test.

Once all the R/Q values were obtained through a systematic sweep of the height and cavity radius, r2 and h respectively (geometry shown Figure in 3.1.8), a contour plot was produced. This plot highlights the region for which the optimum r2 and h can be chosen for a given frequency (indicated by the black line) and R/Q (indicated by the blue dot). Figure 3.1.9 to Figure 3.1.14) features the contour plots for cavities 1 through 6, along with a corresponding table showing the optimum r2 and h values chosen for the required R/Q and frequency along with the measured R/Q and frequency.

Table 3.3: Cavity 1

Parameter	Value	Units
Required R/Q	186.181	Ω
Required f	1.0004	GHz
r2	89.696	mm
h	81.622	mm
Measured R/Q	186.7822	Ω
Measured f	1.0004	GHz

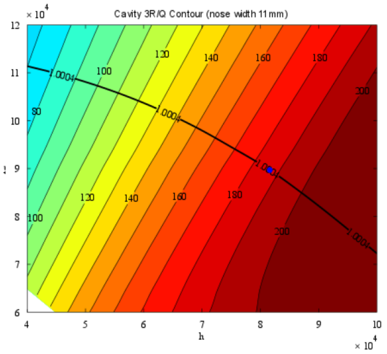

Figure 3.1.9: Cavity 1: R/Q contours plotted against h and r2, including 1.0004 GHz frequency contour line and optimum R/Q (blue dot)

Table 3.4: Cavity 2

Parameter	Value	Units
Required R/Q	189.146	Ω
Required f	1.0005	GHz
r2	87.1566	mm
h	82.436	mm
R/Q	190.0134	Ω
f	1.0005	GHz

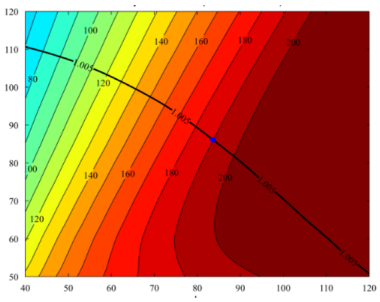

Figure 3.1.10: Cavity 2: R/Q contours plotted against h and r2, including 1.005 GHz frequency contour line and optimum R/Q (blue dot)

Table 3.5: Cavity 3

Parameter	Value	Units
Required R/Q	67.144	Ω
Required f	1.990	GHz
r2	54.994	mm
h	51.5152	mm
R/Q	67.4072	Ω
f	1.990	GHz

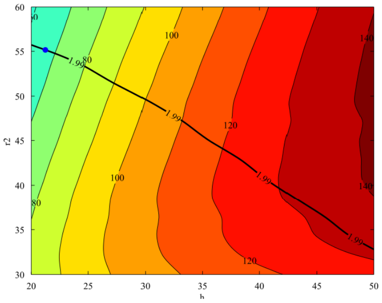

Figure 3.1.11: Cavity 3: R/Q contours plotted against h and r2, including 1.990 GHz frequency contour line and optimum R/Q (blue dot)

Table 3.6: Cavity 4

Parameter	Value	Units
Required R/Q	74.666	Ω
Required f	2.990	GHz
r2	24.7985	mm
h	24.040	mm
R/Q	70.4146	Ω
f	2.990	GHz

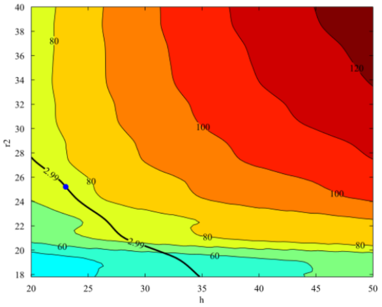

Figure 3.1.12: Cavity 4: R/Q contours plotted against h and r2, including 2.990 GHz frequency contour line and optimum R/Q (blue dot)

Table 3.7: Cavity 5

Parameter	Value	Units
Required R/Q	98.835	Ω
Required f	1.013	GHz
r2	106.206	mm
h	50.909	mm
R/Q	98.284	Ω
f	1.0013	GHz

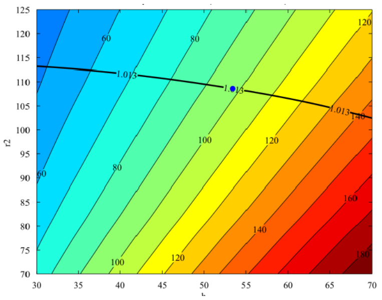

Figure 3.1.13: Cavity 5: R/Q contours plotted against h and r2, including 1.013 GHz frequency contour line and optimum R/Q (blue dot)

Table 3.8: Cavity 6

Parameter	Value	Units
Required R/Q	202.956	Ω
Required f	1.000	GHz
r2	87.235	mm
h	84.848	mm
R/Q	200.3791	Ω
f	1.000	GHz

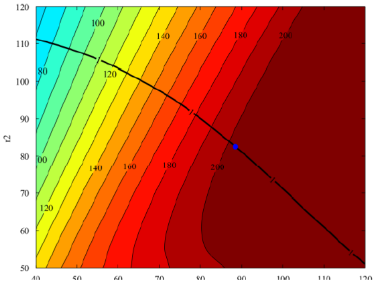

Figure 3.1.14: Cavity 6: R/Q contours plotted against h and r2, including 1.000 GHz frequency contour line and optimum R/Q (blue dot)

From the optimum results chosen you can observe from the frequency that there is no difference between the chosen and required values. However, there is slight differences when comparing the R/Q values. This was expected as the optimal point found is imprecise due to the nature of a colour contour map and the slight variations of R/Q measured at specific geometries.

3.1.3.2 Fine Tunings

Fine tuning each cavity is used to get a more accurate representation of the required frequency and R/Q's without changing the value of r2 and h. This step also involved an iterative process, where by changing the shim and sigma value of each cavity you can further tune the cavity without altering the large geometry scale further. This was required especially for the R/Q's in some cavities as the percentage difference between the measured and required values were as high as 5.5%. The shim command (in MAGIC 2D) is used to add a small, perfectly conducting layer, or shim, to a conformal surface of a perfectly conducting object. By varying the shim you can produce a very fine scale geometric variation on the surface of the conductor, therefore allowing for small changes in the frequency and R/Q. The value of sigma is the electrical conductivity absorbed in each cavity and is controlled by the conductance command. Table 3.9 shows the new values of frequency and R/Q for each cavity after the fine tuning process.

Table 3.9: New values of R/Q and corresponding frequencies after fine tuning

Cavity	New R/Q Value	New Frequency Value
1	186.78	1.0004 GHz
2	189.14	1.005 GHz
3	67.14	1.990 GHz
4	74.67	2.990 GHz
5	92.84	1.013 GHz
6	56.99	1.000 GHz

3.1.3.3 Magic 2D Hot Test Simulations

The hot test simulations were achieved using MAGIC 2D. The main klystron parameters that were input for this simulation is shown in Table 3.10. The main output parameters that were achieved are shown in Table 3.11.

Table 3.10: Input parameters for MAGIC 2D.

Parameter	Value
Operating Frequency	1.0GHz
Beam Voltage	115 kV
Beam Current	8.21 A
Pin	18.25 W
Tube Radius	0.009 m
Beam Radius	0.055 m
Total Length of Tube	1.57 m

Table 3.11: Output Measurements from MAGIC 2D.

Parameter	Value
Output Power	784 kW
Efficiency	79.8 %
Gain	46 dB
Input Cavity Voltage	2.06 kV
Output Cavity Voltage	120 kV

Below (see Figure 3.1.15 shows the graphical results for the output cavity voltage and the FFT for the 2nd and 3rd harmonic cavities. These results importantly show that the tube was stable, as there is no ripple in the output cavity voltage and the frequencies measured show that the cavities are geometrically correct.

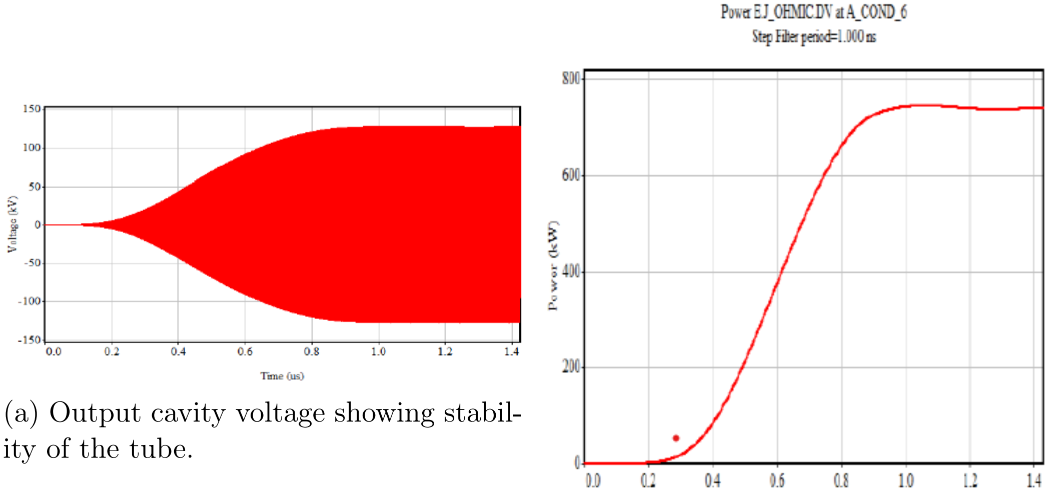

(a) Output cavity voltage showing stability of the tube.

(b) Output power (kW) vs. time (μs

Figure 3.1.15: Output voltage and output power

3.1.3.4 Phase Space Plots

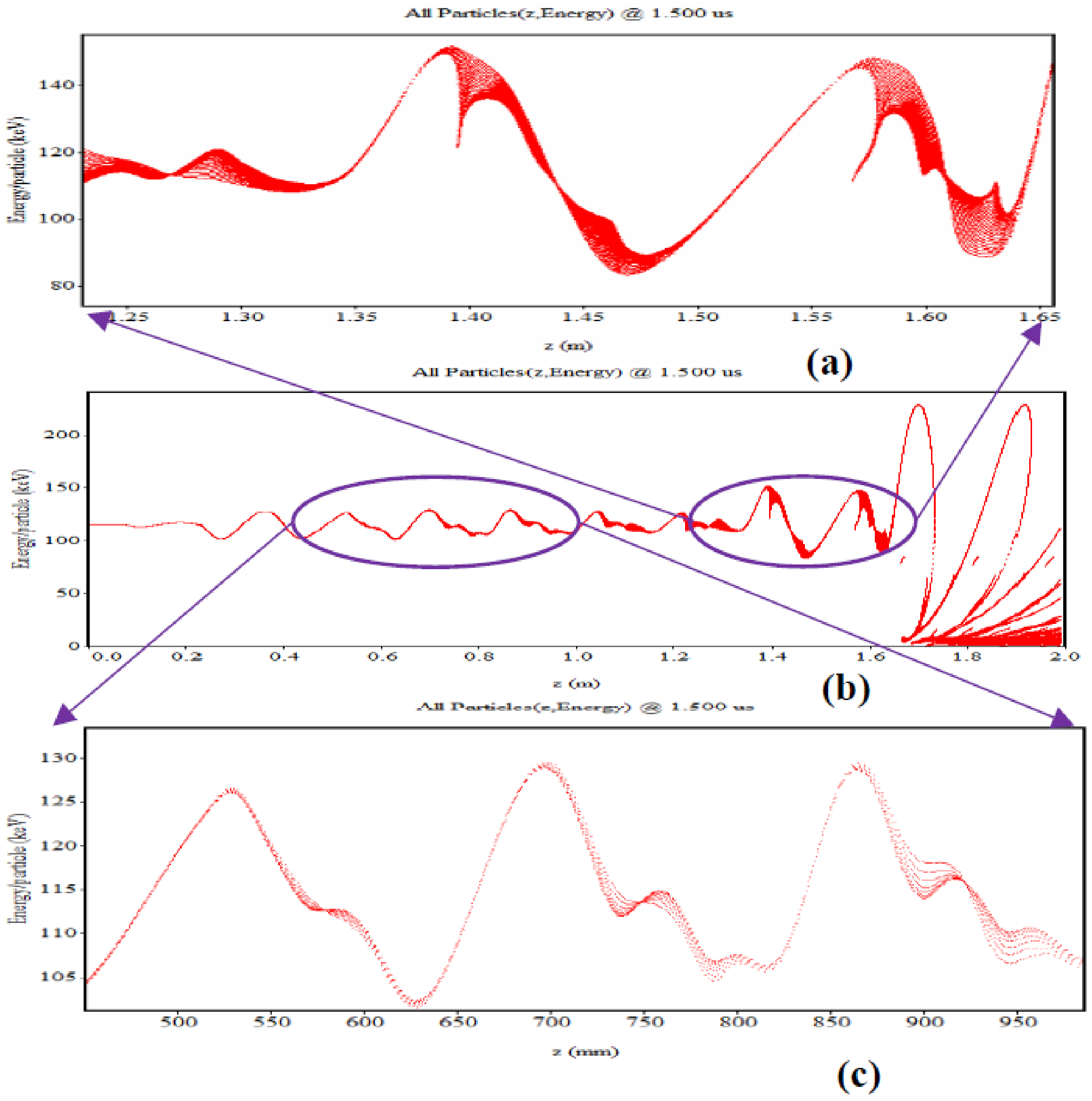

Figure 3.1.16: (a) Zoomed in section of plot (b) showing the particle energy at the 2nd and 3rd harmonic cavities. Showing the formation of the sub-bunches. (b) Shows the energy spread of the particles over the entire F-Tube. (c) Zoomed in section of plot (b) ofthe 5th and 6th cavity showing the sub-bunches merging.

Figure 3.1.16 shows the energy spread of the particles vs. z (m) for the entire length of the tube. Figure 3.1.16 (a) and (b) are zoomed in sections of this phase space plot. It can be seen in both Figures 3.1.16(b) and (c) that as the particles leave the second and third harmonic cavities two subbunches form (for the 2nd harmonic) and three sub bunches form after the 3rd harmonic cavity. As the cavity is resonating at the second harmonic of the drive frequency (of 1 GHz), the harmonic current in the beam is greatly increased. By introducing this non-linear modulation (per RF period) two smaller sub bunches are created. These sub-bunches are caused by the second harmonic field introducing a velocity spread within the initial "uniform" beam. This velocity spread is induced by the natural second harmonic space charge forces in the beam interacting with the second harmonic field. This further leads to space charge forces ultimately being lowered at the centre of the bunch, due to a sparse electron population. Figure 3.1.16(c) clearly shows that a few centimetres after the second harmonic cavity the formation of the sub bunches has occurred. This effect has also occurred at the third harmonic cavity. The harmonic field has induced three sub-bunches within the core bunch. With the space charge forces lowered at the centre, the core of the bunch oscillates reducing the energy spread. This allows for the outside electrons (far from the bunch core) to gradually move towards the core (where space charge forces are lower, with respect to the core), allowing for a "tighter" bunch. This effect can also be seen in Figure 3.1.17 highlighted by the red circles.

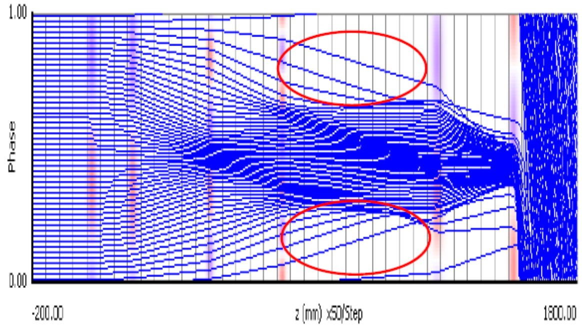

Figure 3.1.17: Applegate diagram highlighting the peripheral electrons circled in red.

At the 5th and 6th cavity these sub-bunches can be seen to have merged to form a single bunch again (Figures 3.1.16(a) and 3.1.17). This is due to the influence of the 1st harmonic field created by the cavities resonating at the drive frequency. The energy spread of the particles has increased due to the velocity spread of the particles being decreased from the harmonic field of the 5th cavity. It can be seen that the shape of the bunch at the entrance of the output cavity has a congregated bunch structure. This structure started forming due to the electrons becoming saturated between the 1st and 2nd cavities and having the same phase velocity allowing for the bunch to be compressed. As the bunch entered the second and third harmonic cavity it began to rotate due to the electrons “seeing” a different electric field (resulting from the sinusoidal nature of the longitudinal electric field) with respect to time. As this rotated bunch enters the output cavity the electrons are decelerated by the gap voltage and arrive with the same velocity, allowing for and extracted power of 746kW (Figure 3.1.15b).

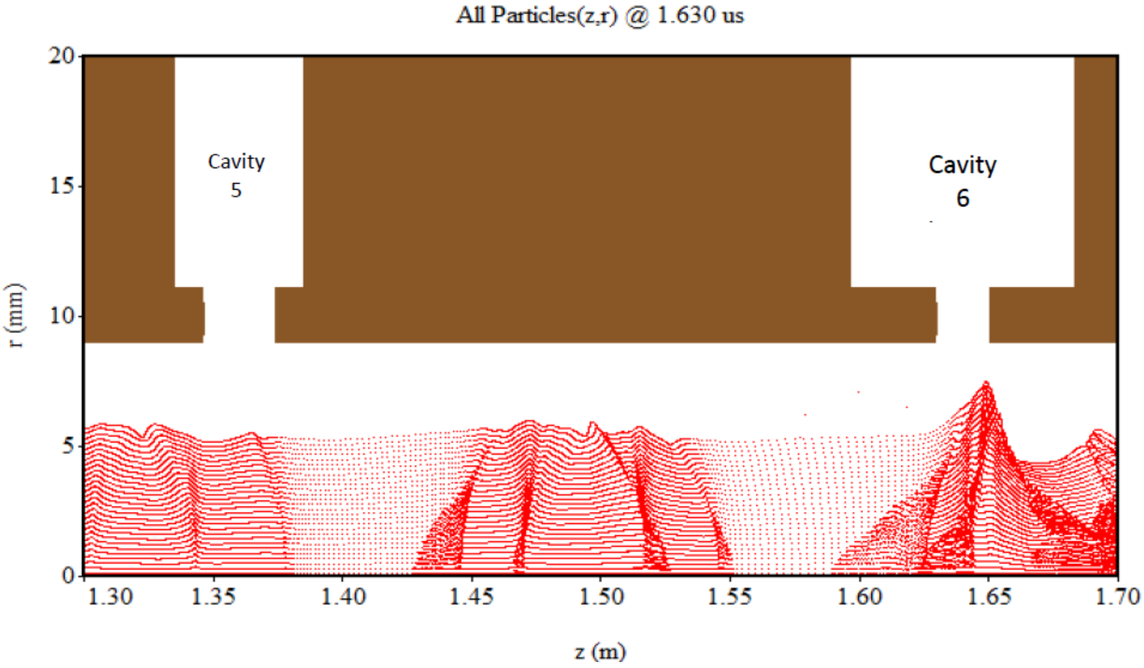

Figure 3.1.18: Phase space plot highlighting a stratified bunch entering the output cavity

Figure 3.1.18 shows the particles leaving the 5th cavity and entering the 6th (output) cavity. It can be seen that there is a "tight" bunch and that the bunch density has increased after the 5th cavity however, there is radial beam stratification (the bunch has a triangular shape). This effect is believed to occur due to the harmonic cavities and the velocity distribution they produce within the sub-bunches. The ideal shape of the bunch (in this phase space form) should be "slab like shape". This shape has less electrons at the pedestal of the bunch and therefore more electrons are giving up their kinetic energy at the same point in time which allows for maximum efficiency. This effect could be minimised by the introduction of a hollow beam rather than using a cylindrical beam. The pedestal effect remains when using a hollow beam however it has been shown to be much less prominent. This stratification can also be seen in Figure 3.1.19. This shows the radial electric field distribution between the fundamental, 2nd and 3rd harmonic cavities, as simulated in CST Microwave Studios and in SUPERFISH. It can be seen from the field maps that the radial distribution becomes increasingly distorted as you move up in harmonics. The field at the first harmonic cavity is consistent in the radial direction but as the relative size of the beam tube increases (with respect to the gap cavity) there is pinching near the middle of the beam tube.

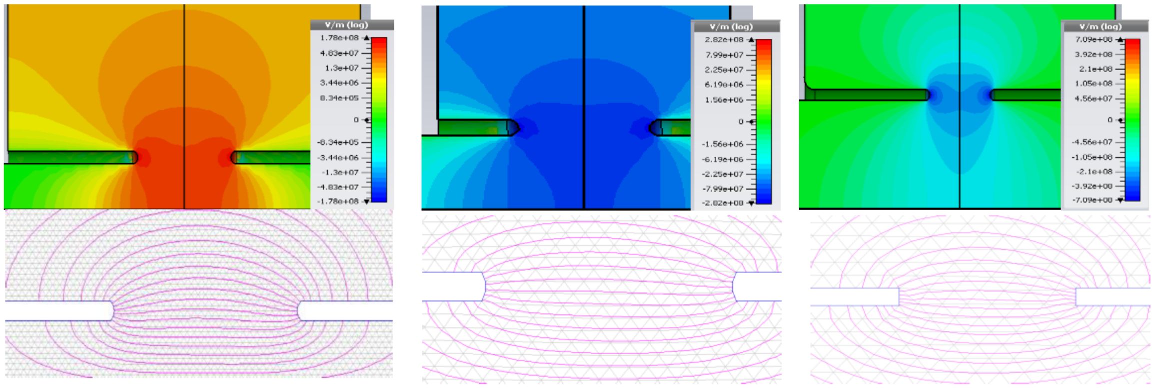

Figure 3.1.19: CST and SUPERFISH simulations of the 1st, 2nd and 3rd harmonic cavities (respectively) showing the radial variation differences between them

3.1.3.5 Output Cavity Analysis - Virtual Cathode Effect

Below shows a trio of graphs showing the particles at the output cavity and their radial position (r) vs. their position in z (m). Figure 3.1.20 shows three time steps, across one RF phase, that particularly emphasises the virtual cathode effect that occurred at this point. It can be seen that a cloud of electrons has built up just after exit gap of the output cavity. This cloud increases and decreases in size over time, that is, it was oscillating with time. This characteristic is known as a virtual cathode. The effect in this instance has occurred due to the electron current from the beam being greater than the space-charge limiting current. This propagating electron beam produced a negative potential because of its own space charge, and when the beam entered the output cavity, the space-charge potential energy increased. At high current levels, the potential barrier produced by the beam space charge exceeded the beam's kinetic energy, and electrons in the beam are reflected back. This current level is called the space-charge limiting current. The potential barrier is called a virtual cathode and is formed at the position where the kinetic energy approaches zero. It was noted from the PIC simulations that with increased output power (>18.25 W) reflected electrons occurred.

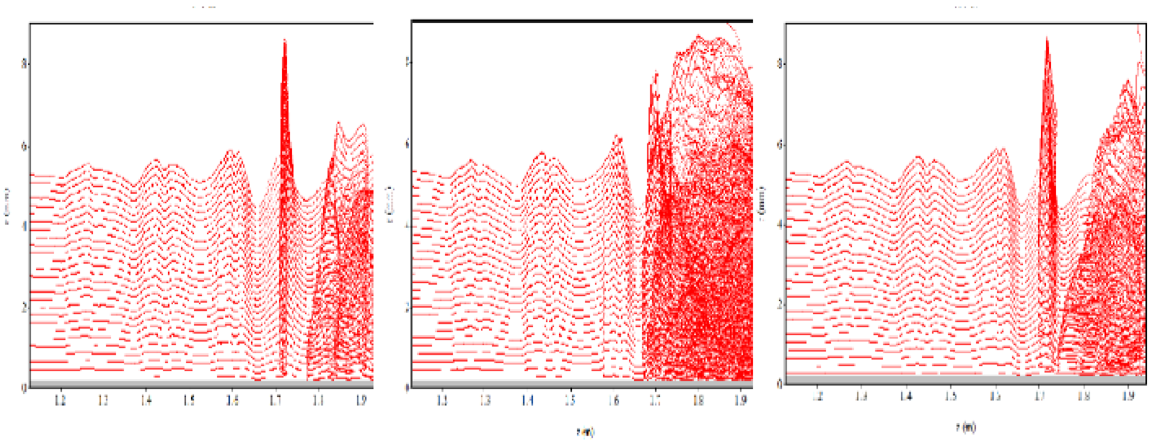

Figure 3.1.20: Phase space plot showing the different phases of the virtual cathode formed at the output cavity.

Figure 3.1.21a shows that as the input power was increased (18.5 W) ripples started to form at the output. These ripples occur as the reflected electrons interfere with the harmonic current of the cavity. If the population of reflected electrons increases it severely decrease the efficiency of a klystron and cause damage to the cathode. Figure 3.1.21b shows the transfer curve of output vs. input power. A transfer curve typically refers to a graph that illustrates the relationship between the input signal and the output signal of the klystron. Specifically, it shows how changes in the input signal, the input power in this case, affects the output signal, the output power. The transfer curve helps to characterise the performance of a klystron and is essential for understanding how best to optimise its operation. To obtain the graph the klystron simulation is run multiple times, with each run the input power is increased and the output is recorded. This is graph also helps to ensure that preceding simulations of the klystron are running at saturation. Figure 3.1.21a highlights the point of saturation when any more increase in input power actually results in a decrease in the output power. In this case the drop in output power was observed at 18.25W. This decrease in the curve after 18.25 W occurs due to the reflected electrons. This again highlights the possible effects of the virtual cathode that occurs after the output cavity. Therefore it is known that the saturation point of this particular klystron was just below 18.25W and any preceding simulations should have an input power of around 18W, to ensure no reflected electrons and maximum output power. It should be noted that all output properties highlighted in the proceeding chapters are given for a klystron that has reached this saturation point, unless otherwise stated.

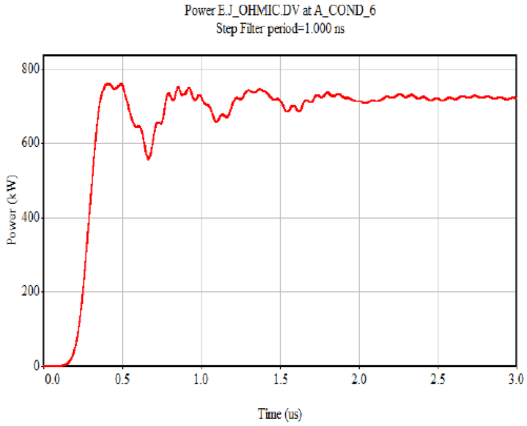

(a) Output power of F-Tube at 18.5 W.

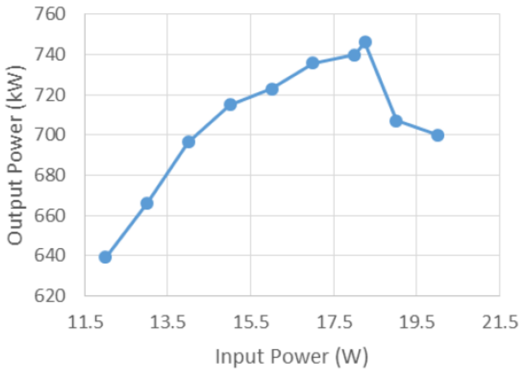

(b) Transfer curve showing all simulated output results vs input power. Also highlighted is the decrease in output power at >18.5W due to reflected electrons.

3.2 Summary

The concept of using harmonic cavities to improve klystron efficiency was initially proposed by E. L. Lien in 1970. By introducing a second harmonic cavity, it was demonstrated that higher efficiencies could be achieved in low perveance klystrons, with a notable increase in output power. The second harmonic cavity creates two sub-bunches in the electron beam, reducing space charge forces near the core and improving particle collection. This approach was further developed in the F-Tube, a six-cavity klystron designed by Chiara Marrelli, which also includes a third harmonic cavity. The combination of second and third harmonic cavities enhances beam stability and efficiency by forming additional sub-bunches. Initial 1D simulations and optimisations using AJDISK, SUPERFISH, and CST confirmed the potential of the F-Tube, with an efficiency of 84.11% and an output power of 790 kW. This chapter demonstrated that harmonic cavities effectively modulate electron velocities, reducing space charge effects and improving klystron performance. Subsequent fine-tuning and hot test simulations in MAGIC 2D refined the design and thus achieved a stable output power with minimal electron reflection.

Chapter 4

Optimisation of the 800 MHz CSM - A Study of Dependencies

From the results of the 1GHz CSM klystron in the previous chapter it was agreed that the core stabilisation method was a method for which high efficiency klystrons could possibly be achieved. The proposed tube had a frequency of 800MHz tube, as required by the FCC (Future Circular Collider) specification, a beam voltage of 133.85KV and beam current of 12.551A corresponding to a perveance (defined in the Child-Langmuir equation) of 0.256 μP. The beam had a radius of 8.63 mm and a tube radius of 15.89 mm giving rise to a fill factor of 0.54. The 1GHz klsytron was scaled using the formula derived from the paper [33]. The tube utilised the core stabilisation method (CSM), and derived the name 800MHz CSM 23, wherein the 23 indicates a second and a third harmonic tube.

Table 4.1 shows the main design parameters used in the KlyC simulation for the six cavity klystron.

Table 4.1: Main beam and tube parameters used for the 800MHz CSM 23 6 cavity klystron.

Parameter	Value
Operating Frequency	800 MHz
Beam Voltage	133.85 kV
Beam Current	12.551 A
Power In	215 W
Tube Radius	0.01589 m
Beam Radius	0.00863 m
Fill Factor	0.54

4.0.1 Gap Coupling Study

Using the above specification the first main design objective is to maximise the efficiency of the tubes using KlyC. The usual method for achieving high efficiency is to fine-tuning the frequencies. However, I conducted a detailed examination of the gap coupling factor (M) and initiated an investigation into its potential impacts. The gap coupling factor, also known as the beam-loading factor, is a parameter that describes the interaction between the electron beam and the RF cavity in a klystron. In a klystron, the electron beam passes through resonant cavities, and the interaction between the beam and the RF fields in these cavities is crucial for the amplification of the RF signal. The gap coupling factor specifically quantifies how much energy is transferred from the electron beam to the RF cavity. It is a dimensionless quantity that represents the efficiency of energy transfer between the beam and the cavity. The gap coupling factor is influenced by the geometry of the resonant cavities (shape of the noses and width of the gap etc.) and the electron beam. Through deliberate manipulation of M, I observed discernible alterations in electron crossovers within the Applegate diagram, see Figure 4.0.1. Specifically, by adjusting M, I identified a direct correlation between its values and the occurrence of electron crossovers. Furthermore, by strategically mitigating the frequency of crossovers consequently enhanced the efficiency values achieved. A high gap coupling factor indicates efficient energy transfer, leading to better RF signal amplification. However, achieving optimal coupling is a delicate balance. If the coupling factor is too high, it can lead to excessive energy transfer and result in the RF fields generated by the beam affecting the beam itself. This can cause variations in the beam velocity and, in turn, impact the overall performance of the klystron.

Figure 4.0.2 shows an optimisation study done to check how the efficiency and stability changed between the two tubes with percentage changes in M across all cavities.

Table 4.2: Original gap coupling factor values (M) for the CSM 23 klystron

Original M's (CSM 23)
0.922
0.970
0.816
0.6620
0.885
0.933

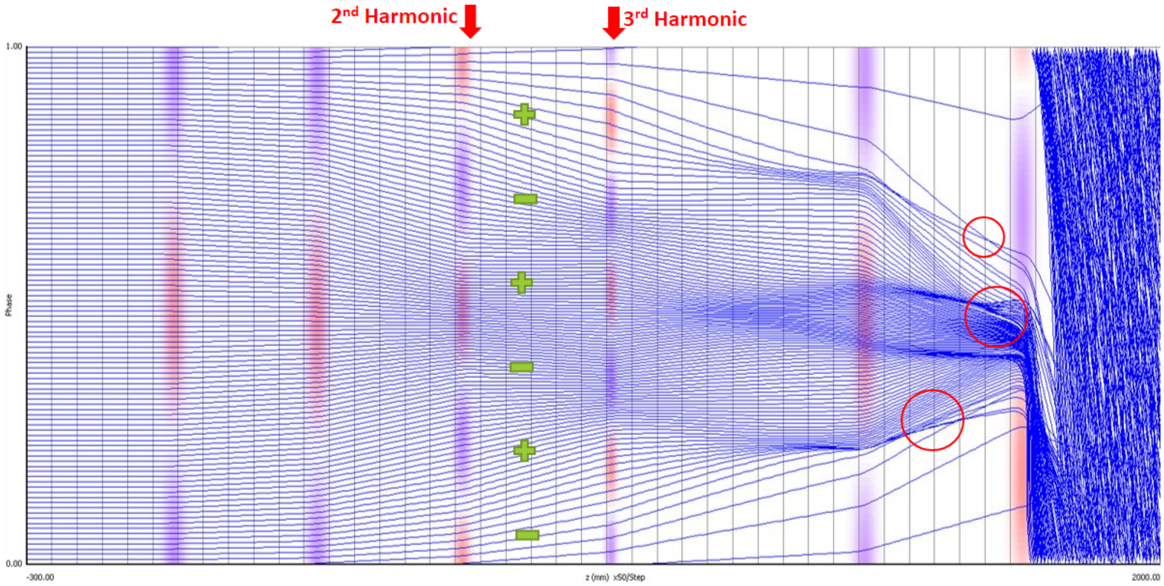

Figure 4.0.1: Example of crossovers before tuning the gap coupling factor in the cavities. The crossovers are highlighted by the red circles and polarities indicated.

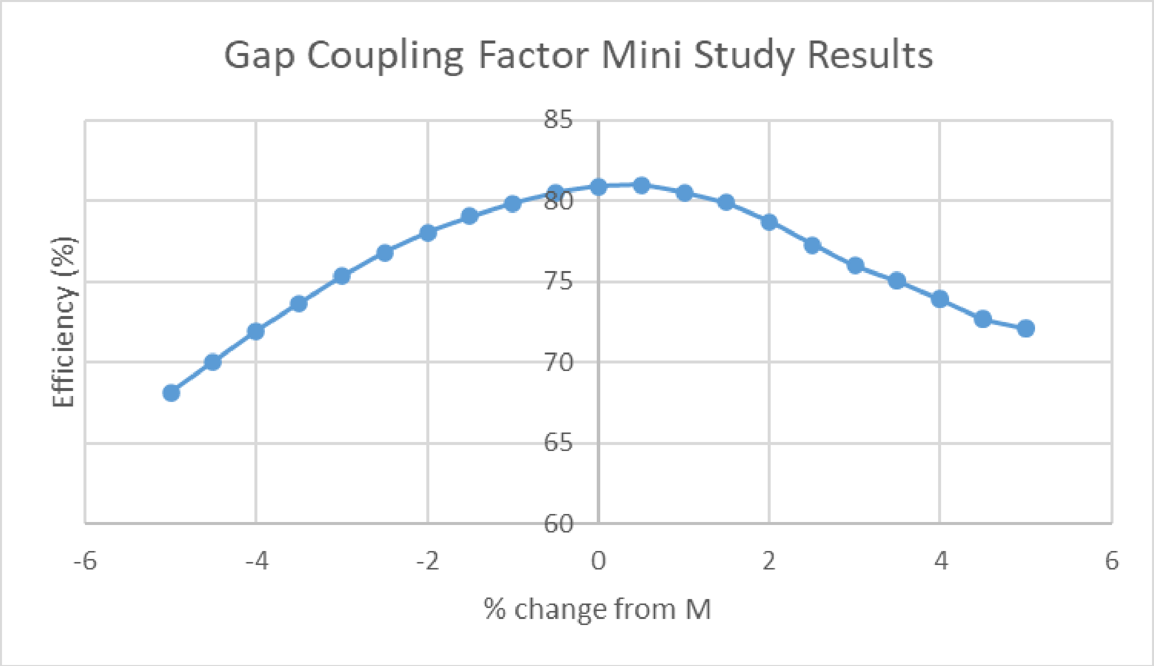

Figure 4.0.2: Efficiency and stability changes between the two tubes with changing M wherein the blue line indicates the CSM 23 800MHz tube

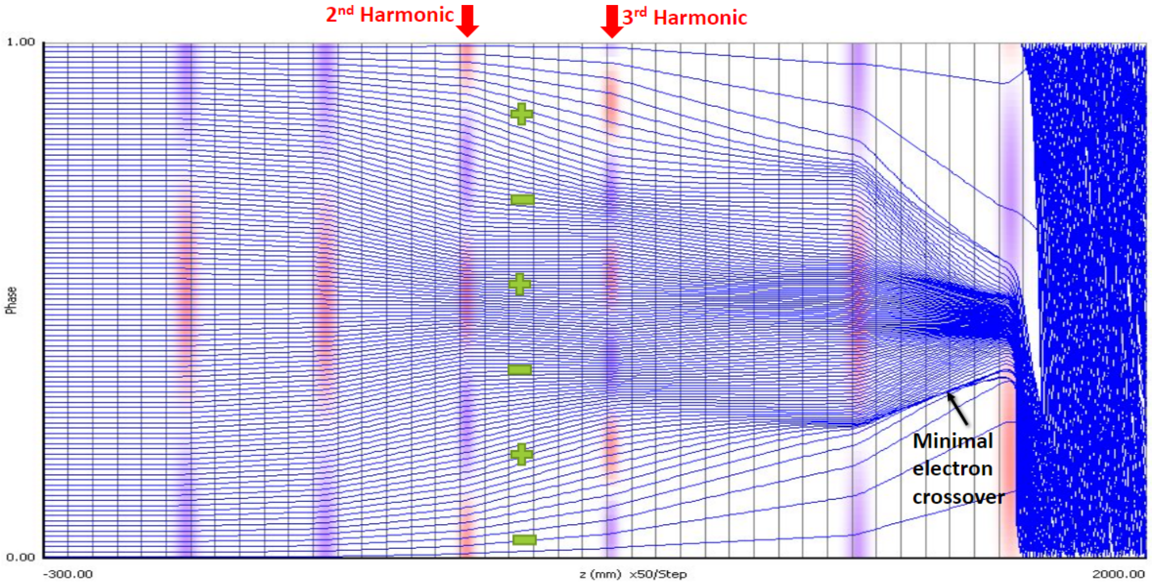

Figure 4.0.3: Applegate diagram of the CSM 23 tube when optimised for minimal electron trajectory crossovers by tuning the gap coupling factor, M

Figure 4.0.1 shows an example of the CSM 23 tube where the gap coupling factors where not optimised and electron crossover has occurred having an efficiency of 78%. This shows an example of where the gap coupling factor could be further optimised whilst, Figure 4.0.3 shows the Applegate diagram when we optimised the gap coupling factor to achieve minimal crossovers. It should be noted that by further increasing the gap coupling factors, a decrease in efficiency does occur as shown in Figure 4.0.2. Contrary, to the other optimisation techniques, high efficiency was not the overall aim for this study. The aim was to create a tube that had a balance between efficiency and stability by minimising the number of electron crossovers per RF phase as shown in the Applegate diagrams.

4.0.2 CSM 23 Optimisation Through a Study of Dependencies

Finally, having optimised the klystron for minimal crossovers, the frequencies were optimised. This not only allowed me to reach a higher efficiency but enabled me to understand the role played by each of the cavities. Therefore, the cavities were detuned to greater level than what would normally occur when shifting frequencies.

Figure 4.0.4 and Tables 4.3 and 4.4 show the parameters, initial results, and the initial frequencies for each cavity from the CSM klystron. This klystron had an initial high efficiency of 78.74%.

Table 4.3: Original Tube Parameters

Operating Frequency (MHz)	**Beam Voltage (KV)**	**Beam Current (A)**	**Beam radius (mm)**	**Tube Radius (mm)**	**Total Length of Tube (m)**
800	133.85	12.551	8.63	15.89	1.58

Table 4.4: CSM Klystron Original Frequencies

Cavity	**1**	**2**	**3** - 2nd Harmonic	**4** - 3rd Harmonic	**5**	**6**
Frequency (MHz)	800.36	804.1	1592.6	2388.5	812.45	799.6

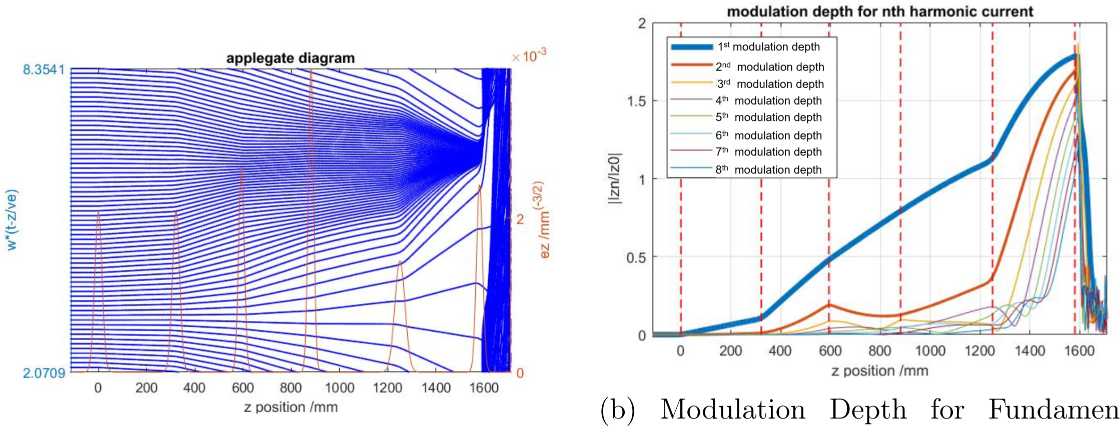

(a) Applegate Diagram

(b) Modulation Depth for Fundamental Harmonics

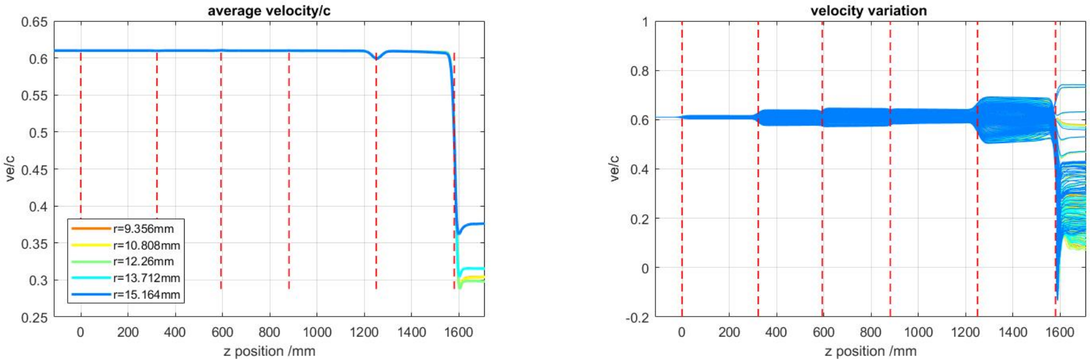

(c) Average Velocity

(d) Velocity Variation

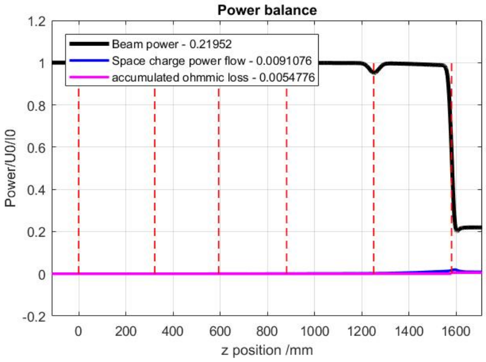

(e) Power Balance

Figure 4.0.4: Original Output Results from CSM Klystron

Using a methodical approach, cavities two through six were individually detuned (from the original frequencies as shown in Table 4.4). Whilst detuning one cavity all other cavities where unaltered and kept at their original frequency. The first approach was to detune each cavity by a maximum of its bandwidth. This produced an insufficient difference to the output results and therefore a larger detuning frequency was required.

Finally, the approach was taken to detune each cavity to a point where the efficiency of the klystron would drop to substantially 70%. This tolerance allowed for an adequate change in the output diagnostics to be noticeable by eye, therefore allowing for a qualitative approach. Every output result was analysed with the aim of determining which element of the beam had been transformed the most with respect to the frequency change. It was crucial to see if this alteration increased in severity as the cavity was detuned further in that direction. It should be noted that during every detune the input power was checked to make sure the klystron was in saturation.

The code used to initially assess the beam profile and output results was KlyC 1/1.5D. This allowed for quicker completion of many simulations compared to a 2D PIC code such as Magic, i.e. a KlyC 1.5D simulation would take approximately 20-25 minutes to converge (whilst calculating over 5 different ring radii of the beam) and a 2D code could take upwards of 20 hours.

4.0.3 Description of Output Results

Table 1.3 gives a description of all the main beam parameter measurements that were taken for each cavity that was detuned. It became quickly apparent that many other parameters that were previously analysed did not provide a consistent result.

Figure's 4.0.5 and 4.0.6 highlight some of the beam parameters: current

(J1) Peak; harmonic amplitude; harmonic current; harmonic spread; position of I_{max}; and the gradient of the knee. The dashed vertical lines show the middle of cavity gap in the beam tunnel.

The ideal for current peak and harmonic amplitude's are to have the peak at the output gap and to be as high as possible.

The absolute peak for I_1/I_0 is 2.0, but a value of of 1.8 is generally accepted as high. The power transferred to the output gap depends on the properties of the gap and the current waveform. Where the DC current is given by equation 4.0.1:

$$I_0 = \frac{1}{2\pi} \int_{\pi}^{-\pi} I(\phi, n) d\phi \tag{4.0.1}$$

and the harmonic currents are 4.0.2:

$$I_m = \frac{1}{2\pi} \int_{\pi}^{-\pi} I(\phi, n) cos(m\phi) d\phi \tag{4.0.2}$$

where m is the harmonic number and n is an integer.

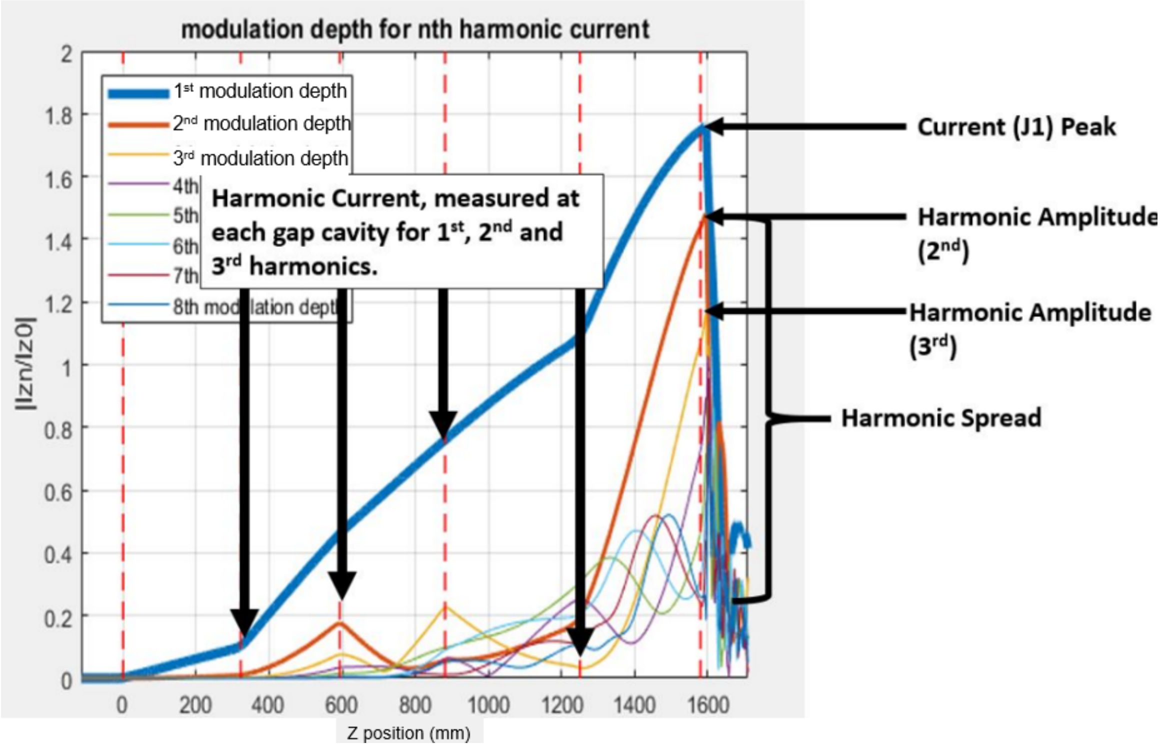

Figure 4.0.5: Graph highlighting current beam parameters such as peak, spread and amplitude

The results that focus on the output of Applegate diagrams are; to analyse the different bunch processes that occur throughout the beam, the density of the bunch at the output and the visibility of sub-bunches or beamlets. Both referring to the spread of the electron trajectories within the bunch. The key output diagram for sub-bunches, bunch length and over/under bunching can be found by analysing an Applegate diagram, illustrated in Figures 4.0.7, 4.0.8 and 4.0.9.

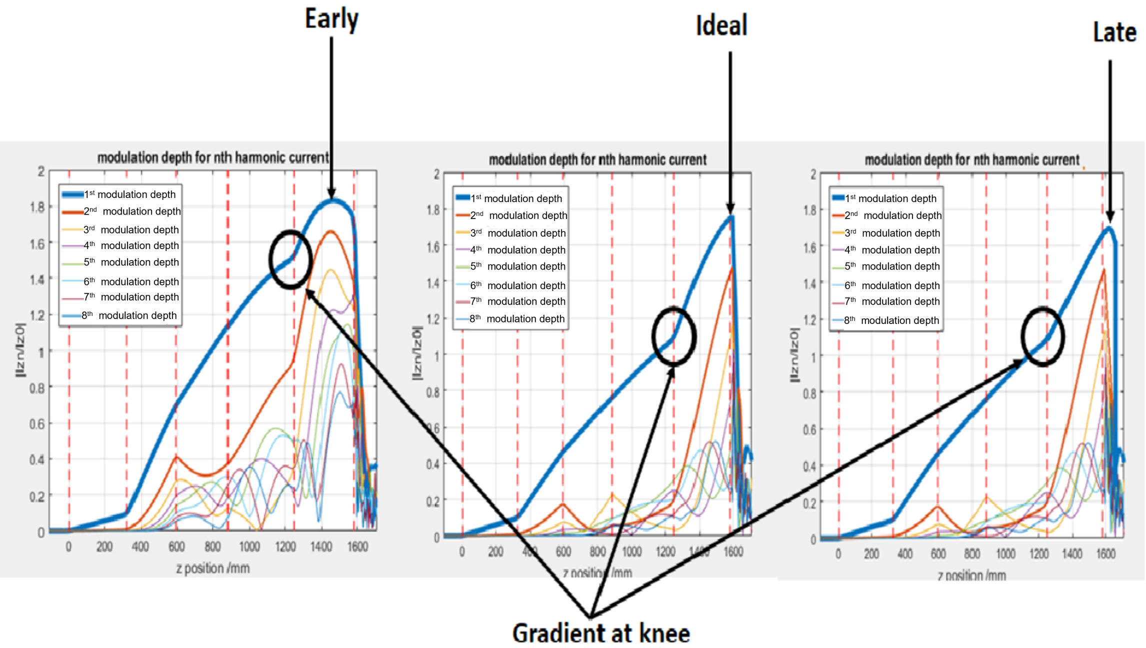

Figure 4.0.6: Graph highlighting movement of I_{max} and the position of the gradient change at the knee

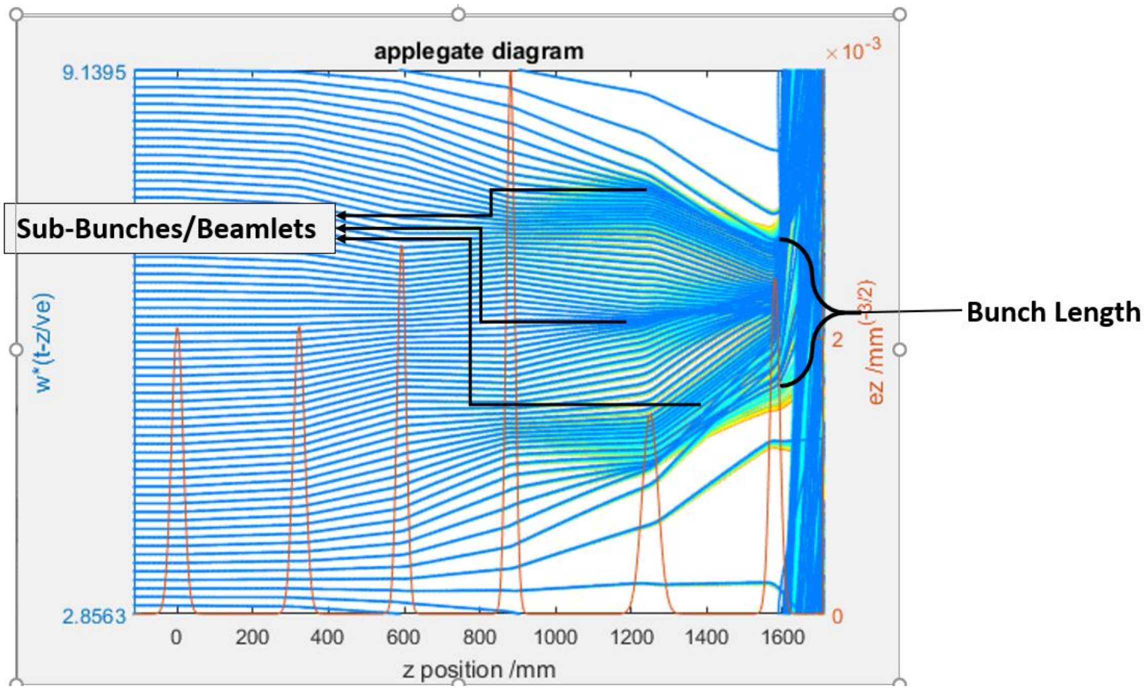

Figure 4.0.7: Applegate diagram highlighting the sub-bunches and the bunch length

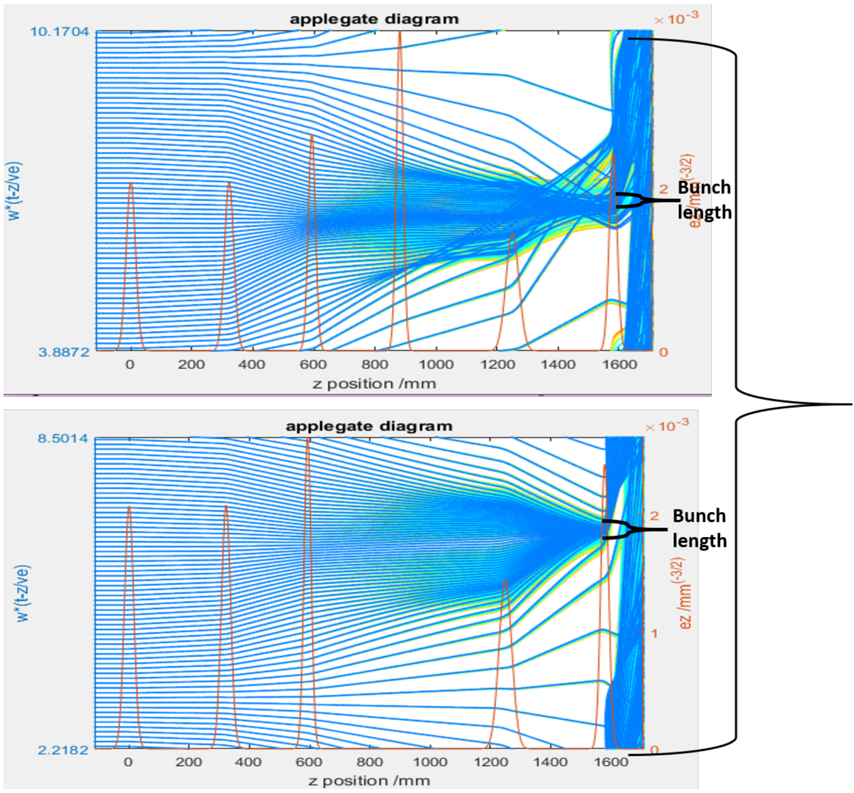

Over-bunched Beams
Top – Overlapping of electrons, visible after cavity 4.
Bottom – Very large velocity change at penultimate gap leading to over bunching

Figure 4.0.8: Applegate diagram's indicting under bunching

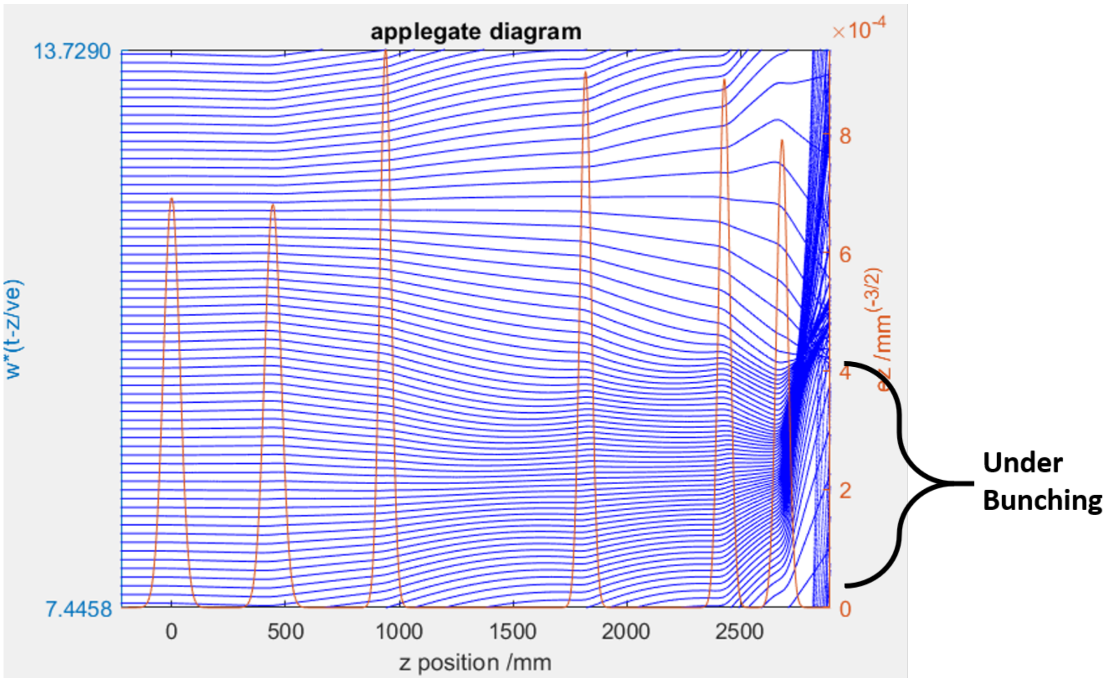

Figure 4.0.9: Applegate diagram's indicting over bunching

4.1 Results

4.1.0.1 Detuned Cavity 2

The key component that cavity 2 affected the most was the position of I_{max}. This component was not affected by any other cavity. Figure's 4.1.1 and 4.1.2 shows the change in position of I_{max} when the frequency is decreased from $f_0 =$ 804.1 MHz at 78.74% to 802.1 MHz at 75.65%, respectively. Also shown are the currents measured at the cavity gaps for the 1st, 2nd and 3rd harmonic currents, the peak values, the currents at specific z (mm) points (in between cavity gaps) and the gradients at these points. From this we can conclude that cavity 2 has a large effect of position of I_{max} for all harmonic currents. With an increase of over 3% in efficiency

Table 4.5: Current parameters of C2 at 802.2 MHz and 75.65% efficiency

Harmonic (H) currents at cavity gaps				Peak harmonic currents		
Cavity	1st H	2nd H	3rd H	H	Current	Z(mm)
C2	0.1006	0.0100	1.082e-3	1st	1.8325	1464.556
C3	0.6945	0.4081	0.2743	2nd	1.6590	1449.372
C4	1.1324	0.3738	0.1233	3rd	1.4464	1449.372
C5	1.5282	0.9639	0.3685	-	-	-
C6	1.6869	1.3487	1.2466	-	-	-

Table 4.6: Gradient of harmonic currents of C2 at 802.2 MHz and 75.65%

Average and Maximum Gradients			Gradients at specific points			
H number	Ave. grad	Max grad	Z(mm)	1st	2nd	3rd
1st	1.75e-5	8.02e-3	737	1.55e-3	1.05e-4	6.88e-4
2nd	1.2e-4	1.74e-3	1065	2.10e-4	1.71e-3	1.47e-3
3rd	1.3e-3	2.98e-2	1415	1.49e-3	1.41e-3	2.52e-3

and a 2 MHz change in frequency this is quiet a sensitive parameter related to this cavity. This equated to a positional change of 0.125m for the 1st harmonic current. This cavity also had an effect on the position of the gradient knee however, however this did not contribute to an increase in efficiency.

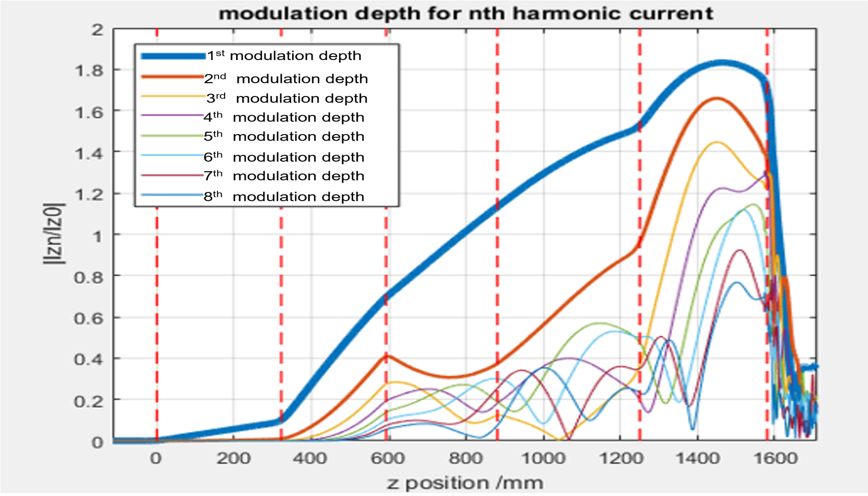

Figure 4.1.1: Current Parameters of C2 at 802.2 MHz at 75.65%

Table 4.7: Current parameters of C2 at 804.1 MHz and 78.74% efficiency

Harmonic (H) currents at cavity gaps				Peak harmonic currents		
Cavity	1st H	2nd H	3rd H	H	Current	Z(mm)
C2	0.1081	0.0113	1.327e-3	1st	1.7948	1589.604
C3	0.4783	0.1888	0.0848	2nd	1.7840	1592.284
C4	0.7912	0.1275	0.0939	3rd	1.8685	1593.177
C5	1.1321	0.3715	0.0505	-	-	-
C6	1.7835	1.6905	1.6001	-	-	-

Table 4.8: Gradient of harmonic currents of C2 at 804.1 MHz and 78.74%

Average and Maximum Gradients			Gradients at specific points			
H number	Ave. grad	Max grad	Z(mm)	1st	2nd	3rd
1st	1.37e-4	6.95e-3	737	1.09e-3	8.86e-4	2.04e-3
2nd	9.50e-5	3.34e-2	1065	2.50e-4	6.20e-4	4.73e-3
3rd	6.18e-5	9.16e-2	1415	4.90-e4	3.60e-5	6.68e-4

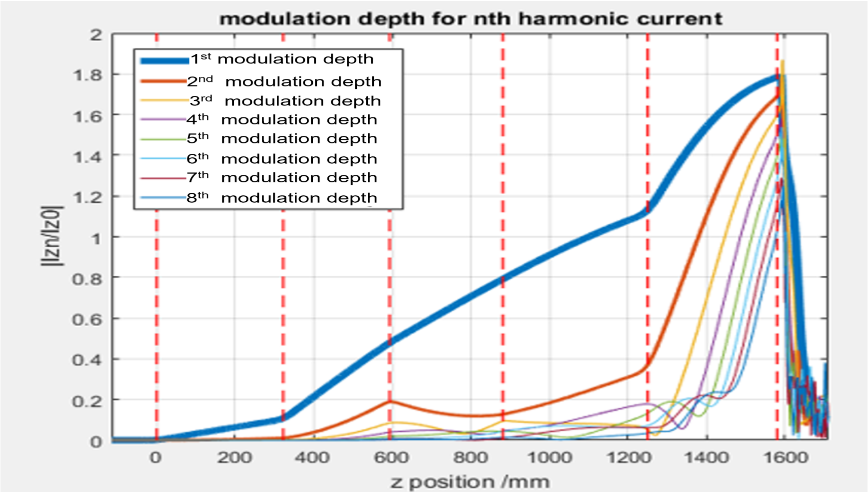

Figure 4.1.2: Current Parameters of C2 at $f_0 = 804.1$ MHz at 78.74%

Another output that was changed by varying the frequency of cavity 2 was the bunch length near the gap output. This can be observed in Figure 4.1.3. One point to consider is the very large increase in input power to reach saturation (110 W to 560 W) when you move from a frequency of 802.1 MHz to 814.1. There is an increase of just over 5% but the decrease in gain would need to be taken into consideration. It is not overly sensitive compared to the change in I_{max}, with an apparent change in the bunch length happening over 12 MHz. Over-bunching at the lower frequency of 802.1 was also noted. This is defined as the overlapping of electrons before the out put cavity. This was also seen in cavity 5. This cavity also had an effect on the position of the gradient knee. Figure 4.1.4 is a comparison of velocity variation along the drift tube for varying cavity 2 frequencies. The graphs show the velocity spread (in terms of v/c) as a function of the z position (in mm). The red dashed lines represent the cavity positions. As the frequency increases from 802.1 MHz to 804.1 MHz, the efficiency improves, indicating a better bunching of electrons. However, as the frequency increases above 804.1 MHz, changes in the spread become minimal.

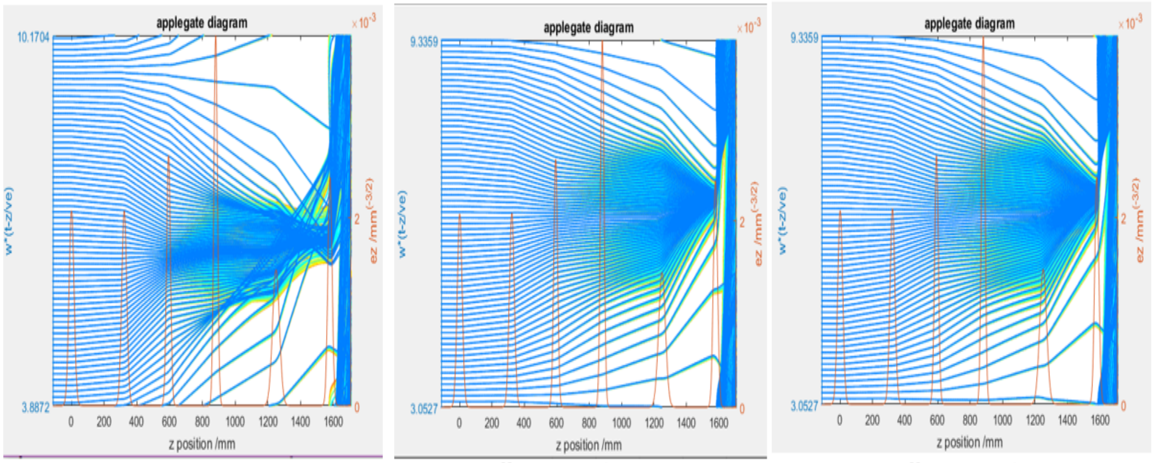

802.1, Eff = 75.65%, Pin = 110
804.1, Eff = 78.74, Pin = 140
806.6, Eff = 79.74, Pin =270

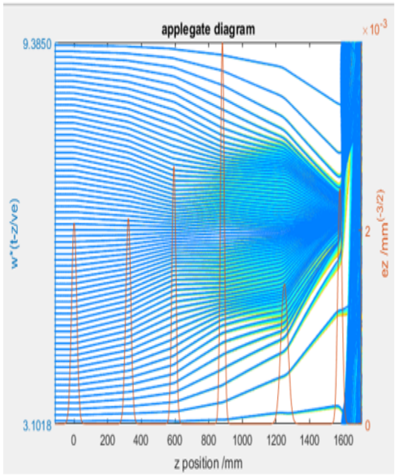

814.1, Eff = 80.49, Pin = 560

Figure 4.1.3: Change in the bunch length from 802.1 MHz to 814.1 MHz

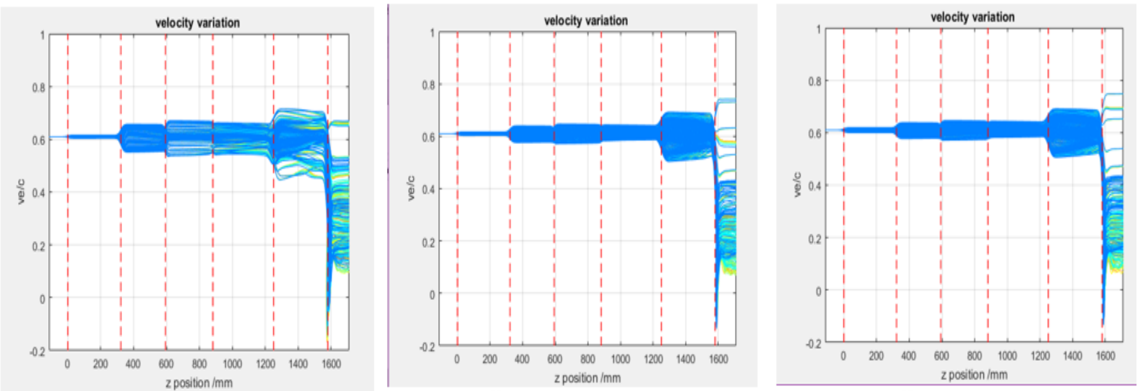

802.1, Eff = 75.65%, Pin = 110

804.1, Eff = 78.74, Pin = 140

806.6, Eff = 79.74, Pin =270

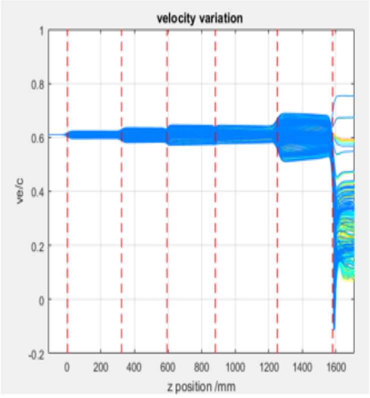

814.1, Eff = 80.49, Pin = 560

Figure 4.1.4: Changes in velocity variation along the tube when changing the frequency of cavity 2 from 802.1 MHz to 814.1 MHz

4.1.1 Cavity 3

The following diagrams are from the detuning process of cavity 3. This was the cavity found to have the most substantial effect on the Applegate when detuned. Figure 4.1.5 shows the evolution of the sub-bunches in an Applegate diagram, the first, third and forth are the detuned cavities, with the second being the original at f_0 = 1592.65. The largest calculated efficiency was 79.61% and this occurred at 1595.65 MHz, 3 Mhz above f_0. All the figures show the trajectories of 64 electrons over one

RF period, from the input cavity to the output. The slopes are an indication of the electrons velocity, with a downward slope indicating an increase in velocity and vice versa, and horizontal lines indicating no change in velocity ($\mu 0$). The sub-bunches are more pronounced due to the harmonic space charge fields of the 2nd harmonic cavity overcoming the harmonic space charge forces. This phasing of the the sub-bunches was almost symmetrical around the middle of the final bunch, as seen in further cavities this was not always the case.

It is also clear that this cavity had an effect on the length of the bunch. With the bunch length increasing as the frequency increased. This parameter was also defined as a high sensitive parameter with a large increase in diameter within a relatively small frequency change.

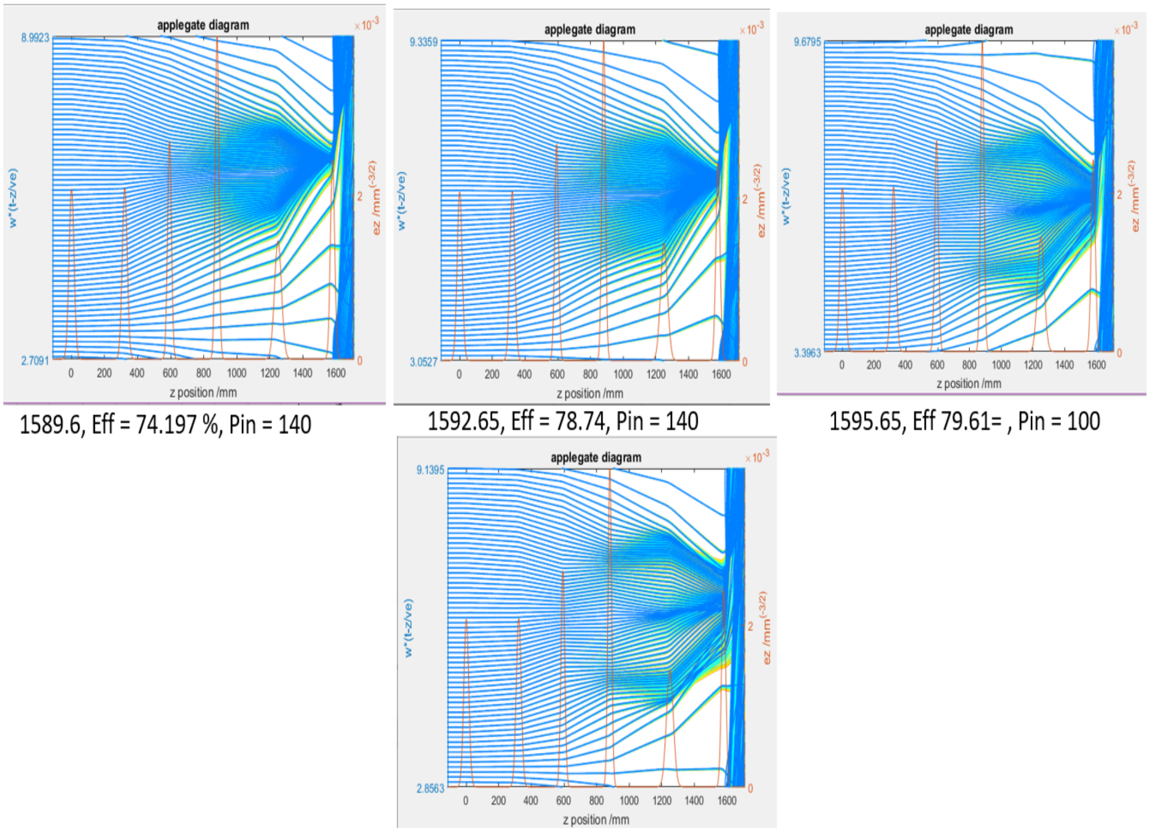

1589.6, Eff = 74.197 %, Pin = 140

1592.65, Eff = 78.74, Pin = 140

1595.65, Eff 79.61= , Pin = 100

1596.7, Eff = 75.19, Pin = 80

Figure 4.1.5: Change in the bunch length from 1589.6 MHz to 1596.7 MHz

4.1.2 Cavity 4

This cavity was the least sensitive, with only one parameter making a minimal effect. This was the currents of the harmonics at key points in z, in particular the the third to the eighth harmonic current. This was considered a "noise" increase, as all the elements increased in amplitude and spread of amplitudes across z. These elements were increased as you increased in frequency from $f_0 = 2380.5$ MHz to 2399.5 MHz, shown in Figures 4.1.6 and 4.1.7 respectively. This is almost 20 MHz difference, allowing for the lack of sensitivity with this cavity.

Table 4.9: Current parameters of C4 at 2380.5 MHz

Harmonic (H) currents at cavity gaps				Peak harmonic currents		
Cavity	1st H	2nd H	3rd H	H	Current	Z(mm)
C2	0.1081	0.0113	1.327e-3	1st	1.7773	1586.031
C3	0.4783	0.1888	0.0848	2nd	1.8039	1589.604
C4	0.7913	0.1250	0.0948	3rd	1.7875	1590.497
C5	1.1389	0.3644	0.1375	-	-	-
C6	1.7825	1.6839	1.5956	-	-	-

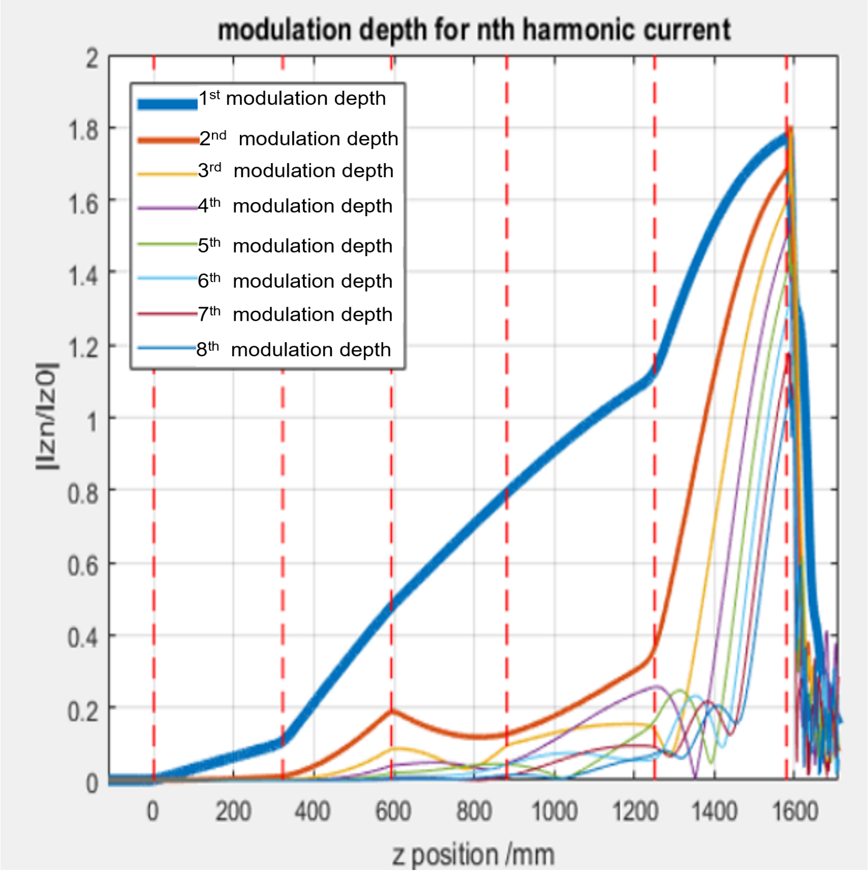

Figure 4.1.6: Cavity 4 harmonic structure at $f_0 = 2380.5$ MHz

Table 4.10: Current parameters of C4 at 2399.5 MHz

Harmonic (H) currents at cavity gaps				Peak harmonic currents		
Cavity	1st H	2nd H	3rd H	H	Current	Z(mm)
C2	0.1081	0.0113	1.327e-3	1st	1.8046	1586.138
C3	0.4783	0.1888	0.0848	2nd	1.7211	1589.604
C4	0.7915	0.1294	0.0895	3rd	1.6691	1590.497
C5	1.1316	0.3818	0.2829	-	-	-
C6	1.8022	1.6479	1.4774	-	-	-

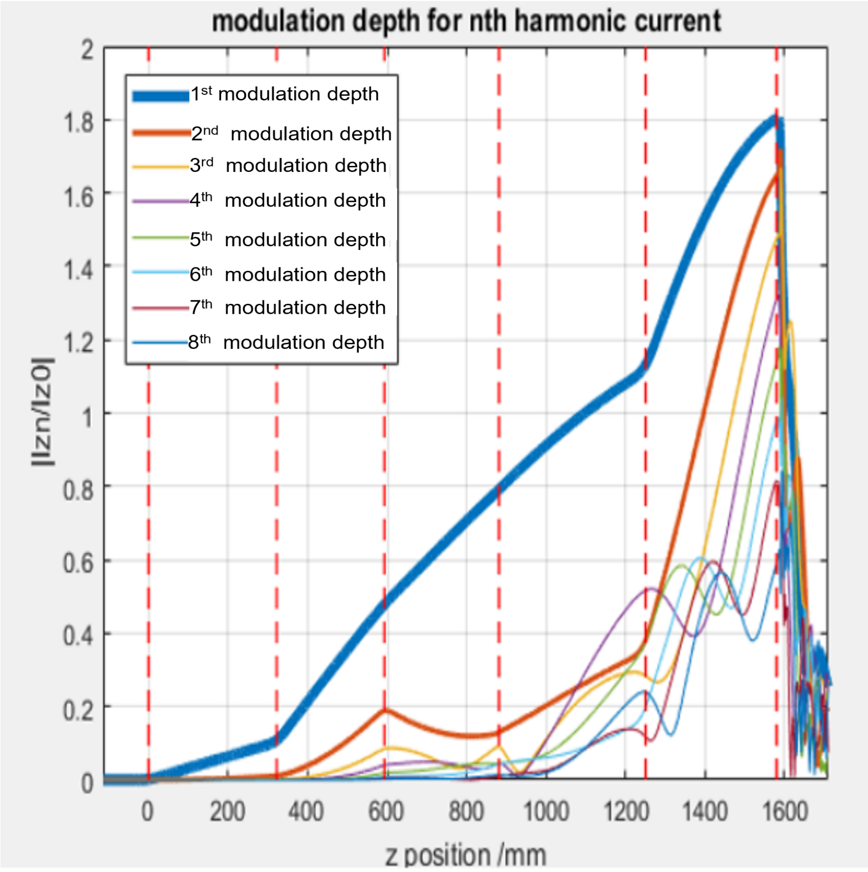

Figure 4.1.7: Cavity 4 harmonic structure at 2399.5 MHz

4.1.3 Cavity 5

The key component that cavity 5 affected the most was the bunch length. This can be ascertained in Figure 4.1.8. As you increase the frequency of cavity 5 from 809.45 MHz to 816.45 MHz you increase the length of the bunch along with enhancing the sub-bunch density. This has shown that having the shortest bunch does not equate to the highest efficiency. Sub-bunches are a benefit to the maximum RF energy to be extracted. This is due to an increased number of electrons that enter the output cavity at the correct phase compared to a shorter bunch with more electrons in the anti-bunch, i.e. these electrons do not contribute to the output power. The sub-bunches or beamlets are spaced evenly throughout the electron beam and are an indication that the space charge forces have been distributed radially within the bunch when the frequency is 818.45 MHz with an efficiency of 82.54% and an input power of 130 Watts. Unlike cavity 2 which also showed a decrease in bunch length the number of beamlets did not change. The cavity is most sensitive between 809.45 MHz and 814.45 MHz, a change of 5 MHz. After 814.47 MHz the change in the bunch width is much smaller, therefore the higher you tune cavity the less of an impact the cavity has on bunch length.

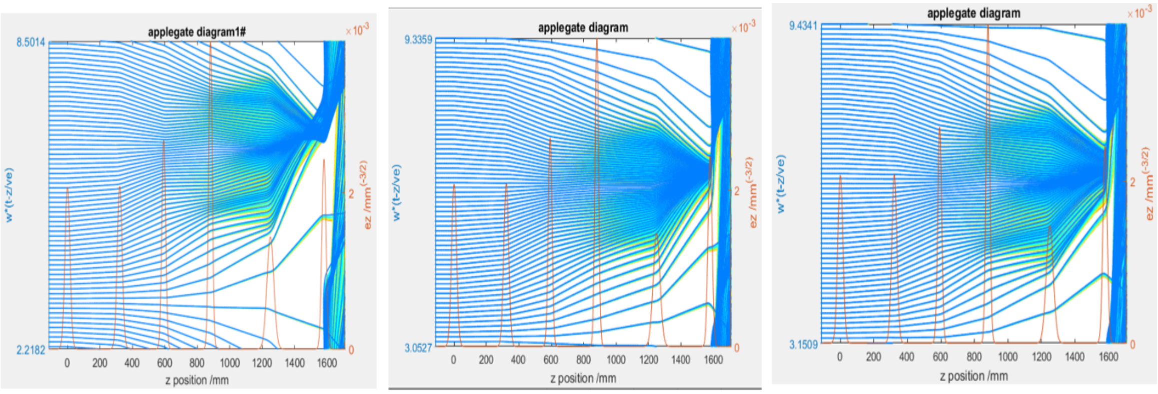

809.45, Eff = 70.53 Pin = 140

812.45, Eff = 78.74, Pin = 140

814.45, Eff = 79.94 Pin = 130

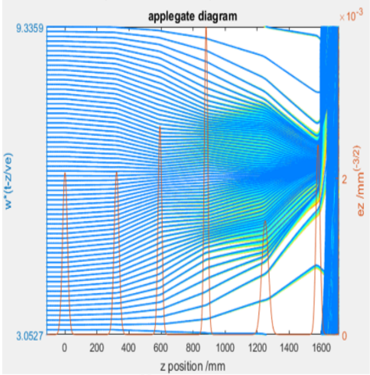

816.45, Eff = 82.27 Pin = 130

Figure 4.1.8: Cavity 5 detuning. Original Frequency = 812.45 MHz at 78.74%. Showing the change in bunch length with an increase in frequency

This cavity also had an impact on the peak values of the harmonic currents. The lower the frequency the higher the peak current from the 2nd to the 8th harmonics. This comparison is shown in Figures 4.1.9 and 4.1.10.

Table 4.11: Current parameters of C2 at 809.45 MHz and 70.53%

Harmonic (H) currents at cavity gaps				Peak harmonic currents		
Cavity	1st H	2nd H	3rd H	H	Current	Z(mm)
C2	0.1081	0.0113	1.325e-3	1st	1.8699	1541.371
C3	0.4790	0.1873	0.0843	2nd	1.7844	1530.653
C4	0.7851	0.0577	0.2454	3rd	1.6787	1526.187
C5	1.1404	0.2416	0.0315	-	-	-
C6	1.7962	1.6989	1.2898	-	-	-

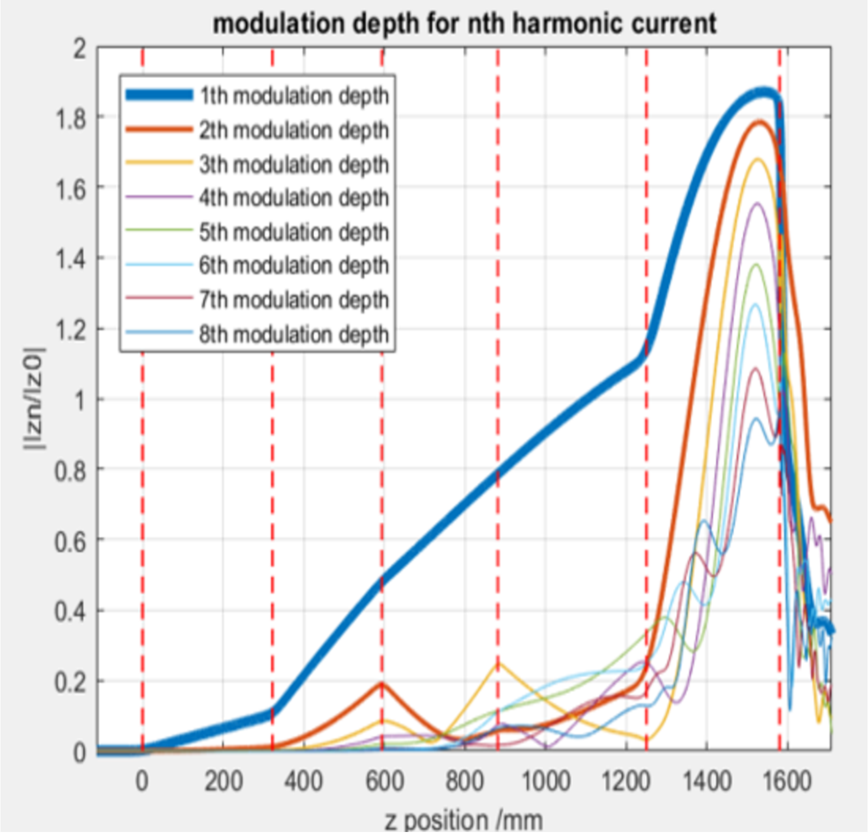

Figure 4.1.9: Higher peak harmonic currents

Table 4.12: Current parameters of C2 at 818.45 MHz and 82.14%

Harmonic (H) currents at cavity gaps				Peak harmonic currents		
Cavity	1st H	2nd H	3rd H	H	Current	Z(mm)
C2	0.1042	0.0105	1.188e-3	1st	1.7619	1594.07
C3	0.4614	0.1739	0.0754	2nd	1.4804	1593.177
C4	0.7599	0.0566	0.2243	3rd	1.1621	1594.07
C5	1.0956	0.1996	0.0333	-	-	-
C6	1.7469	1.4385	1.0699	-	-	-

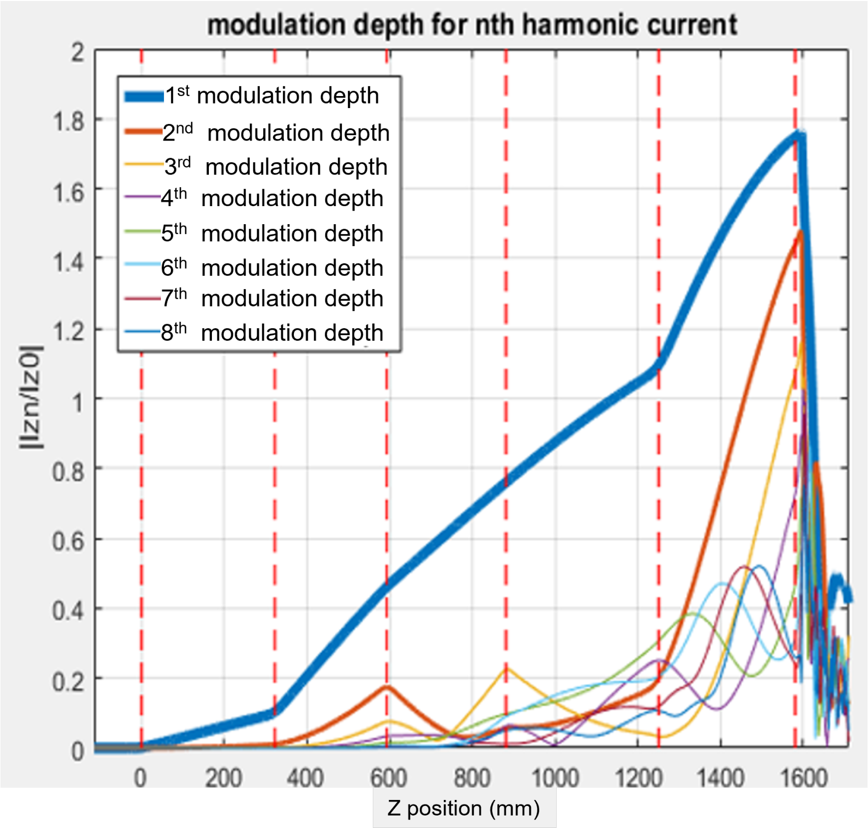

Figure 4.1.10: Lower peak harmonic currents

4.1.4 Cavity Responses

Table 4.13 shows a breakdown of all cavities and how each parameter responds to the detuning of therein.

Table 4.13: Summary of each cavities response to a parameter after detuning

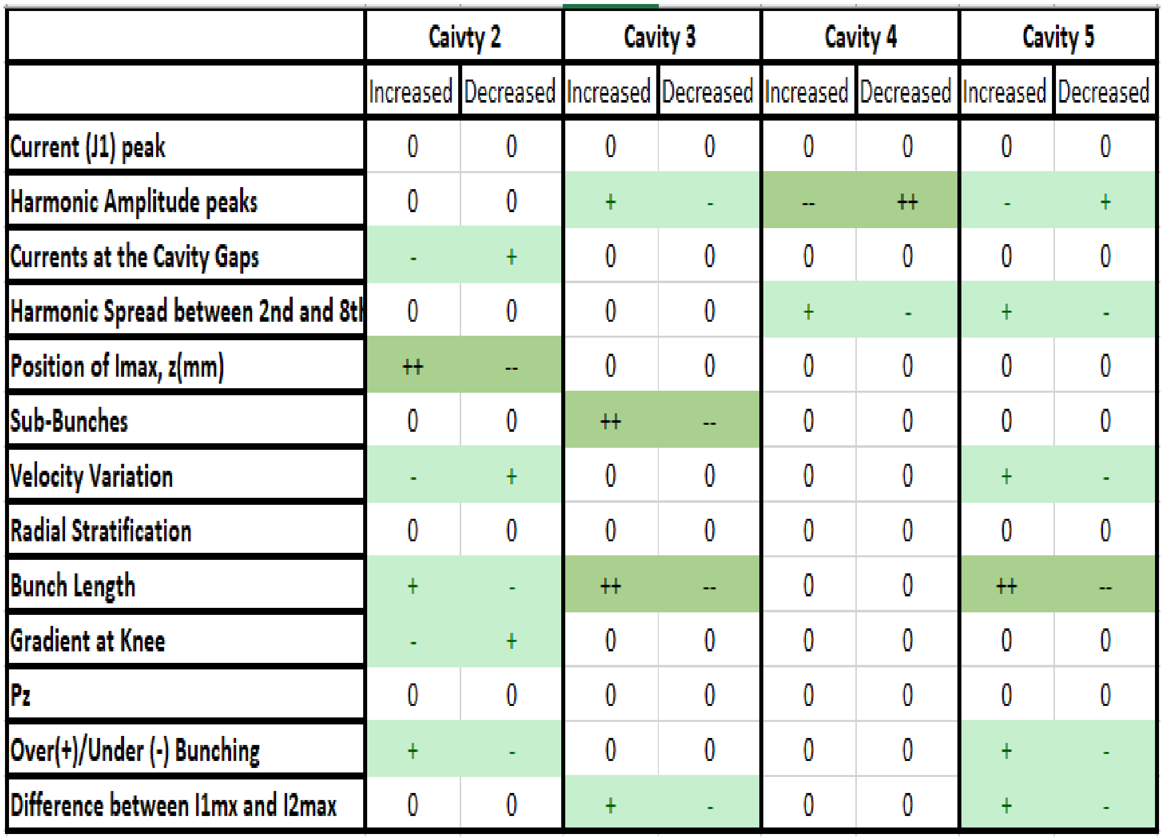

	Caivty 2		Cavity 3		Cavity 4		Cavity 5	
	Increased	Decreased	Increased	Decreased	Increased	Decreased	Increased	Decreased
Current (J1) peak	0	0	0	0	0	0	0	0
Harmonic Amplitude peaks	0	0	+	-	--	++	-	+
Currents at the Cavity Gaps	-	+	0	0	0	0	0	0
Harmonic Spread between 2nd and 8th	0	0	0	0	+	-	+	-
Position of Imax, z(mm)	++	--	0	0	0	0	0	0
Sub-Bunches	0	0	++	--	0	0	0	0
Velocity Variation	-	+	0	0	0	0	+	-
Radial Stratification	0	0	0	0	0	0	0	0
Bunch Length	+	-	++	--	0	0	++	--
Gradient at Knee	-	+	0	0	0	0	0	0
Pz	0	0	0	0	0	0	0	0
Over(+)/Under (-) Bunching	+	-	0	0	0	0	+	-
Difference between I1mx and I2max	0	0	+	-	0	0	+	-

A green box exhibits a parameter that was affected by a cavity, wherein dark green defines the most dominated parameter for said cavity. A + (positive) sign indicates an increased response in a parameter and a - (negative) sign specifies a decreased response, wherein a ++ or a

——

highlighted the largest response for a given interaction. A 0 (zero) indicated that the parameter was either not affected or the response was non-linear. For example, one of the parameters that was not affected by the detuning of cavities was the peak current of J1 max, i.e. the 1st harmonic modulation The cavities were detuned until the efficiency was in between the 70% and 90% threshold, but not below. Due to the relatively high ending efficiency of each cavity, I_{1max} never dropped to a point below 1.6. This affect is worth looking into for efficiencies below 70%.

Another parameter that was not affected by any cavity was stratification. Stratification is a phenomenon seen in many core stabilisation method tubes such as the one above. Figure 4.1.11 and 4.1.12 shows the difference between a tube with stratification and one with minimal stratification. Radial bunch stratification is the radial variation of the RF current modulation depth. In a system with axial symmetry, with respect to the beam centre, the effect is originated by radial variations of the space charge forces and cavities impedance's. This phenomenon was further confirmed with a Pz plot, another parameter showing no changes with each cavity detuning.

Figure 4.1.11: Klystron showing effects of high stratification

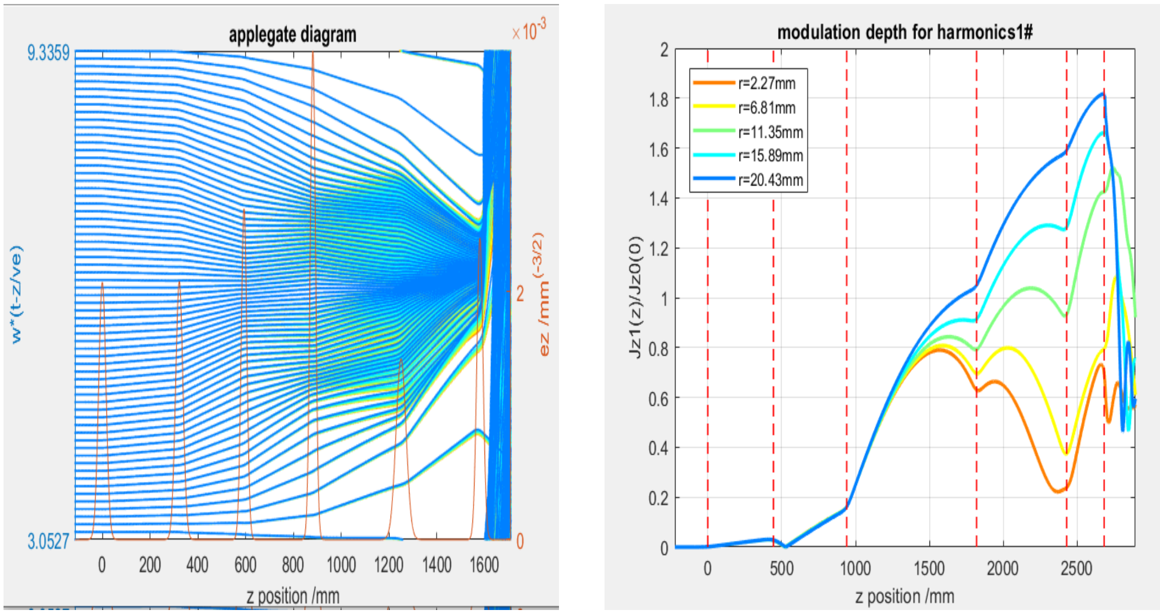

(a) Applegate Diagram showing stratification effects beginning before cavity 4

(b) First harmonic current showing radial modulation depth

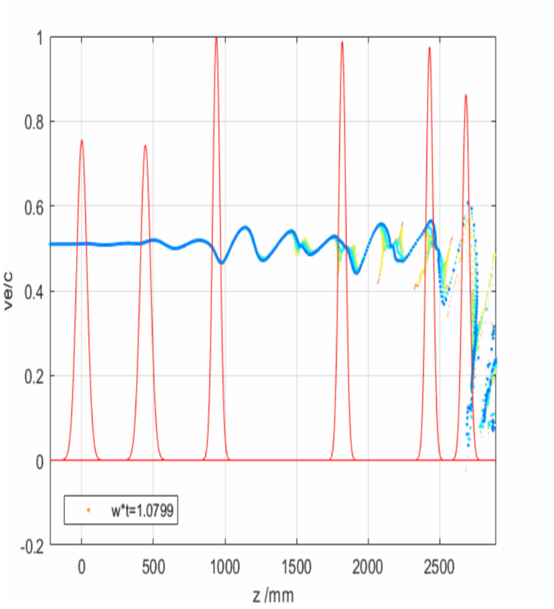

(c) PZ Diagram showing stratification effects before output

Figure 4.1.12: Klystron showing minimal stratification effects

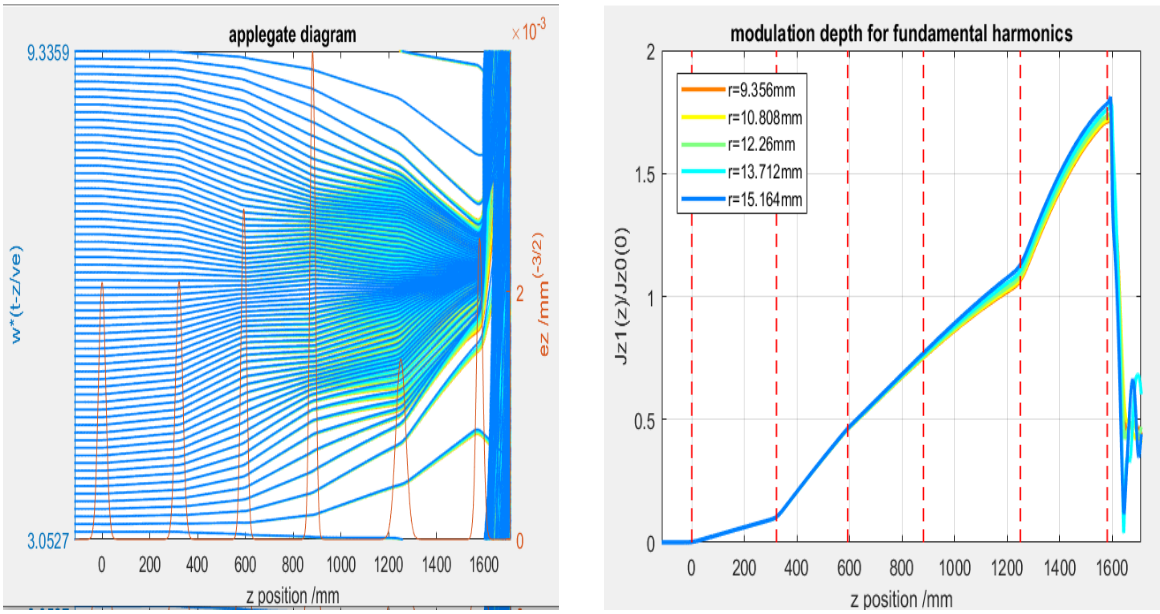

(a) Applegate Diagram

(b) First harmonic current showing radial modulation depth

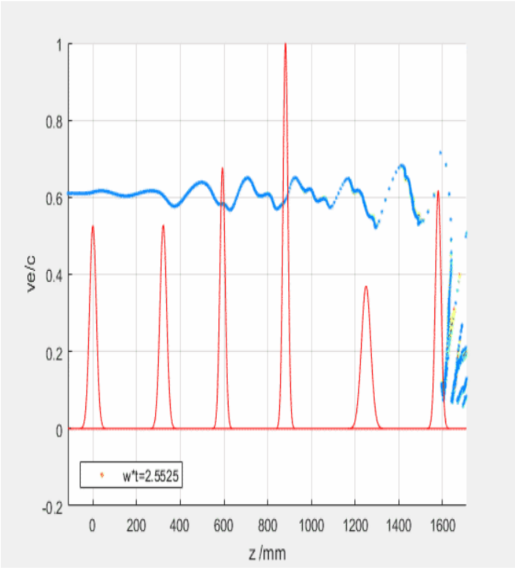

(c) PZ Diagram showing minimal stratification effects before output

4.1.5 Summary of Cavities and Results

Table 4.14 summarises the main diagnostic changes observed after detuning each cavity in the klystron. The detuning process involved shifting the frequency of each cavity from its original resonant frequency and analyzing the effects on the various beam properties. The table highlights how specific cavity adjustments influenced these key parameters and includes the position of maximum current, the formation of beamlets within the electron bunch, the spread of harmonic current amplitudes, and the density and current gradients of the electron bunch as it progresses through the system. Specifically, the detuning of cavities lead to changes in the beam dynamics with the majority effects occurring in the final cavities, where the beam density and current modulation were adjusted for an optimal output.

Table 4.14: Table summarising the main diagnostic changes after detuning each cavity

Cavity	**Description of Main Diagnostic Change**
2	Moved position of Imax in the z direction. When detuned down from the original frequency, f0, the position of Imax was moved to the right.
3	Varies the number of "beamlets" within each bunch of the beam. Beamlets are the sub bunches created due to disproportionate space charge forces between the core and the peripheral of the bunch. Decreasing the frequency from f0, increases the number of beamlets.
4	Changed the spread of the final amplitudes of the harmonic currents, when detuned below f0 the spread of the final harmonic current values decreased. There was a strong correspondence with detuning C4 and the peak current values from the 2nd to the 8th cavities. Decreasing the frequency decreased the spread of final amplitudes between the 2nd and 8th harmonic modulation.
5	It varied the density of the bunch at the final cavity. Decreasing the frequency from f0, increases the density of the bunch at the output cavity. Alters the amplitude of the 1st harmonic current at the 5th cavity. By decreasing the frequency from f0 the amplitude of the current decreases at this point. This in turns decreases the gradient change between the 4th and 5th cavities leading to a flatter overall current gradient. This change in gradient is referred to as the knee.

In this chapter, the 800 MHz CSM (Core Stabilization Method) klystron model was investigated using various design parameters, including a beam voltage of 133.85 kV and beam current of 12.551 A. The primary objective was to enhance the efficiency of the six-cavity klystron by fine-tuning both the frequency and the gap coupling factor (M), a parameter that describes the interaction between the electron beam and the RF cavities. Through simulation studies using KlyC, it was found that optimising the gap coupling factor led to noticeable improvements in efficiency and stability by reducing electron crossovers in the Applegate diagram. The investigation showed that a balance between high efficiency and minimal electron crossovers could be achieved by manipulating M values, although increasing M beyond certain thresholds reduced efficiency. Further tuning of cavity frequencies was conducted to enhance performance, where the relationship between each cavity's frequency and beam parameters like current, bunch length, and beamlet or sub-bunch formation was studied. Cavity detuning had effects on several parameters, such as the position of maximum current, the spread of harmonic current amplitudes, and the density of the electron bunch, all contributing to the overall behavior of the klystron.

In conclusion, the study demonstrated that fine-tuning the gap coupling factor and detuning each cavity could lead to substantial efficiency improvements in the 800 MHz CSM klystron, showing that the Core Stabilisation Method is a suitable direction for high-efficiency klystron design.

Chapter 5

Fuzzy Logic Table Analysis and Creation

5.1 Introduction

5.1.1 Basic Theory of Fuzzy Logic

Introduced in 1965 by Lotfi Zadeh, fuzzy logic was derived from fuzzy set theory which deals with finding approximate answers, truths, or patterns rather than precise answers thereof. In mathematics and computing, fuzzy logic sets can be thought of as a multi-valued logic system where the truth values can be any real number between 0 and 1, degrees of membership. This contrasts with Boolean logic where the truth values can only be the integer values 0 (false) or 1 (true), a crisp membership. Fuzzy logic can also be used to represent vagueness or imprecise statements such as decrease/increase or smaller/bigger when there is no specific value assigned to said statements. The characteristic crisp set function is defined as:

$$\begin{aligned} &f_A(x) : X \to 0, 1 \\ &f_A(x) = \begin{cases} 1, & \text{if } x \in A \\ 0, & \text{if } x \notin A \end{cases} \end{aligned} \tag{5.1.1}$$

Fuzzy Logic sets are represented by the membership function,

$$\begin{aligned} &\mu_A(x) : X \to [0, 1] \\ &\mu_A(x) = 1 \text{ if } x \text{ is totally in } A; \\ &\mu_A(x) = 0 \text{ if } x \text{ is not in } A; \\ &0 < \mu_A(x) < 1 \text{ if } x \text{ is partly in } A \end{aligned} \tag{5.1.2}$$

where known membership functions can be described graphically as triangular, trapezoidal, Gaussian and the like. This method of working can be especially helpful when making decisions based on imprecise or non-numerical information. Using these ideas, we based a fuzzy logic model around the speed and accuracy at which we can effectively optimise a klystron using a 2.5D PIC (Particle-in-a-cell) code. By formulating several fuzzy logic style tables that involve the use of imprecise statements, we can direct the user in which way to optimise a given klystron, therefore reducing the time and effort it takes to complete such a task.

5.1.1.1 Fuzzy Logic, a 'Simple' Solution to the Complexities of Klystron Optimisation

Using fuzzy logic to break down the complexities and time-consuming activity of klystron optimisation when using a 1D code such as AJDisk or KlyC is described. By getting the user to take a qualitative rather than quantitative approach, a quicker systematic response can be achieved.

Through observation of the beam profile and output diagnostics (from Chapter 4), and by choosing which aspects of the beam could be enhanced or diminished the user will be capable of selecting which cavities to alter via the information given in the fuzzy logic tables. This has been achieved by analysing and recording the beam diagnostics along the length of the beam tube and at the output cavity of a single klystron, during various stages of a detuning process. Each cavity was detuned individually, and results were recorded. This enabled us to characterise and segment the differences between the cavity's position and the change in output. Through this, fuzzy logic tables were established.

5.2 Methodology

The initial decision was to choose an appropriate klystron as a basis for the inputs and output results. It was suitable to use a klystron model that had been studied previously. Throughout this project there has been developed a greater understanding of modeling CSM (Core Stabilisation Method) klystrons and therefore it was appropriate to formulate the initial parameters and results from this study.

From Table 4.14 relationships between corresponding cavities and their output effect driven by changes in frequency were combined and organised into a pair of fuzzy logic Tables 5.1 and 5.2. The first fuzzy logic Table 5.1 shows the relationship between the second and the fifth cavity. Following on from analysis of the Applegate diagrams it had to be taken into consideration that both had an affect on the bunch length. When the frequencies of either were too low the bunch was considerably dense, however this influence had different outcomes for both. At a frequency too low for cavity 3 there would be no sign of sub-bunches. Contrarily at a frequency too low for cavity 5 sub-bunches are present.

Table 5.1: Fuzzy Logic Table 1

	Bunching Content		
	Bunched too much	**Good**	**Not enough bunching**
No Beamlets	Increase C3 and Increase C5	Increase C3	Increase C3 and Decrease C5
Good	Increase C5	Do nothing	Decrease C5
Strong Beamlets	Increase C5 and Decrease C3	Decrease C3	Decrease C3 and C5

Table 5.2 shows a more orthogonal response for the parameters chosen for cavity 2 and 4. With regards to the peak harmonic current, it was found that the 2nd

harmonic current was higher than the 1st when you decreased the frequency of below f_0 cavity 4. This was only detected for cavity 4.

Table 5.2: Fuzzy Logic Table 2

Harmonic Content			
	Peaks too high	**Good**	**Peaks too low**
I_{max} **Too early**	Increase C2 and Decrease C4	Increase C2	Increase C2 and Increase C4
I_{max} **Good**	Decrease C4	Do nothing	Increase C4
I_{max} **Too Late**	Decrease C2 and C4	Decrease C2	Decrease C2 and Increase C4

These tables show when optimising for a CSM tube the output diagrams and graphs you should consider are the Applegate diagrams (to tune the second and fifth cavity) and the harmonic modulation graphs (to tune for third and fourth cavity).

After discussion of the above tables, it was agreed that a flow chart was an alternative method for which a simple optimiser could be established. The flow chart below (Figure 5.2.1 highlights the relationships between each of the cavities and the order to apply the frequency changes. The order in which the tables are presented is an important factor to be considered. It became apparent from Table 4.13 that some parameters were influenced by more than one cavity. For example, following on from the analysis of the Applegate diagrams both cavity 3 and cavity 5 had an effect on the bunch length. When the frequencies of either were too low the bunch was considerably dense, however, this influence had different outcomes for both. At a frequency too low for cavity 3 there would be no sign of sub-bunches. Contrarily, at a frequency too low for cavity 5 sub-bunches were present. With this in mind, a logical order to respond to a given set of parameters has to be determined.

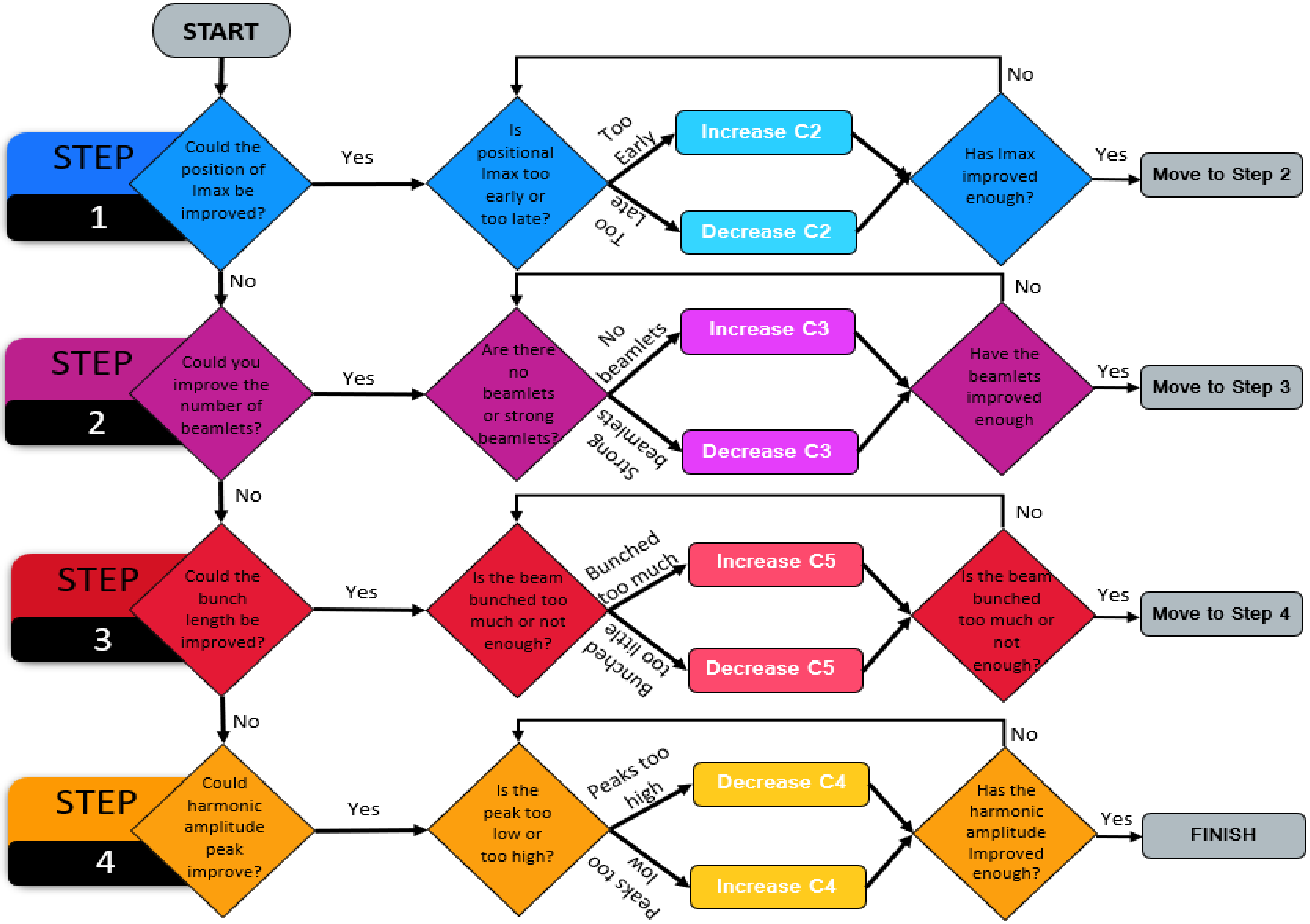

Figure 5.2.1: Flowchart for optimising klystron

The use of the above fuzzy logic tables and flowchart contributes to the beginnings of a streamlined method for the optimisation process and minimizing computational overhead in KlyC. However, the primary objective extends beyond this to encompass the expansion of such applications into more intricate simulations, with a specific focus on 2D PIC codes, such as Magic for this purpose. Although using a 1D large signal code offers a valuable insights into klystron dynamics, the transition to a 2D PIC code introduces heightened complexity by incorporating spatial variations and particle interactions. Demonstrating the efficacy of the fuzzy logic-based approach in Magic simulations adds a layer of reliability to the methodology, highlighting its adaptability across diverse simulation platforms and reinforcing its potential as a versatile tool for enhancing klystron efficiency. This validation across different simulation techniques contributes to a better understanding of the methodology's effectiveness in various modeling environments.

5.2.1 CSM Results

To further justify the methodology behind altering the frequency of a specific cavity to enhance the overall efficiency of a klystron, the original CSM tube (seen in Table 4.4) was subjected to a random detuning, shown in Table 5.3, wherein the detuned frequencies are marked in blue text. At 69.78% this is a tube close to being classified as high efficiency however, after analysis of the output graphs in Figure 5.2.2 the tube can clearly be enhanced further. The next section presents the step by step logic taken to increase the efficiency by using the fuzzy logic tables and the analysis of each result.

Table 5.3: CSM Klystron Random Cavity and Frequency Detuning

Cavity	**1**	**2**	**3** - 2nd Harmonic	**4** - 3rd Harmonic	**5**	**6**
Original Frequency (MHz)	800.36	802.56	1592.6	2394	810.78	799.6
Detuned Frequency (MHz)	800.36	802.1	1590	2394	810.78	799.6

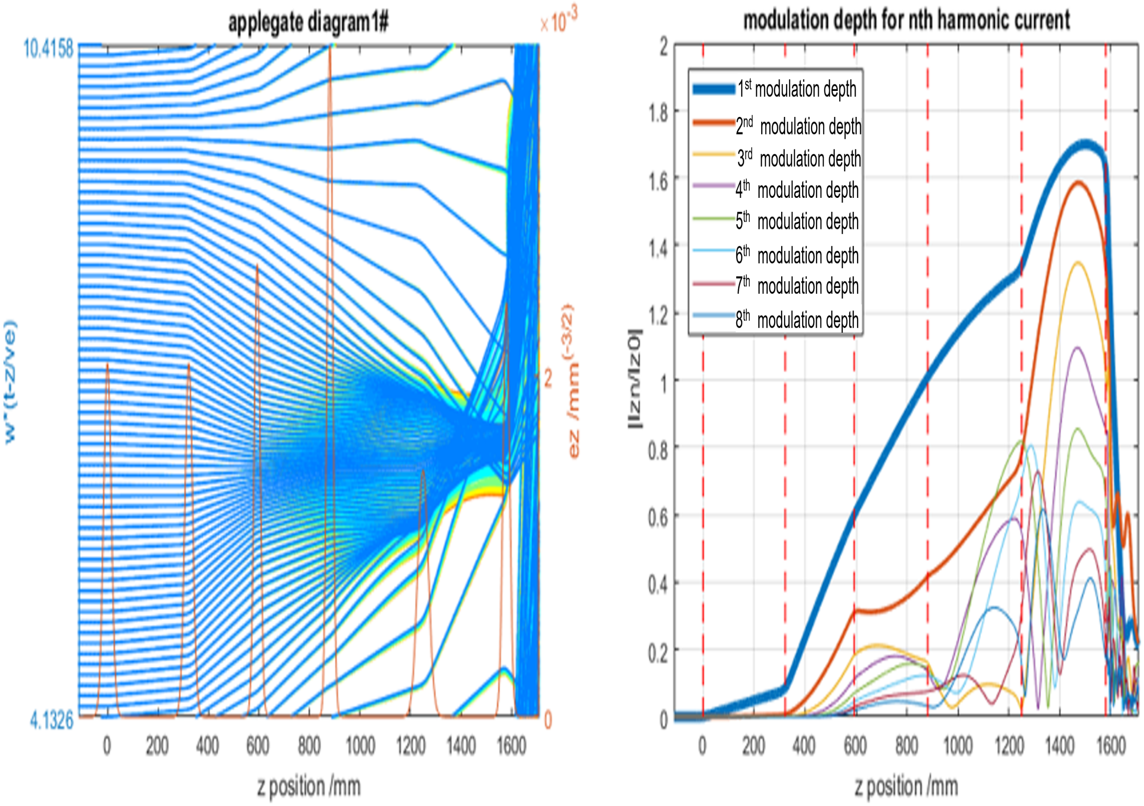

Figure 5.2.2: Initial detuning results with an efficiency of 68.97%.

5.2.1.1 Step 1 - Initial Analysis

From the Applegate diagram there is a high concentration of electron cross-over starting just after the fifth cavity (around 1300 mm), occurring at both the tail and head of the bunch. This also causes the bunch to become very narrow by the time just before reaching the output cavity, causing slight debunching before it enters the gap. The harmonic current is also seen to increase, across all higher harmonic currents at this position too.

5.2.1.2 Step 2 - First Fuzzy Logic Table

The location of I_{max} for all harmonic currents is to the left of the output gap. From the fuzzy logic Table 5.2, we know that cavity 2 has an orthogonal effect on I_{max} position. Table 5.2 also looks at the harmonic content of the peaks, that is, are the peaks too low, good or too high. Visually the harmonic current graph looks to have “good” peaks, that is they are not too high not too low. This would therefore suggest that by increasing the frequency of cavity 2 and keeping the frequency of cavity 4 the same will have an affect on the position of I_{max}. It was therefore hypothesised that I_{max} would move to the right increasing the efficiency. This is also indicated as steps one and four of the flowchart of Figure 5.2.1.

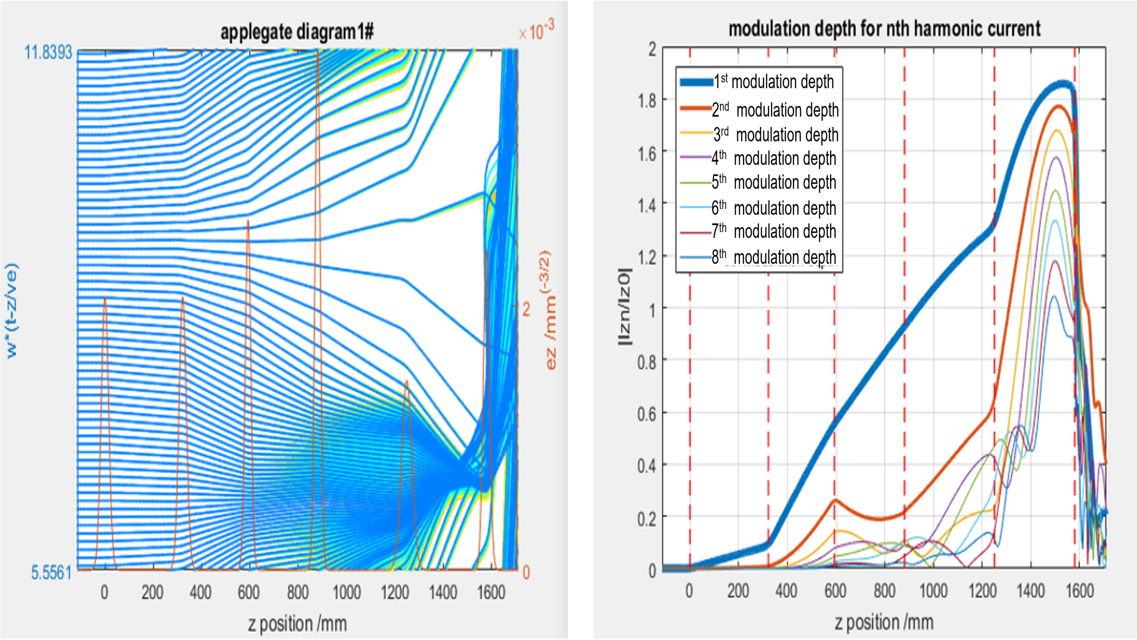

Figure 5.2.3: Efficiency = 73.05%.

5.2.1.3 Step 3 - Second Fuzzy Logic table

From increasing the frequency of cavity 2 from 802.1 MHz to 803 MHz Figure 5.2.3 it has been shown that our hypothesise was correct and the position of I_{max} has moved to the right along with an efficiency increase to 75.03%. However, the Applegate diagram in Figure 5.2.2 also showed that the beam was over bunched after the 5th cavity and included electron cross-overs (as a results of over bunching). However, the level of sub-bunching was good with three clear sub-bunches being presented in the Applegate diagram. From looking at fuzzy logic Table 5.1 you can see that for a beam that is bunched too much, but has an overall good number of sub-bunches, the cavity that should be changed is cavity 5 whilst keeping cavity 3 the same. This is also indicated as steps 2 and 3 in the flowchart on Figure 5.2.1.

Therefore it was hypothesised that by increasing the frequency of cavity 5 from 810.78 MHz to 816 MHz we would see the strong bunching diminish and the level of electron crossover decrease.

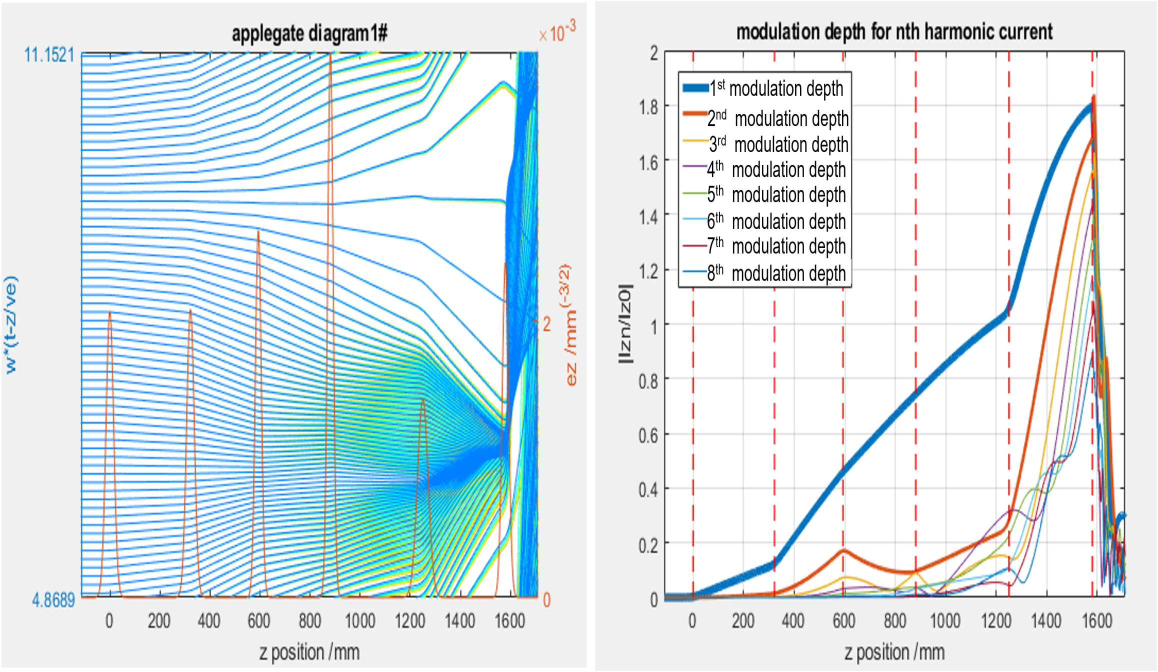

Figure 5.2.4: Efficiency = 78.97%.

5.2.1.4 Step 4 - Final Analysis

From increasing the frequency of cavity 5 from 810.78 MHz to 816 MHz as shown in Figure 5.2.5 it has been shown that the hypothesise was correct. From Figure 5.2.5 it can be seen that the strong bunching after the 5th cavity has decreased and the presence of cross-over electrons have disappeared leading to efficiency increase of 78.97%.

Figure 5.2.5 shows the final result from a two step optimisation of a CSM klystron having an initial efficiency of 68% to an increased efficiency 79%. The final result showed that by using the fuzzy logic tables, I have been able to show how to refine the design of a random seed CSM klystron. Wherein, the main steps implemented for this particular design where through changing the position of I_{max}, electron cross-overs through over-bunching. And that the steps taken, by looking at the tables, was the logical order to respond for this given set of output parameters. Tables 5.4 show the beam parameters for the random seed CSM 23 tube whilst Table 5.5 highlights the final optimised frequencies for said tube.

Table 5.4: Original tube parameters.

Operating Frequency (MHz)	**Beam Voltage (KV)**	**Beam Current (A)**	**Beam radius (mm)**	**Tube Radius (mm)**	**Total Length of Tube (m)**
800	133.85	12.551	8.63	15.89	1.58

Table 5.5: CSM klystron final frequencies with an efficiency of 79% (from an initial efficiency of 68%) , where the blue text indicates which frequencies where changed

Cavity	**1**	**2**	**3**	**4**	**5**	**6**
Frequency (MHz)	800.36	803	1590	2394	816	799.6

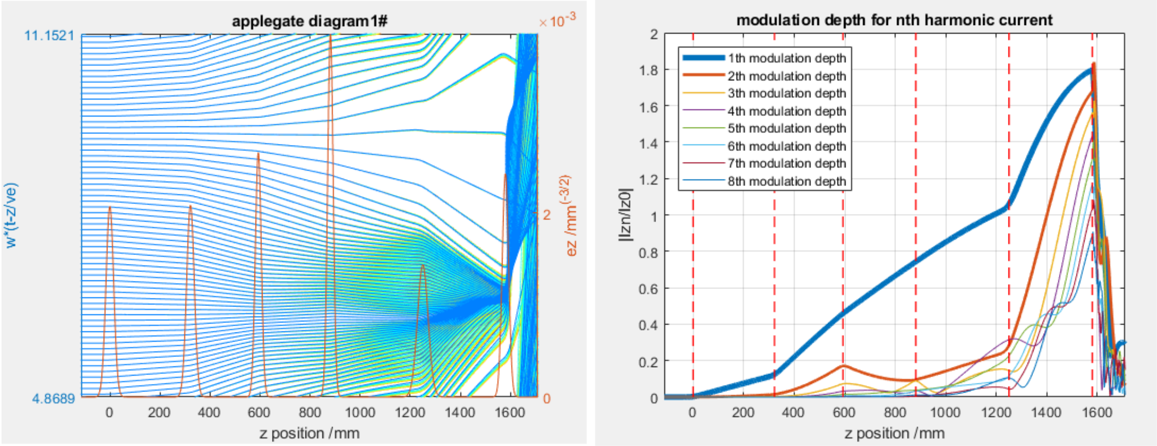

Figure 5.2.5: Final optimised Applegate and harmonic current diagrams.

Figure 5.2.5 shows the final output results and through this the efficiency achieved was elevated from from 68% to 79%.

5.3 Summary

This chapter provided an overview of fuzzy logic theory and its application to optimise the klystron design and efficiency of a Core Stabilization Method (CSM) klystron. Fuzzy logic, introduced by Lotfi Zadeh, deals with multi-valued logic systems, which helps in making decisions based on imprecise or non-numerical data. The method used fuzzy logic to quicken the klystron optimisation by applying rules from qualitative analysis instead of relying solely on quantitative measures. Using the fuzzy logic tables, relationships between different cavities and their effects on beam diagnostics (like beam bunching and harmonic currents) were explored to improve the efficiency of the CSM klystron design.

Fuzzy logic was to optimise the performance of a CSM (Core Stabilization Method) klystron. A series of steps were taken to adjust the frequencies of specific cavities, following an iterative process that used fuzzy logic tables to guide decision-making. The main aim was to increase efficiency by tuning the cavity parameters based on the output diagnostics including Applegate diagrams and harmonic modulation graphs.

The initial step involved analysing the electron beam dynamics and identifying over-bunching and harmonic issues by adjusting the frequency of individual cavities. By following the fuzzy logic presented in the Tables 5.1 and 5.2 and by following the steps in Figure 5.2.1, changes to specific cavities were made giving an improvement in the efficiency.

The following Table 5.6 summarises the key changes made along each step and includes the outcomes of those changes:

Table 5.6: Summary of Changes at Each Step in the Optimization Process

Step	**Analysis or Change Made**	**Description**	**Outcome/Effect**
Step 1	Analysis, Initial efficiency 68%	Parameters of note that need changing are position of I_max and the over bunching	Look at fuzzy logic tables and/or flowchart. Understood that the cavities to change were C2 and C4.
Step 2	Harmonic Content fuzzy logic table - Increased freq of cavity 2 from 802.1 MHz to 803 MHz	Cavity 2 frequency was adjusted to move the position of I_{max} to the right.	Efficiency increased to 73.05%. The position of I_{max} shifted to the right
Step 3	Bunching Content fuzzy logic table - Increased freq of cavity 5 from 810 MHz to 816 MHz	Cavity 5 frequency was adjusted to decrease over bunching and mitigate electron cross-over.	Efficiency increased to 78.97%. Over bunching decreased, as a result cross-overs were mitigated

Chapter 6

PIC Results for CSM 23

6.1 Magic Results for CSM 23

It should be noted that the 2D Magic simulations were conducted on a klystron that had not undergone full optimisation prior to the implementation of the fuzzy logic method. This decision was driven by time constraints within the project, necessitating the need to obtain initial insights and performance assessments of the CSM tube through 2D Magic simulations. Despite the time limitations, these preliminary simulations provided usable data and characteristics of the klystron design under consideration. Subsequently, the fuzzy logic method was employed to further optimise the klystron design, from the initial Magic 2D simulations to refine and improve its performance. This iterative approach allowed for a systematic and efficient optimisation process, ultimately leading to the development of an enhanced and more efficient klystron design.

For the initial tuning of CSM 23 klystron two steps were implemented to ensure that the each cavity geometry resonated at the required frequency and R/Q.

These steps include an eigenmode test and a cold test. The eigenmode simulation is used to compute frequency eigenvalues for each cavity at a given geometry and mesh. The radius, r2, and height, h, of a cavity are given a minimum and maximum value and a step size (this is the parameter space). Whilst r2 is kept constant, h is iterated according to the step size. When the maximum value of h is reached r2 is iterated and the first step is repeated until r2 has reached its maximum. All frequencies are recorded over the entire parameter space of h and r2 (usually around 225 results per cavity). A cold test is then performed to get the corresponding R/Qs for each individual structure and cavity number. Using the data obtained from this a contour plot is extracted for each cavity that enables the user to obtain the optimum value of r2 and h, this corresponds to the value of R/Q and frequency stated in the original simulation code. Fine tuning is used to get a more accurate measurement of the frequency and R/Q without changing the value of r2 and h. This step also includes tuning the Qe and Qin values by inputting an appropriate sigma value. The shim command (in MAGIC 2D) is used to add a small, perfectly conducting layer, or shim, to a conformal surface of a perfectly conducting object. By varying the shim you can produce a very fine-scale geometric variation on the surface of the conductor, therefore allowing for small changes in the frequency and R/Q. The value of sigma is the electrical conductivity of the absorber in each cavity and is controlled by the conductance command. This is used to replicate the ohmic losses found in a real cavity.

The Q factor in all cases is tuned to 2% of the desired value, R/Q is tuned within 4%, whilst the frequency is tuned to the exact value given. Furthermore, the cold tests allowed me to measure and calculate each gap coupling factor (M) for a given cavity. For each given value of M (as calculated in AJDisk) the width of the gap was changed until it matched the value as given in the 1D simulations. Another note of particular importance is when trying to match the input powers given in AJDisk versus Magic 2D. The calculation for a given input power between these two codes is not the same. When matching for input power it was necessary to always match the cavity voltage at cavity 1 as measured between Magic and AJDisk. This was a method used to ensure that the input power was comparable between the two codes.

Figure 6.1.1 highlights the structure of the CSM 23 klystron simulated in Magic. Table 6.1 shows the frequencies and drift lengths between each cavity along with the R/Qs. Furthermore, the B_z used for this particular simulation was 0.043 tesla.

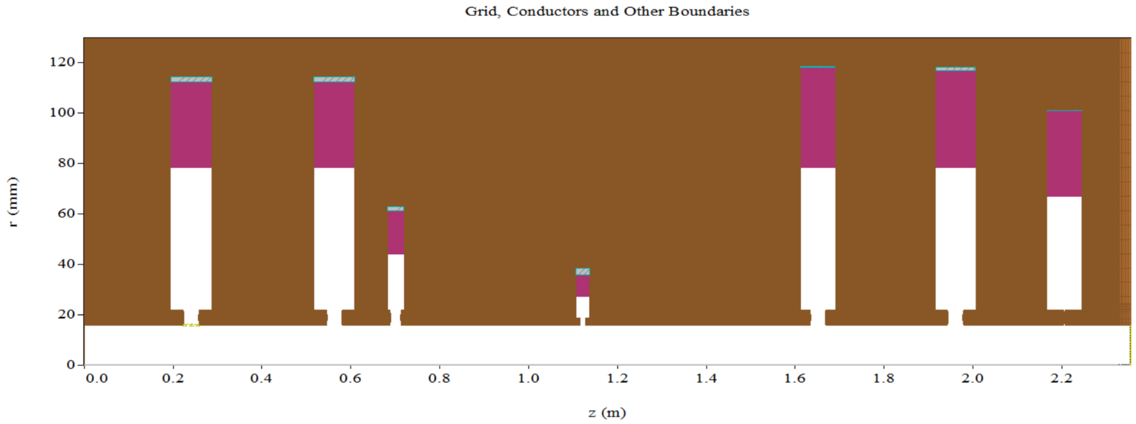

Figure 6.1.1: Structure of the CSM 23 klystron, a six cavity klystron including a 2nd and a 3rd harmonic idler cavity

First, on the simulating FCC CSM 23 in MAGIC2D, the maximum output power of 1.31 MW in saturation was achieved for an input power of 90W, corresponding to power gain of 41.6 dB.

For all input power levels considered, the output power was stable and no

Table 6.1: Frequency and drift lengths and R/Qs used for the 2D Magic simulation

Cavity Number	Frequency (MHZ)	Drift length between cavities (mm)	R/Qs
1	800.36	482	141.4
2	804.1	162	140.2
3	1592.65	114	68.4
4	2388.55	728	85.4
5	812.45	330	129.3
6	799.6	290	136.7

reflected electrons were predicted. The instantaneous bunch profiles in PZ-Z and R-Z phase spaces at the location of final two cavities are shown in Figures 6.1.2 and 6.1.4. The simulated efficiency was as high as 78.1% [34]. The PZ-Z plot showed a stable tube and a decreased bunch saturation length whilst also highlighting a reduced beam core modulation along with enhanced modulation of the electrons at the periphery of the bunch. Comparing to a COM klystron one can conclude that CSM 23 has lower level of the bunch saturation and stronger radial bunch stratification. However, the compact layout with simple 6-cavity configuration makes CSM technology very attractive for the L-band klystrons.

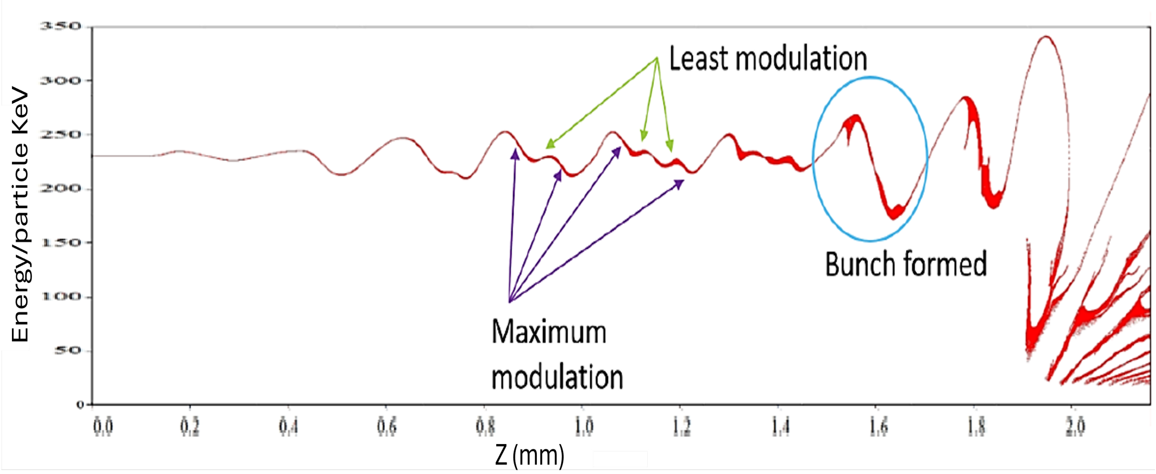

Figure 6.1.2: PZ-Z phase space profile of the electron beam at the final two cavities for CSM 23, highlighting the sub-bunches having been formed after the second and third harmonic cavity and the reformed bunch after the fifth cavity in Magic

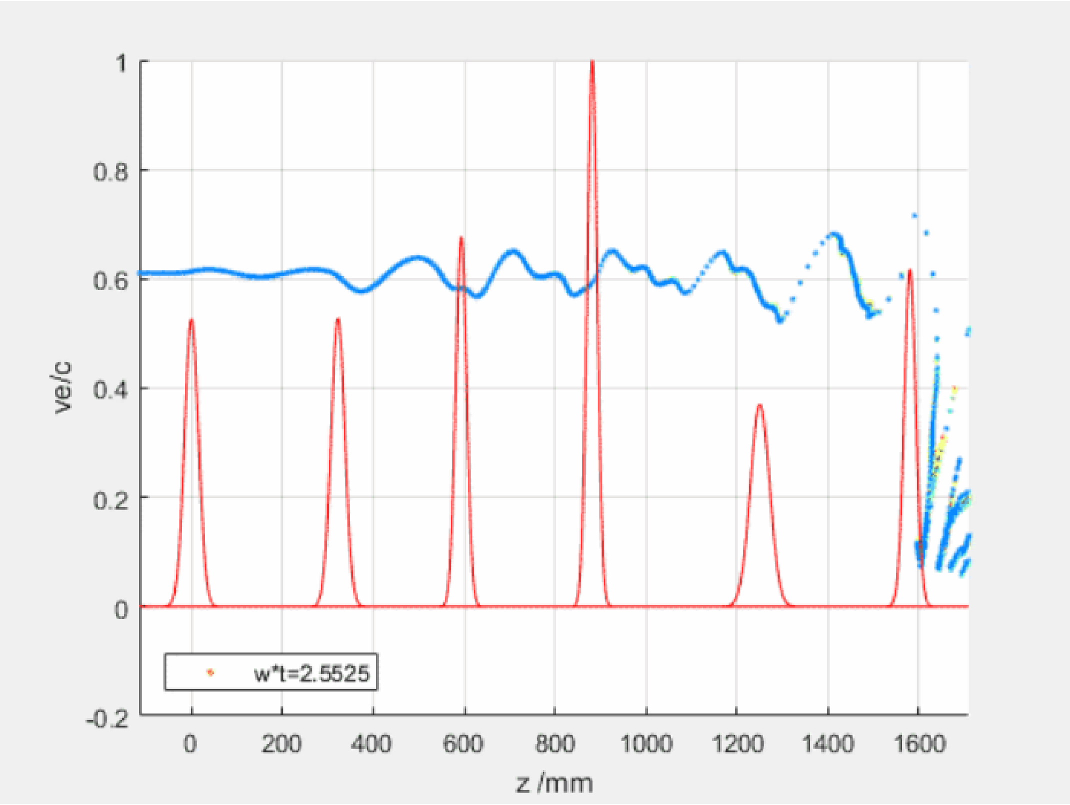

Figure 6.1.3: PZ-Z phase space profile of the electron beam at the final two cavities for CSM 23, highlighting the sub-bunches having been formed after the second and third harmonic cavity and the reformed bunch after the fifth cavity in KlyC

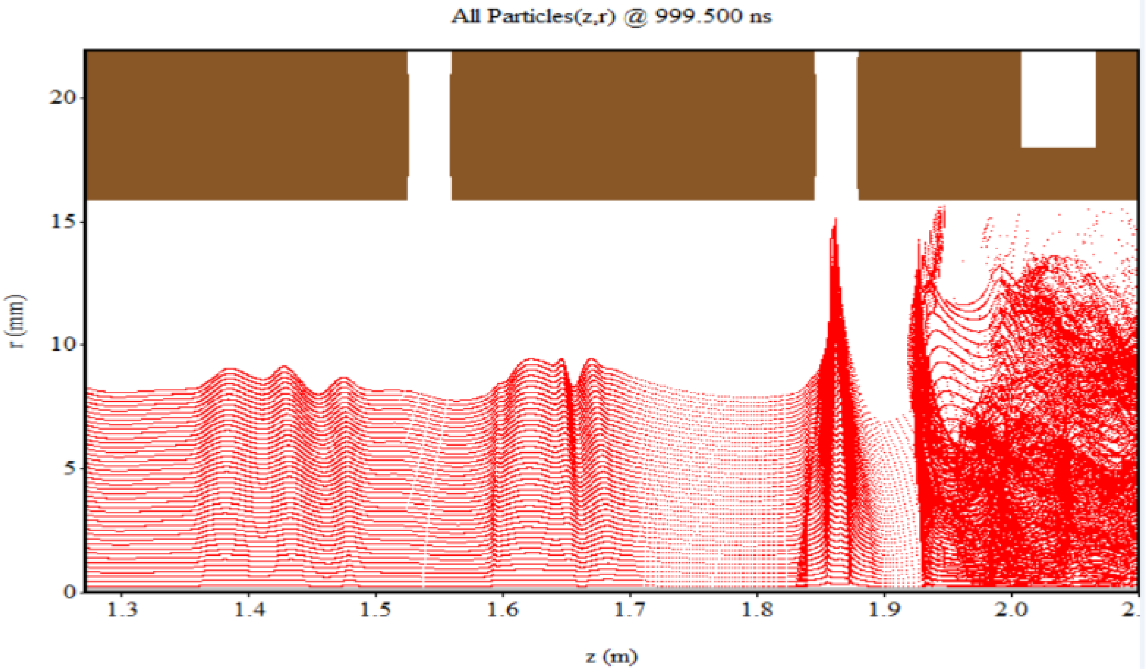

Figure 6.1.4: RZ phase space profile of the electron beam at the final two cavities for the CSM 23 800MHz klystron. This graph aims to highlight minimal stratification, and the recombination of the subbunches after cavity 5.

By comparing results between the original CSM 23 klystron in KlyC (Chapter 4) and the PIC results shown above we can determine a reasonable correlation between the two codes. The simulated efficiency in KlyC was 78.54% whilst the simulated efficiency as given in Magic was 78.1%. Furthermore, the PZ-Z plots shown in Figures 6.1.2 and 6.1.3 emphasise the similarities between the velocity distribution of the electrons throughout the tube. This ultimately could present a foreseeable high efficiency output for the optimised CSM 23 tube in a 2.5D code, such as Magic, at an efficiency of just below 82.27%.

6.2 Summary of PIC Results

In this chapter, the 2D MAGIC simulations for the CSM 23 klystron were conducted on a non-fully optimised model due to time constraints. Despite this, the simulations provided data to guide further optimisations through fuzzy logic methods. Initial tuning was carried out by performing eigenmode and cold tests to determine the cavity geometries and resonance frequencies. The simulation fine-tuned parameters like R/Q and Q factors for more accurate results, followed by gap coupling factor adjustments to match with previous simulations from AJDisk. The structure of the CSM 23 klystron, a six-cavity model incorporating second and third harmonic cavities, is illustrated in Figure 6.1.1, while Table 6.1 lists the key simulation parameters.

The simulations resulted in a maximum output power of 1.31 MW with an efficiency of 78.1%. Phase space plots (PZ-Z and R-Z) revealed stable bunch formation with reduced beam core modulation and enhanced modulation of peripheral electrons. The PZ-Z profile emphasized sub-bunch formation and recombination after the fifth cavity. A comparison with the KlyC results showed close agreement in efficiency values and electron velocity distributions between the two codes, indicating that the optimized CSM 23 tube could achieve high efficiency (just below 82.27%) in further simulations.

Chapter 7

Conclusion and Further Work

The design of a high efficiency klystron remains a complex task. A number of design decisions have been made which will aid further work on this topic. In addition a new fuzzy logic technique to simplify the beginning optimisation of a klystron in and its properties have been developed.

7.1 Core Stabilisation Method

7.1.1 Original Idea

The original idea of using harmonic cavities was from E. L. Lien's work in 1970. He was able to show that by the implementation of a cavity resonating at the second harmonic in a low microperveance klystron proved instrumental in achieving higher efficiencies. By replacing the third cavity with a second harmonic cavity in a 5-cavity klystron, Lien demonstrated an efficiency exceeding 65% for 100 kW output power, compared to 54% without the second harmonic cavity. This work into the use of harmonic cavities has been further tested and studied by the High Efficiency Klystron Activity (HEIKA) collaboration including Lancaster University and CERN. This concept was developed further by implementing a second and a third harmonic cavity for 1 GHz, low microperveance (0.21) klystron. This technique, called the core stabilisation method (CSM) allowed for non-monotonic bunching in the electron beam over a shorter tube length than compared to the core oscillation method (COM), and in a similar way to the bunch alignment collection (BAC) method. Using a plurality of higher harmonic cavities facilitated the formation of two smaller sub-bunches within the electron beam, reuniting at the penultimate cavity in the klystron. These sub-bunches effectively reduced the space charge forces on peripheral particles. Coupled with velocity modulation, this process improved the "collection" of particles located far from the bunch core. Consequently, the enhanced bunching at the output cavity led to the attainment of higher efficiencies. This method used the third harmonic cavity to produce three “virtual” cores in the bunch and the peripheral electrons are collected even faster than in the BAC method, as the needed debunching is not as strong because the central core neutralizes the two others. As a result the “global” core can be transported without distortion over the tube.

7.1.2 CSM 1GHz and 800MHz

The CSM technique was used and optimisation of two tubes were established. The first was the 1Ghz tube and the second was an 800MHz tube. The second and third harmonic, 1 GHz, low microperveance (0.21) klystron with a beam current of 8.21 A and beam voltage of 115 kV was optimised with AJDisk, and the RF design of the cavities was carried out using SUPERFISH by Chiara Marrelli. Further optimisation and a full PIC code model was achieved using CST Microwave Studio, AJDisk, and MAGIC 2D. Figure 7.1.1, and Tables 7.1 and 7.2 show the final output results for the AJDisk and Magic simulations. These results providing evidence that the CSM technique could provide the efficiency required for future klystrons.

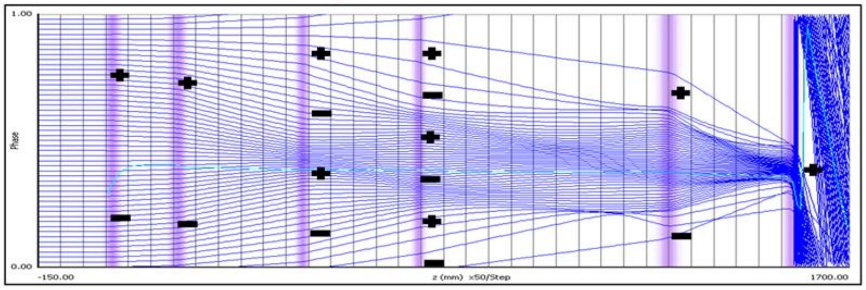

Figure 7.1.1: AJDisk prediction showing the Applegate diagram of 1GHz klystron with second (cavity 3) and third harmonic (cavity 4) with corresponding poles. Having a predicted efficiency of 88%

Table 7.1: Output Measurements from AJDisk

Parameter	Value
Operating Frequency	1.0GHz
Beam Voltage	115 kV
Beam Current	8.21 A
Gain	39 dB
Output Power	833.069 W
Efficiency(%)	88.65

Table 7.2: Output Measurements from MAGIC 2D.

Parameter	Value
Output Power	784 kW
Efficiency	79.8 %
Gain	46 dB
Input Cavity Voltage	2.06 kV
Output Cavity Voltage	120 kV

The 800MHz tube was scaled using the scaling process outlined in [33]. From here the tube was optimised through a study of the frequency dependencies and by taking a closer look at the gap coupling factors. The original efficiency from the scaled tube was 78.54%. Through detailed analysis of each cavity and its impact on the electron beam and its corresponding output parameters a thorough understanding of the optimisation process (by detuning the frequency) was met.

Table 7.3: Summary of each cavities response to a parameter after detuning.

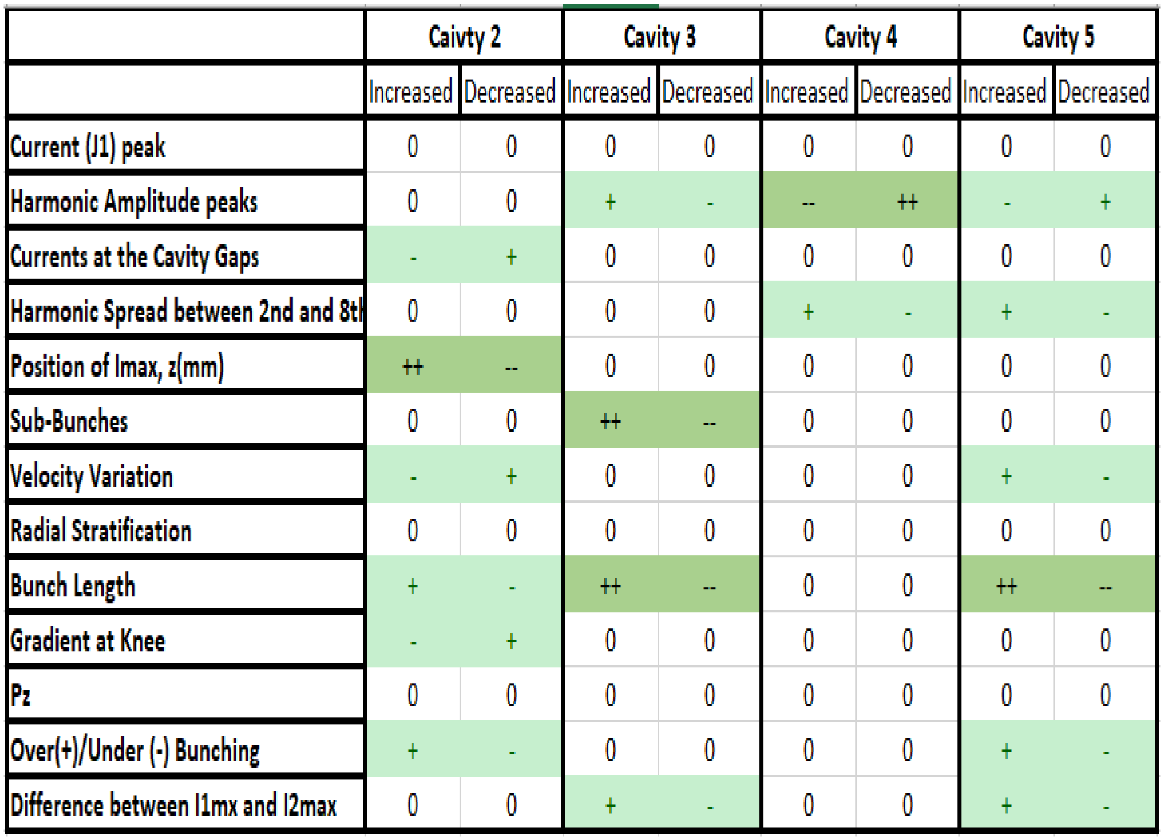

	Caivty 2		Cavity 3		Cavity 4		Cavity 5	
	Increased	Decreased	Increased	Decreased	Increased	Decreased	Increased	Decreased
Current (J1) peak	0	0	0	0	0	0	0	0
Harmonic Amplitude peaks	0	0	+	-	--	++	-	+
Currents at the Cavity Gaps	-	+	0	0	0	0	0	0
Harmonic Spread between 2nd and 8t	0	0	0	0	+	-	+	-
Position of Imax, z(mm)	++	--	0	0	0	0	0	0
Sub-Bunches	0	0	++	--	0	0	0	0
Velocity Variation	-	+	0	0	0	0	+	-
Radial Stratification	0	0	0	0	0	0	0	0
Bunch Length	+	-	++	--	0	0	++	--
Gradient at Knee	-	+	0	0	0	0	0	0
Pz	0	0	0	0	0	0	0	0
Over(+)/Under (-) Bunching	+	-	0	0	0	0	+	-
Difference between I1mx and I2max	0	0	+	-	0	0	+	-

This analysis and the frequency optimisation produced a final optimised design with an efficiency of 82.27%.

As discussed in chapter 4 however, the final optimised design was not simulated in Magic due to time constraints. However, the design as simulated produced a decent efficiency of 78.1%. However, this was still a favorable result highlighting the benefits of using the core stabilisation method as compared to COM. That the CSM 23 had lower level of the bunch saturation and stronger radial bunch stratification leading to a more stable, high efficient and smaller tube.

7.2 Further Work

While the fuzzy logic tables, as designed in Chapter 5, played a role in beginning the streamlining process for the optimization process and reducing computation time in KlyC, the broader objective was to establish the application of this methodology to more sophisticated simulations, specifically employing 2D PIC (Particle-in-Cell) code such as Magic. Using a 1D large signal computer code provides valuable insights into the dynamics of the klystron, yet the transition to a 2D PIC code introduces a higher level of complexity by accounting for spatial variations and particle interactions. Demonstrating the effectiveness of the fuzzy logic-based approach in Magic simulations adds a layer of robustness to the methodology, showcasing its adaptability across different simulation platforms and reinforcing its potential as a versatile tool for optimising klystron efficiency. This cross-validation across simulation techniques contributes to a more comprehensive understanding of the methodology's efficacy in diverse modeling environments.

Bibliography

[1] Antonella Del Rosso. "Higgs: the beginning of the exploration". In: *CERN Bulletin* BUL-NA-2012-357. 47/2012 (Nov. 2012), p. 3.

[2] Lyndon Evans. *The Large Hadron Collider: a Marvel of Technology*. Ed. by Lyndon Evans. 1st. EPFL Press, 2009.

[3] Alexander Wu Chao and Maury Tigner. *Handbook of Accelerator Physics and Engineering*. Ed. by Alexander Wu Chao and Maury Tigner. World Scientific Publishing Co. Pte. Ltd., 2002.

[4] James Benford, John A. Swegle, and Edl Schamiloglu. "Chapter 1: Introduction to High Power Microwaves". In: *High Power Microwaves*. 3rd. Boca Raton, FL: CRC Press, 2015, pp. 1–21. ISBN: 978-1-4665-9833-8.

[5] G. Gautier et al. "352.2 MHz 150 kW Solid State Amplifiers at the ESRF". In: *Conf. Proc. C* 110904 (2011). Ed. by Christine Petit-Jean-Genaz, pp. 71–73.

[6] M. Di Giacomo. "Solid state RF amplifiers for accelerator applications". In: *Particle Accelerator Conference PAC09*. May 2009.

[7] J. Jacob et al. "COMMISSIONING OF FIRST 352.2 MHz - 150 kW SOLID STATE AMPLIFIERS AT THE ESRF AND STATUS OF R&D". In: *IPAC2013:*

Proceedings of the 4th International Particle Accelerator Conference. May 2013, pp. 2708–2710.

[8] R. G. Carter. “Review of RF power sources for particle accelerators”. In: *CERN Accelerator School : Radio Frequency*. Ed. by J. Miles. 2005, pp. 107–145.

[9] X. Chang et al. “DEVELOPMENT OF THE ENERGY-EFFICIENT SOLID STATE RF POWER SOURCE FOR THE JEFFERSON LABORATORY CEBAF LINAC”. In: *Proceedings of IPAC 2012, New Orleans, Louisiana, USA*. 2012.

[10] P. Marchand et al. “DEVELOPMENT OF HIGH RF POWER SOLID STATE AMPLIFIERS AT SOLEIL”. In: *Proceedings of IPAC2011, San Sebastián, Spain*. 2011.

[11] M. J. Smith and G. Philips. *Power Klystrons Today*. Research Study Press Ltd., 1995.

[12] Russell H. Varian. “Electrical translating system and method”. US2242275A. May 1941. URL: `https://patents.google.com/patent/US2242275A`.

[13] A. S. Gilmour(Jr). *Klystrons, Travelling Wave Tubes, Magnetrons, Crossed-Field Amplifers and Gyrotrons*. Artech House, 2011.

[14] Yiman Wang, Jinshu Wang, and Wei Liu. “Development of scandate cathode and its prospect: A review”. In: *Vacuum Electron Sources Conference IVESC, 2012 IEEE Ninth International*. Apr. 2012, p. 41.

[15] C. Lingwood. “High Power High Efficiency Multiple-Beam Klystron Design”. PhD thesis. Lancaster University, 2010.

[16] George Caryotakis. “The Klystron: A Microwave source of surprising range and endurance”. In: *39th Annual Meeting of the Division of Plasma Physics of the American Physical Society (DPP 97)*. Jan. 1998.

[17] Y. H. Chin et al. “DEVELOPMENT OF TOSHIBA L-BAND MULTI-BEAM KLYSTRON FOR EUROPEAN XFEL PROJECT”. In: *Proceedings of 2005 Particle Accelerator Conference, Knoxville, Tennessee*. 2005.

[18] F. Gerigk. “Cavity Types”. In: *CERN Accelerator School : RF for accelerators*. June 2010, pp. 277–298.

[19] G. Burt. *Lecture 1: Introduction to RF for accelerators*. Dec. 2014.

[20] M Aicheler et al. *A Multi-TeV Linear Collider Based on CLIC Technology: CLIC Conceptual Design Report*. CERN Yellow Reports: Monographs. Geneva: CERN, 2012. DOI: `10.5170/CERN-2012-007`. URL: `https://cds.cern.ch/record/1500095`.

[21] Erk Jensen. “FCC RF Overview”. In: *First Annual Meeting of the Future Circular Collider study*. 2015.

[22] Arnold Vlieks. “X-BAND KLYSTRON DEVELOPMENT AT SLAC”. In: *X-BAND KLYSTRON DEVELOPMENT AT SLAC*. Aug. 2009.

[23] Y.H. Chin et al. “Development of 10 MW L-Band Multi-Beam Klystron (MBK) for european X-FEL project”. In: *2007 IEEE Particle Accelerator Conference (PAC)*. 2007, pp. 2098–2100. DOI: `10.1109/PAC.2007.4441162`.

[24] C. Marrelli. *HE Klystron Summary Report*. Tech. rep. European Spallation Source ESS AB, 2014. URL: `https://www.europeanspallationsource.se/publications`.

[25] Andrey Yu Baikov, Chiara Marrelli, and Igor Syratchev. "Toward High-Power Klystrons With RF Power Conversion Efficiency on the Order of 90%". In: *IEEE Transactions on Electron Devices* 62.10 (2015), pp. 3406–3412. DOI: `10.1109/TED.2015.2464096`.

[26] A. V. Konnov, I. A. Guzilov, and O. Yu. Maslennikov. "A Way to Increase the Efficiency of Klystrons". In: *Proceedings of the International Vacuum Electronics Conference (IVEC)*. IEEE. 2013. URL: `https://ieeexplore.ieee.org/document/6571181`.

[27] Roman Egorov et al. "BAC-Klystrons: A New Generation of Klystrons in Vacuum Electronics". In: *Moscow University Physics Bulletin* 74 (Jan. 2019), pp. 38–42. DOI: `10.3103/S0027134919010077`.

[28] E. Wright et al. "Development of a 10-MW, L-band, multiple-beam klystron for TESLA". In: *Proceedings of the 2003 Particle Accelerator Conference*. Vol. 2. 2003, 1144–1146 Vol.2. DOI: `10.1109/PAC.2003.1289633`.

[29] In: *Design of a High-Power Sheet Beam Klystron", in Proc. IEEE Part. Accel. Conf., Washington D.C.* Mar. 1997.

[30] E. R. Colby et al. "E.Schamiloglu J.Bedford J.A.Swegle. High Power Microwavesd sheet beam klystron simulation". In: *AIP Conference Proceedings* 474.1 (May 1999), pp. 74–90. ISSN: 0094-243X. DOI: `10.1063/1.59037`. eprint: `https://pubs.aip.org/aip/acp/article-pdf/474/1/74/11498469/74\_1\_online.pdf`. URL: `https://doi.org/10.1063/1.59037`.

[31] A. Jensen et al. "Developing Sheet Beam Klystron Simulation Capability in AJDISK". In: *IEEE Transactions on Electron Devices* 61.6 (June 2014). ISSN:

0018-9383. DOI: `10.1109/TED.2014.2298753`. URL: `https://www.osti.gov/biblio/1133383`.

[32] E.L. Lien. “High efficiency klystron amplifier”. In: *1969 International Electron Devices Meeting*. 1969, pp. 98–98.

[33] Jinchi Cai, Igor Syratchev, and Zening Lui. “Scaling Procedures and Post-Optimization for the Design of High-Efficiency Klystrons. Scaling Procedures and Post-Optimization for the Design of High-Efficiency Klystrons”. In: *IEEE Trans. Electron Devices* 66.2 (2019), pp. 1075–1081. DOI: `10.1109/TED.2018.2887348`. URL: `https://cds.cern.ch/record/2655910`.

[34] Victoria C. R. Hill et al. “Particle-in-cell simulation of second and third harmonic cavity klystron”. In: *2017 Eighteenth International Vacuum Electronics Conference (IVEC)*. 2017, pp. 1–2. DOI: `10.1109/IVEC.2017.8289626`.